February 2022
PhD Dissertation

# Reactive and Proactive Resource Allocation for LoRa-Enabled IoT Applications

Graduate School of Chosun University

Department of Information and Communication Engineering

Arshad Farhad

# Reactive and Proactive Resource Allocation for LoRa-Enabled IoT Applications

# LoRa 기반 사물인터넷 응용을 위한 Reactive 및 Proactive 자원 할당

February 25, 2022

Graduate School of Chosun University

Department of Information and Communication Engineering

Arshad Farhad

# Reactive and Proactive Resource Allocation for LoRa-Enabled IoT Applications

Advisor: Prof. Jae-Young, Pyun

A dissertation submitted in partial fulfillment of the requirements for the Degree of Doctor of Philosophy

October 2021

Graduate School of Chosun University

Department of Information and Communication Engineering

Arshad Farhad

# This is to certify that the Doctor's thesis of

# Arshad Farhad

has been approved by the examining committee for the thesis requirement for the Doctor's degree in Engineering

**Committee Chairperson**
**Chosun University** **Prof. Goo-Rak Kwon** **(Sign)**

**Committee Member**
**Sunchon National University** **Prof. Eui-Sung Kang** **(Sign)**

**Committee Member**
**Sunchon National University** **Prof. Sang-Hyun Park** **(Sign)**

**Committee Member**
**Chosun University** **Prof. Ji-Hwan Moon** **(Sign)**

**Committee Member**
**Chosun University** **Prof. Jae-Young Pyun** **(Sign)**

January 2022

Graduate School of Chosun University

*Dedicated to my mother and family members.*

# Abstract

## Reactive and Proactive Resource Allocation for LoRa-Enabled IoT Applications

Arshad Farhad
Advisor: Prof. Jae-Young Pyun
Department of Information and Communication Engineering
Graduate School of Chosun University

In recent times, LoRa has become a de-facto technology for the Internet of Things (IoT) owing to its long-range connectivity support for a large number of end devices, low deployment cost, and ultra-low energy consumption. The adaptive data rate (ADR) in LoRaWAN is a widely adopted strategy for resource assignment to end devices recommended for static IoT applications, such as smart grid and metering. ADR manages the spreading factor (SF) and transmit power (TP) of an individual end device (ED). However, the ADR performance can be reduced significantly under a highly dense network and variable channel conditions. Also, the mobility of EDs causes frequent alterations in the topology, which influences the signal strength between EDs and a gateway (GW). ADR of LoRaWAN is unsuitable and inadequate when the EDs are mobile because it requires hours to converge to a stable and energy-efficient communication state by adapting an appropriate SF. The new SF and TP configured by the NS do not guarantee efficient communication between mobile ED and GW. In such a case, the propagation environment may change radically when an ADR command reaches the mobile ED, and the newly assigned parameters may no longer be valid. Hence, a new packet from this ED with newly adopted parameters may be lost owing to the inappropriate use of both SF and TP. This packet loss compels EDs to retransmit the packet, resulting in further packet loss due to interference. Therefore, this dissertation resolves the packet loss issue caused due to inappropriate SF using reactive, proactive, and hybrid paradigms. The reactive paradigms

comprise channel-adaptive SF allocation (C-ASFA), Gaussian-ADR (G-ADR), and Exponential moving average-ADR (EMA-ADR). The proactive paradigms include mobility-aware SF assignment (M-ASFA), retransmission-assisted resource management (RA-ARM), and artificial intelligence-empowered resource allocation (AI-ERA). Finally, a hybrid-ADR (HADR) is presented. Simulation results showed an improved packet success ratio, energy consumption, and convergence period compared to state-of-the-art ADR schemes.

**Index Terms:** LoRa, LoRaWAN, Internet of Things, Adaptive Data Rate, Resource Allocation, Artificial Intelligence

# 요 약

## LoRa 기반 사물인터넷 응용을 위한 Reactive 및 Proactive 자원 할당

Arshad Farhad
Advisor: Prof. Jae-Young Pyun
Department of Information and Communication Engineering
Graduate School of Chosun University

최근 LoRa는 다수의 단말에 대한 장거리 연결 지원, 낮은 배포 비용 및 적은 에너지 소비로 인해 사물인터넷 (IoT)을 위한 통신기술이 되었다. LoRaWAN의 ADR (adaptive data rate)은 스마트 그리드 및 계량과 같은 정적 IoT 애플리케이션에 권장되는 단말에 자원을 할당하기 위해 널리 채택된 전략이다. ADR은 개별 단말의 SF (spreading factor)와 TP (transmit power)를 관리한다. 그러나 고밀집 네트워크 및 가변 채널 조건에서는 ADR 성능이 크게 저하될 수 있다. 또한 단말의 이동성으로 인해 전송 환경이 자주 변경 되어 단말과 게이트웨이 간의 신호 강도에 영향을 준다. LoRaWAN의 ADR은 적절한 SF를 적용하여 안정적이고 에너지 효율적인 통신 상태로 수렴하는데 많은 시간이 소모되기 때문에 단말이 이동하는 경우에 부적절하다. 또한, LoRaWAN 네트워크 서버에 의해 새로 구성된 SF 와 TP 같은 통신 파라미터는 이동 단말과 게이트웨이 간의 효율적인 통신을 보장하지 않는다. 즉, 단말이 이동하는 경우 전파 환경이 급격히 변하여 새로 발행된 ADR 명령이 더 이상 유효하지 않아 단말은 적응적이지 못한 SF와 TP의 사용으로 인해 패킷 전송이 실패할 수 있다. 이 패킷 손실은 단말이 재전송 절차를 수행하도록 하여 패킷 간 간섭으로 인한 추가적인 손실을 일으킨다. 따라서 본 논문에서는 적응적이지 못한 SF로 인한 패킷 손실 문제를 reacitve, proactive, hybrid와 같은 다양한 자원 할당 접근 방식을 통해 해결한다. reacitve 접근 방식에는 채널 적응형 SF 할당(C-ASFA), 가우시안-ADR (G-ADR) 및 지수 이동 평균-ADR (EMA-ADR)이 포함된다. Proactive 방식으로는 M-ASFA (mobility-aware SF assignment), RA-ARM (retransmission-assisted resource management ADR), AI-ERA (artificial intelligence-empowered

resource allocation)가 있다. 마지막으로는 hybrid ADR (HADR)를 제안한다. 제안한 방법의 주요 목표는 패킷 전송 성공률을 높이고 에너지 소비를 줄이는 것이다. 시뮬레이션 결과는 제안한 ADR 방식에 향상된 성능을 보여준다.

**Index Terms:** LoRa, LoRaWAN, Internet of Things, Adaptive Data Rate, Resource Allocation, Artificial Intelligence

# Acronyms

| | |
|---|---|
| ACK | Acknowledment |
| ADR | Adaptive Data Rate |
| CIR | Cumulative Interference Ratio |
| CSS | Chirp Spread Spectrum |
| DL | Downlink |
| DR | Data Rate |
| E-ADR | Enhanced ADR |
| ED | End Device |
| GW | Gateway |
| I-ASF | Adaptive SF Assignment Based on the Interference |
| IoT | Internet of Things |
| LOG | Log-Distance |
| LoRaWAN | Long-Range Wide Area Network |
| LPWAN | Low-Power Wide Area Network |
| MAC | Medium Access Control |
| M-ASFA | Mobility-Aware SF Assignment Scheme |
| MCS | Modulation and Coding Schemes |
| NS | Network Server |
| OH | Okumura-Hata |
| PER | Packet Error Rate |
| PLR | Packet Loss Ratio |
| PSR | Packet Success Ratio |
| RF | Radio Frequency |
| RSSI | Received Signal Strength Indicator |
| RX | Receive Window |
| SF | Spreading Factor |
| SINR | Signal-to-Interference-plus-Noise Ratio |
| SNR | Signal-to-Noise Ratio |
| ToA | Time-on-Air |
| TP | Transmit Power |
| UL | Uplink |

# Contents

# List of Figures

# List of Tables

# List of Algorithms

# Chapter 1
# Introduction

The Internet of Things (IoT) allows people and things to be connected Anytime, Anyplace, with Anything and Anyone, using Any network and Any service. The IoT is massive and growing exponentially, comprising a large number of devices scattered over a wide geographical area, thus creating a high-density and large-scale environment. Low Power Wide Area Network (LPWAN) is an umbrella of IoT technologies to fulfill application requirements. IoT applications can be categorized into nine groups: smart metering, agriculture, tracking, smart grids, health, industrial, smart city, home automation, and vehicle telematics [1].

LPWAN technologies have risen in licensed and unlicensed markets, such as Long Term Evolution for Machines (LTE-M), SigFox, Long-Range Wide Area Network (LoRaWAN), and Narrowband (NB)-IoT. LoRaWAN [2] is among the leading LPWAN technologies and has been extensively adopted by academia and industries for the IoT. Specifically, the IoT requires a communication protocol that can satisfy application requirements such as long-range, energy efficiency, and scalability [3].

Long-Range (LoRa) specifies the physical layer, which employs chirp spread spectrum (CSS) modulation, enabling long-range and low-energy communication [4, 5]. LoRa operates in the unlicensed ISM bands of 433, 868, and 915 MHz in Asia, Europe, and North America, respectively [6]. In LoRa technology, *Class A* end devices (EDs), which support bidirectional communication, always initiate uplink (UL) transmission by using six spreading factors (SFs $\in$ [7, 8, 9, 10, 11, 12]) with an ALOHA channel access mechanism. In LoRa, an SF represents the size of the chip sequence applied to the original data signal [7]. Furthermore, it indicates the number of maximum raw bits that can be encoded. For example, SF7 indicates that a chirp can be encoded in seven bits. When the value of SF increases, the signal-to-noise ratio (SNR) and time-on-air (ToA) increase, resulting in increased coverage range and sensitivity [8].

The rest of the chapter is organized as follows: Section 1.1 presents the motivation. Section 1.2 highlights the problem statement. Section 1.3 describes the research objectives. Section 1.4 elaborates on the contributions, while last Section 1.5 presents the organization of the dissertation.

## 1.1 Motivation

LoRaWAN is the most widely adopted technology for the IoT due to its long-range, ultra-low power consumption, and low-cost solutions. To fulfill IoT application requirements [1], *Class A* devices are utilized because of high energy efficiency and bi-directional behavior. However, the *Class A* devices utilize an

ALOHA channel access method during the communication, resulting in packet collisions caused by intra- and inter-SF interferences. This situation causes massive packet loss and high energy consumption. To this end, LoRaWAN offers an energy-efficient Adaptive Data Rate (ADR) for resource [e.g., transmit power (TP) and SF] allocation to IoT applications.

In LoRaWAN, EDs and network server (NS) utilize ADR concurrently for dynamic resource management. For example, LoRa Alliance suggested using the ED-side ADR in [2, 9], which is primarily designed to re-establish reliable communication links by stepping up the SF and allocating the maximum power (i.e., 14 dBm). Additionally, the network operator can set up the NS-side ADR (e.g., The Things Network) to manage the SF and TP by investigating the UL history of $M$ packets (i.e., $M = 20$), thereby providing reliability and efficiency [10]. Once the ADR is adjusted, the SF and TP parameters are periodically maintained. Hence, this provides a suitable environment for high-capacity, and static applications such as metering [11]. However, the channel condition changes drastically due to the ED movement, resulting in a massive packet loss ratio (PLR), excessive energy consumption, and a significantly long convergence period in static and mobile application scenarios. Therefore, this dissertation reactively and proactively assigns resources to mobile and static IoT applications to improve the scalability, convergence period, energy consumption, and packet success ratio (PSR).

## 1.2 Problem Statement

ADR is a widely adopted resource assignment approach for static IoT applications, such as smart grid and metering. However, for mobile IoT applications, for instance, pet and industrial asset tracking, blind ADR (BADR) is recommended. Both ADRs cannot consider any appropriate measures to predict and provide evasive measures to alleviate the massive packet loss that is caused due to the inefficient SF and TP adopted by EDs.

## 1.3 Research Objectives

The application requirements of static and mobile IoT applications are not the same, such as UL period, bi-directionality, PSR, and scalability. Resource management in a uni-directional network is not challenging due to the absence of an acknowledgment (ACK); such network in LoRa is called unconfirmed mode. However, resource management is demanding in a bi-directional network (also known as a confirmed mode) since most IoT applications require monitoring (e.g., asset-tracking). The current ADR of LoRaWAN is specifically designed

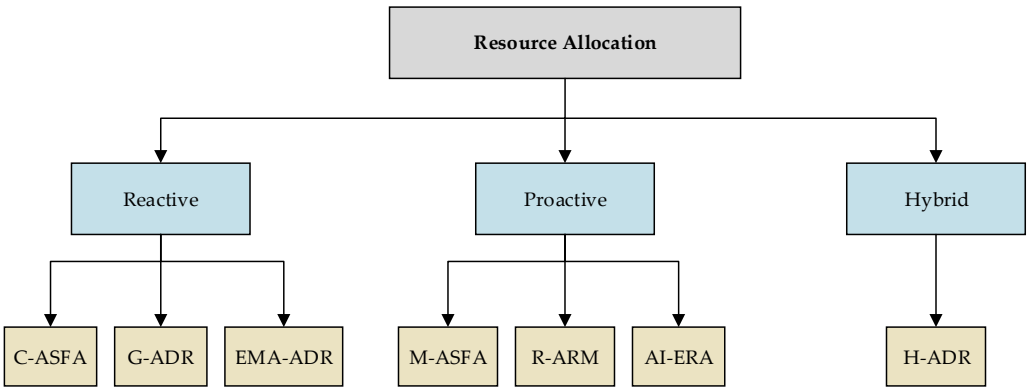


Figure 1.1: Reactive, proactive, and hybrid resource allocation in LoRa-Enabled IoT applications.

to manage the resources of only static EDs. Therefore, Semtech suggests utilizing a BADR for mobile applications (e.g., pet-tracking). However, many aspects of the IoT applications are ignored (e.g., UL period and bi-directionality). Thus, resource management should be done in both confirmed and unconfirmed modes for mobile and static applications to fulfill their requirements.

The primary objective of this dissertation is to study the LoRaWAN, the typical ADRs, highlight issues, and then suggest some distinctive approaches to improve the PSR, convergence period, and energy consumption of the static and mobile IoT applications.

## 1.4 Contributions of Dissertation

This dissertation contributes to the Internet of Things (IoT) field by utilizing a long-range wide area network (LoRaWAN) in static and mobile IoT applications. This dissertation targets the LoRaWAN, which is the Medium Access Control (MAC) layer. It is primarily responsible for the resource management of end device (ED) through ED- and NS-sides ADR. This dissertation presents reactive, proactive, and hybrid approaches for resource allocation to static and mobile IoT applications, as shown in Figure 1.1.

### 1.4.1 Reactive Resource Allocation

A reactive paradigm is based on responding to events after they have happened in the communication network (such as collision, interference, and channel variations). In the reactive paradigm category, Channel-Aware Spreading Factor Allocation (C-ASFA at ED-side), Gaussian- and Exponential Moving Average ADR

(G-ADR and EMA-ADR) are proposed to resolve the resource assignment issue. The C-ASFA increases/decreases the SF of ED by utilizing the channel information. While G- and EMA-ADRs are primarily designed to smooth the SNR of $M$ packets (i.e., $M = 20$ UL packets) for efficient SF and TP parameters. Results showed that these approaches have assigned resources to EDs efficiently and improved the network performance in terms of PSR and energy consumption.

### 1.4.2 Proactive Resource Allocation

A proactive approach focuses on eliminating problems before they have a chance to appear (e.g., interference, collision, and packets arriving under the required SF sensitivity due to channel variations). In this category, Mobility-Aware Spreading Factor Allocation (M-ASFA), Retransmission-Assisted Resource Management (R-ARM), and Artificial Intelligence-Empowered Resource Allocation (AI-ERA) are proposed to allocate resources to static and mobile EDs, respectively. Results showed that proactive approaches have assigned resources to EDs efficiently and improved the network performance in terms of PSR, convergence period, and energy consumption.

### 1.4.3 Hybrid Resource Allocation

A hybrid paradigm utilizes both reactive and proactive approaches at the same time. The hybrid ADR (HADR) first finds the ED status (e.g., static or mobile). For example, if an ED is determined as mobile, it will use BADR+, otherwise ADR. Simulation results showed enhanced PSR, convergence period, and energy consumption.

## 1.5 Organization of Dissertation

Chapter 2 presents an overview of LoRaWAN and background study. Chapter 3 presents the network model, definitions, assumptions, and performance indicators utilized in the dissertation, along with problem formulation. Chapter 4 elaborates on the proposed reactive resource allocation paradigm. Chapter 5 presents the proposed proactive resource allocation paradigm. Chapter 6 illustrates the proposed hybrid resource allocation paradigm. Chapter 7 provides detailed experimental results and analysis of the proposed paradigms in comparison with the typical ADRs and existing state-of-the-art approaches. Finally, Chapter 8 concludes this dissertation and suggests some future directions.

# Chapter 2
# LoRaWAN Overview and Background Study

The LoRa was started in 2009 by Nicolas Sornin and Olivier Seller to create a low-power, long-range modulation technology, targeting the metering industry by introducing long-range wireless communication capabilities to meters. They used CSS modulation technology to achieve long-range communication, primarily for sonar in the maritime and aviation radar industries. In May 2012, Semtech collaborated with Nicolas and Olivier to further develop the technology and finalize the hardware chips needed for the EDs (SX1272 and SX1276) and the gateways (SX1301). Simultaneously, developing a proprietary MAC protocol called "LoRaMAC" by defining message formats and security layers for an open networking protocol. As a result, the LoRa Alliance® was created in February 2015, and the networking protocol was called " Long-Range Wide Area Network (LoRaWAN)." The primary goal of LoRa Alliance was to help and encourage the global adoption of the LoRaWAN by ensuring that all LoRaWAN products and technologies are interoperable. A LoRaWAN is a long-range and low-power technology that focuses on multi-year battery life. Thus, LoRaWAN provides EDs with cheap costs and the best solution for the IoT.

The rest of this chapter is structured as follows: Section 2.1 elaborates on the LoRa. Section 2.2 describes the LoRaWAN. Section 2.3 highlights the typical ADR approaches of LoRaWAN for confirmed and unconfirmed modes both at ED and NS sides. Section 2.4 presents the background studies on the enhancement of the LoRaWAN performance, while last Section 2.5 presents some concluding remarks.

## 2.1 LoRa

LoRa [7] is a radio frequency (RF) modulation technology designed for LPWANs. LoRa defines the physical layer features for long-range communication.

### 2.1.1 LoRa Modulation

LoRa is a proprietary physical layer modulation based on the CSS modulation to achieve the long-range communication [12]. CSS is a subset of Direct-Sequence Spread Spectrum (DSSS), helping the GW to recover a weak signal and achieve high sensitivity, enabling increased coverage at a lower data rate (DR) [13, 14]. In CSS, data is distributed via chirps, which are sinusoidal sounds whose frequency rises linearly with time and span over the available bandwidth. CSS is based on the notion that a chirp signal, a sinusoidal signal with a set frequency and duration, may be used to “spread" information over a larger spectrum than it

Table 2.1: End device and gateway sensitivity thresholds for each SF with 125-kHz mode.

| Data rate | Spreading factor | $S_g$ [dBm] | $S_e$ [dBm] | SNR [dB] |
|---|---|---|---|---|
| 0 | 12 | -142.5 | -137.0 | -20 |
| 1 | 11 | -140.0 | -135.0 | -17.5 |
| 2 | 10 | -137.5 | -133.0 | -15 |
| 3 | 9 | -135.0 | -130.0 | -12.5 |
| 4 | 8 | -132.5 | -127.0 | -10 |
| 5 | 7 | -130.0 | -124.0 | -7.5 |

would otherwise need. Furthermore, CSS is resistant to multi-path interference and the Doppler effect than other more traditional modulation techniques if some additional measures are taken.

### 2.1.2 Spreading Factor

The number of bits encoded in a symbol by LoRa, which is an adjustable resource parameter known as the spreading factor (SF). For example, SF7 indicates that a chirp can be encoded in seven bits. This means that a chirp with the SF represents $2^{SF}$ bits using a symbol and that a chirp can have $K = 2^{SF}$ different starting frequencies. Duration of a symbol for any SF can be determined using (2.1.1).

$$T_s = \frac{2^{SF}}{B}, \tag{2.1.1}$$

where $T_s$ is the LoRa symbol time and $B$ is bandwidth in (2.1.1). The increase in SF doubles the $T_s$, increasing the energy consumption and making the signal more robust to noise and interference, reaching longer distances. However, SF also influences the DR: for the raw DR $R_b$ at physcial (PHY) layer is represented in (2.1.2)

$$R_b = SF \times \frac{B}{2^{SF}}. \tag{2.1.2}$$

On the other hand, when SF increases, DR decreases, resulting in increased coverage range and sensitivity. However, this further increases the chances of collision and interference [8]. In addition, the choice of SF affects the receiver sensitivity ($S$), as defined in (2.1.3) [15].

$$S = -174 + 10log10(B) + NF + SNR, \tag{2.1.3}$$

Furthermore, Table 2.1 presents the required sensitivities for each SF [16,17]. For both the EDs ($S_e$) and GW ($S_g$), the sensitivity decreases with an increasing SF. However, this also further increases the ToA.

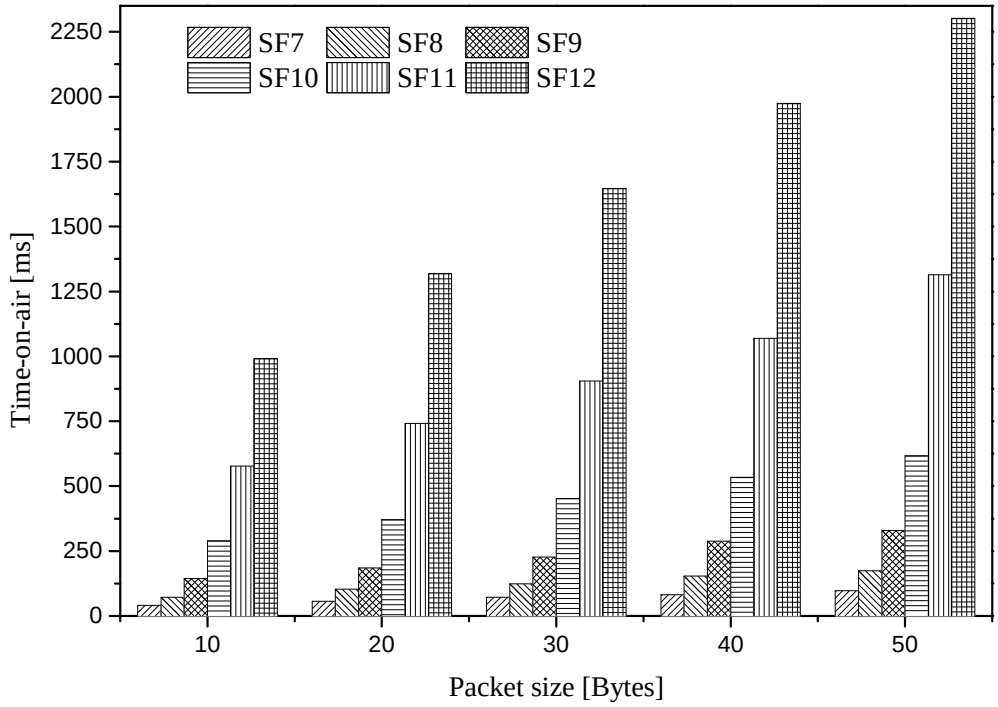


Figure 2.1: Time on air of each SF for different packet sizes.

### 2.1.3 Time-On-Air

ED in a LoRa network uses an SF to transmit payload to a GW. The choice of SF utilized by an ED during the communication plays a significant role owing to different reasons: a higher SF (e.g., 11, 12) comply with a high distance coverage. However, it indicates a low DR and high ToA. The ToA is computed using (2.1.4 [17]) and shown in Fig. 2.1. ToA increases with SF and packet size.

$$ToA = T_{preamble} + T_{payload}. \tag{2.1.4}$$

$$T_{preamble} = N_{preamble} + 4.25) \times T_s, \tag{2.1.5}$$

$$T_{payload} = N_{payload} \times T_s, \tag{2.1.6}$$

$$N_{payload} = 8 + max \times \left\lceil \frac{8PL - 4SF + 28 + 16CRC - 20IH}{4(SF - 2DE)} \right\rceil (CR + 4), 0. \tag{2.1.7}$$

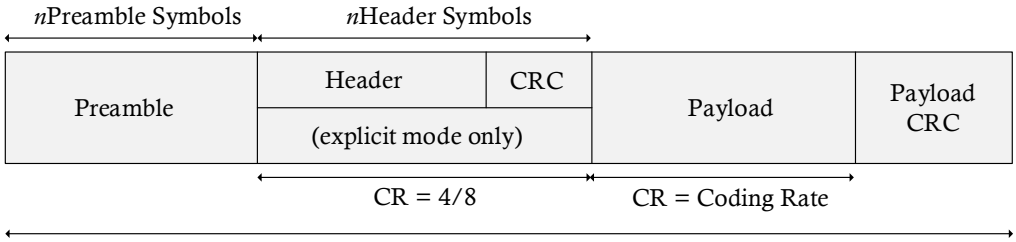


Figure 2.2: LoRa packet structure.

In (2.1.4), the $T_{preamble}$ is an interval to transmit the preamble bits, and $T_{payload}$ is a time to transmit a packet, as shown in the LoRa packet structure of Fig. 2.2. The $T_{preamble}$ is computed in (2.1.5), where $N_{preamble}$ is the payload size in symbols and $T_s$ is the time duration of a symbol. The $N_{payload}$ is determined by (2.1.7), where $PL$ is the size of a packet in Bytes, cyclic redundancy check (CRC) is equal to 1 when the CRC field is present, $IH$ represents the PHY layer header, which is 1 when enabled or 0 when disabled. Similarly, the $DE$ value is based on the DR optimization option, and it is either 0 or 1 if it is disabled or enabled, respectively. At the same time, $CR$ is the coding rate defined by $CR = 4$ and is set to 1.

## 2.2 LoRaWAN

LoRaWAN defines an open-source MAC layer protocol developed by the LoRa Alliance. As part of this protocol, a star-of-stars topology is formed that comprises a large number of EDs, GW, NS, and application servers, as shown in Fig. 2.3.

### 2.2.1 Types of End Devices in LoRaWAN

The EDs in LoRaWAN network are classified as *Class A*, *Class B*, and *Class C* [18]. *Class A* EDs are battery-powered and consume ultra-low energy. These EDs are bi-directional and receive ACK from NS with in two available receive windows (*RXs*). *Class B* EDs are also battery-powered and provide bi-directional communication. These devices support unicast and multicast transmission; though, it has more *RXs* as compared to *Class A* EDs. *Class B* EDs are synchronized with a beacon frame transmitted by the GW after a certain amount of time. Finally, *Class C* EDs use more power than to *Class A* and *B*. Besides, *Class C* EDs listen all the time, excluding transmission time. Among them, *Class A* EDs deal with sensors and are implemented in IoT applications, owing to their energy efficiency and bi-directional communications. The rest of the requirements

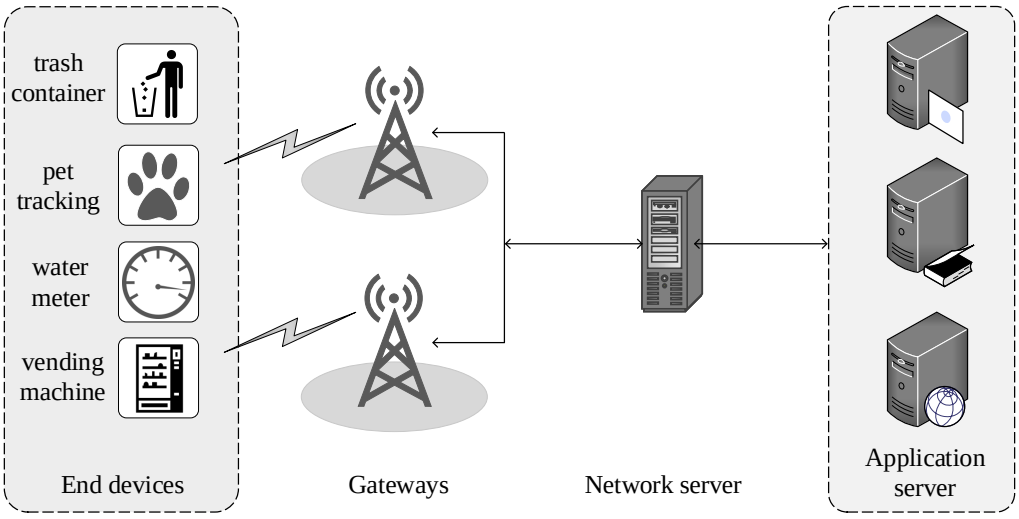


Figure 2.3: LoRaWAN network architecture.

Table 2.2: End device requirements under bi-directional communication mode.

| Class | Type | Transmission | *RXs* | Channel Access | Energy |
|---|---|---|---|---|---|
| A | Battery powered | Unicast | 2 | ALOHA | Energy efficient |
| B | Battery powered | Unicast and Multicast | More | Slotted with beacon | High |
| C | Main powered | Unicast and Multicast | Always open | Slotted with beacon | Highest |

of these ED classes are shown in Table 2.2. This dissertation utilizes *Class A* EDs throughout. Furthermore, LoRaWAN supports two communication modes: confirmed and unconfirmed.

### 2.2.2 Confirmed Mode

In the confirmed mode, after every UL packet transmission, the *Class A* ED requires an ACK from the NS, as highlighted in Figure. 2.4. *RX*1 commences operation after the end of the UL packet transmission, where *Receive_Delay* 1 ($RX_{d1}$) is typically 1 s long. The NS sends an ACK through the DL channel using the same SF and channel in RX1. In the absence of the ACK in RX1, ED opens RX2, which normally starts operating 2 s after the UL packet transmission ends. The NS transmits an ACK to the ED using SF12 in RX2 using the dedicated 869.525 MHz channel [10]. However, $RX_{d1}$ and $RX_{d2}$ of RX1 and RX2 are programmable, depending on the IoT application requirement [19]. When the ED does not receive the ACK in both RXs, retransmission is initiated after waiting for at least $RETRANSMIT\_TIMEOUT$ seconds (i.e., 2 s with a random delay between 1 and 3 s) [2].

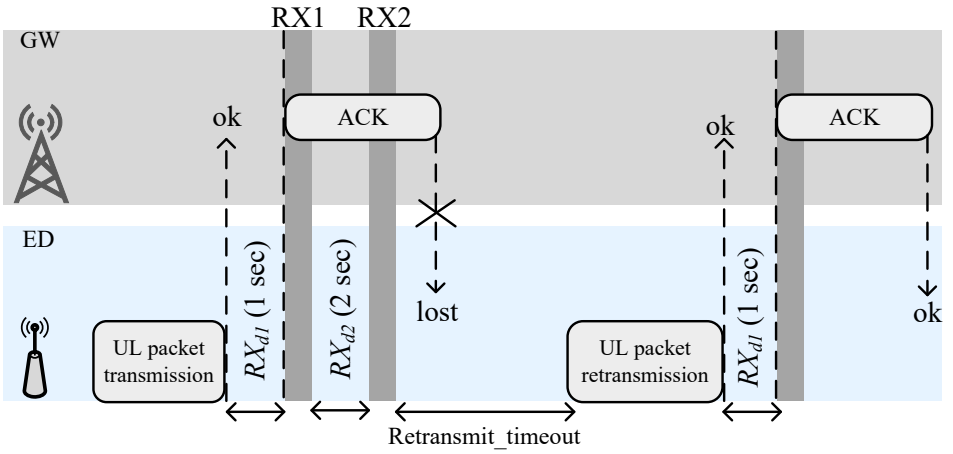


Figure 2.4: Confirmed mode: uplink packet and downlink acknowledgment operation of the LoRaWAN.

### 2.2.3 Unconfirmed Mode

A DL ACK from the NS to ED is not required in this mode. However, to determine the connectivity loss between the ED and GW, the ED enables ADR ACK bit by sending it in a MAC command *ADRACKReq* in the LoRa frame header (FHDR) after 64 (default) UL packets [2]. This instructs the NS to send an ACK, but not necessarily immediately. On the other hand, if *ADRACKReq* is not enabled during communication, the NS does not send any DL ACK notification. In both confirmed and unconfirmed modes, LoRaWAN utilizes an energy-efficient ADR for resource management (e.g., SF and TP) of the EDs involved in communication.

## 2.3 Adaptive Data Rates in LoRaWAN

LoRaWAN defines the ADR at the ED and NS. The ADR at the ED is specified by the LoRa Alliance [2], whereas the network operator defines the ADR at the NS. ADR at the ED side increments only SF, while ADR at the NS alters both the SF and TP. By managing both SF and TP, the ADR mechanism provides reliable energy-efficient communication and enhances the network capacity [10, 20, 21]. The ADRs in both confirmed and unconfirmed modes at the ED-side are slightly different, while the NS-side ADR is common for both modes.

**Algorithm 2.1:** ED-managed ADR in confirmed mode.

**Input :** SF = SF 7∼ SF 12, $\alpha = 2$, $Tx_{limit} = 8$, $TP = 14$ dBm
**Output:** SF and TP

```
At each uplink transmission
if (mType == CONFIRMED_DATA_UP) then
    ▷ it is a confirmed uplink transmission
  if (TX == True) then
      ▷ it is a new transmission
    continue transmission with current SF
  else
      ▷ it is a retransmission
    if (ReTx_CNT % α == 0) then
        ▷ if SF is < 12
      SF = SF + 1
      TP = 14
    else
      continue transmission with current SF
    end
  end
end
    ▷ it is unconfirmed uplink transmission
```

### 2.3.1 ED-Managed ADR in Confirmed Mode

In the confirmed mode of LoRaWAN, an ED can transmit a packet up to a maximum of 8 times. If the UL packet is a new transmission, it is transmitted to NS through GW by enabling the *ADRACKReq* bit in the FHDR. It indicates that the ED requires an ACK upon the reception of the UL packet from the ED. If ACK was failed in the $RX1$, the NS transmits the ACK again in the $RX2$ using a dedicated channel of 869.525 MHz and SF12. When ED fails to receive ACK in both $RXs$, ED initiates retransmission after $RETRASNMIT\_TIMEOUT$. A retransmission counter ($ReTx\_CNT$) is incremented in the next iteration. To this end, the Algorithm 2.1 at the ED side verifies if $ReTx\_CNT$ is a multiple of $\alpha$ ($\alpha$ = 2). If the condition holds, SF is increased by 1 to regain connectivity [22].

### 2.3.2 ED-Managed ADR in Unconfirmed Mode

The two parameters, $ADR\_ACK\_LIMIT$ and $ADR\_ACK\_DELAY$ with default values of 64 and 32, respectively, control the working of the ADR, as shown in

**Algorithm 2.2:** ED-managed ADR in unconfirmed mode.

**Input :** SF = 7 ∼ 12, *ADR_ACK_LIMIT* = 64, *ADR_ACK_DELAY* = 32, *ADR_ACK_CNT* = 0, *TP* = 14 dBm
**Output:** SF and TP

```
At each uplink packet transmission
if (mType == UNCONFIRMED_DATA_UP) then
    ADR_ACK_CNT += 1
    if (ADR_ACK_CNT == ADR_ACK_LIMIT) then
        ED enables ADRACKReq bit in the FHDR
        if (ADR_ACK_CNT ≥ ADR_ACK_LIMIT + ADR_ACK_DELAY) then
            SF = SF + 1
        end
        if (ACK == True) then
            reset ADR_ACK_CNT
        end
    end
end
                ▷ it is a confirmed uplink transmission
```

Algorithm 2.2 [23]. In addition, the *ADR_ACK_CNT* parameter increases by one for every UL packet that an ED transmits to the GW. If *ADR_ACK_CNT* reaches *ADR_ACK_LIMIT*, the ED enables *ADRACKReq* bit in all UL transmissions. This indicates that the ED requires a DL ACK confirmation message from the NS to verify its connectivity with the GW. If the ED detects that several successive UL packets (i.e., 64 + 32 = 96 UL packets) are not acknowledged from the NS, it assumes that the connectivity with GW is lost. Therefore, it starts incrementing the SF to improve the robustness of the link [24].

### 2.3.3 NS-managed ADR

On the other hand, an ED can request the NS to step in and monitor the quality of *M* UL recent past packets received (i.e., M=20) [25, 26]. If the link quality calculated over the last *M* packets is too high compared to the minimum receiver sensitivity threshold, the NS decides to reduce SF and reduce or increase TP. The NS-managed ADR takes the maximum SNR value among the last 20 UL packets received from an ED, as shown in Algorithm 2.3. However, when ED receives the ADR command containing new SF and TP from NS, the propagation situation might have changed so radically that the SF and the link budget, would

**Algorithm 2.3:** NS-managed ADR of LoRaWAN at NS-side.

**Input :** TP = 2∼14, SF = 7∼12, $M$, $SNR_{req}$, $device_{margin}$
**Output:** SF and TP
// computes
a. $SNR_m$ = Max(SNR of last $M$ UL packets) ▷ $M$=20 UL packets
b. $SNR_{req}$ = demodulation $floor$ (current DR/SF)
c. $device_{margin}$ = 10 ($LoRaWAN\ default$)
d. $SNR_{margin}$ = ($SNR_m$ - $SNR_{req}$ - $device_{margin}$)
e. $steps$ = $int$ ($SNR_{margin}$/3)
**while** ($steps > 0$ and $SF > SF_{min}$) **do**
    $SF = SF + 1$
    $steps = steps - 1$
**end**
**while** ($steps > 0$ and $TP > TP_{min}$) **do**
    $TP = TP - 2$
    $steps = steps - 1$
**end**
**while** ($steps < 0$ and $TP < TP_{max}$) **do**
    $TP = TP + 2$
    $steps = steps + 1$
**end**
NS transmits *LinkADRReq*

no longer be valid, resulting in massive packet loss and retransmissions.

The NS-managed ADR takes the maximum SNR ($SNR_m$) value among the $M$ UL packets and computes $SNR_{margin}$ using (2.3.1), where $SNR_{req}$ (DR) is the required SNR to successfully demodulate as a function of DR given in Table 2.1, and $margin_{dBm}$ is 10 dBm (default). Lastly, NS-managed ADR computes the $N_{step}$ using (2.3.2), where $int$ is the integer part, which can be negative or positive.

$$SNR_{margin} = SNR_m - SNR_{req}(DR) - margin_{dBm}, \tag{2.3.1}$$

$$N_{step} = int\left(\frac{SNR_{margin}}{3}\right). \tag{2.3.2}$$

In (2.3.2), $N_{step}$ represents the number of times the ADR is executed [20]. When $N_{step}$ is 0, the ED is already using the best possible configuration of SF and TP. If $N_{step}$ is greater than 0, it indicates that there is still a reasonable margin to optimize these two parameters. First, the SF is decreased until it reaches a

minimum limit. Second, the TP is decreased by 2 until it reaches a minimum limit (i.e., 2 dBm). Finally, when $N_{step}$ is negative, only the TP is increased by 2 until the maximum limit is reached (i.e., 14 dBm).

### 2.3.4 Blind Adaptive Data Rate

The BADR uses three SFs (i.e., 7, 10, and 12): SF 7 (three times), SF 10 (twice), and SF 12 (once) in 60 minutes, as shown in Fig. 2.5 [11]. However, BADR restricts the network capacity by utilizing only three SFs the entire time, which is inefficient in terms of ToA (in the case of SF 12).

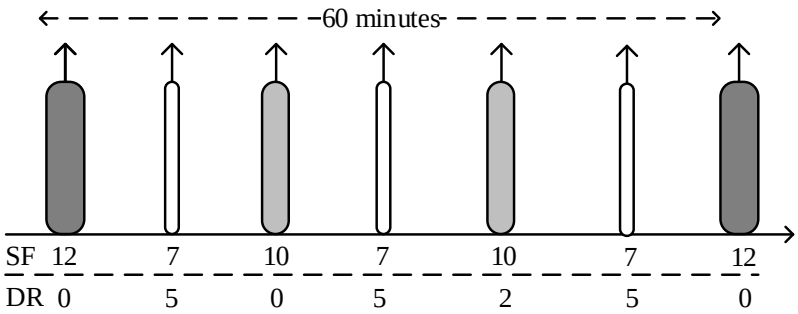


Figure 2.5: SF utilization of the blind ADR for mobile IoT applications.

## 2.4 Background Studies

This section briefly surveys the existing resource allocation solutions in the LoRaWAN network. These existing solutions are divided into five broad categories: interference-based, link- and system-based, mathematical model-based, improvements in typical ADR, improvements in convergence period, and AI-based approaches, as shown in Figure 2.6.

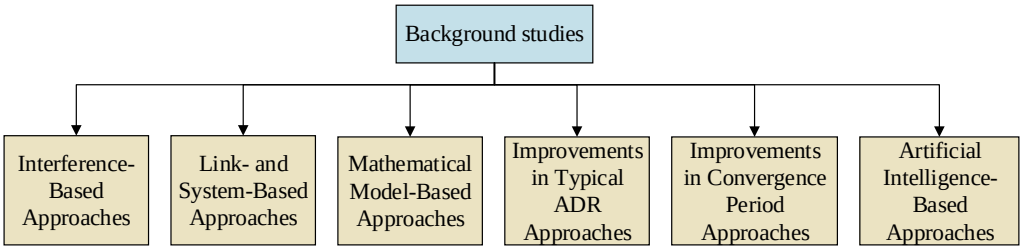


Figure 2.6: Categorization of the background studies.

### 2.4.1 Interference-Based Approaches

Another work based on collision types to manage the SF is presented in [27]. Two types of collisions are observed during communications: (a) Collision of two packets with the same SFs and (b) collision of two packets with different SFs. The primary aim of this collision-aware SF assignment method is to improve the PER by enhancing channel fairness. Firstly, this method categorizes the EDs to form groups based on the radio frequency (RF) coverage and path loss, wherein each group uses a distinct channel. Secondly, the lowest SF is selected and allocated to each group based on the observed cumulative interference ratio (CIR). The proposed scheme in [4] decreases the PER up to 42% overall.

An SF assignment mechanism for the LoRaWAN network introduced in [28] aims to improve the success ratio by reducing the interference caused by the same SFs and channels. To categorize the interference of two packets, [9] measures the signal-to-interference-plus-noise ratio (SINR) of packets transmitted with the same SFs over the same channels. If the measured SINR is larger than the threshold limit, the packets survive the interference in the simulation. Otherwise, the packets are lost to interference. However, [9] does not take into account the interferences between packets with different SFs over the same channel, as these SFs are not entirely orthogonal [29–33].

A similar scenario related to the impact of non-orthogonality concerning the data extraction rate is presented in [30]. The study in [30] reveals that the impact of non-orthogonality is limited when the traffic load in the network is low. The authors of [30] also show that higher SFs (e.g., 10, 11, 12) are more venerable to interference due to their high ToA.

It is also assumed in [16] that a collision occurs due to the simultaneous transmission of the packets over the same SF and channel. However, the analysis in [16] is limited to the case with an SF of 12 only. Furthermore, the effect of the non-orthogonality concerning SFs is further deliberated in [17], where it computes the probabilities of successful UL packet and coverage based on [30]. The study in [34] shows that UL packets transmitted with different SFs can collide as long as their received power at GW is different. It also reveals that the impact of inter-SF interference can be high enough in a significantly large network. However, in a short distance (i.e., less than 1 km), the effect of inter-SF interference is less.

Additionally, the scalability of LoRaWAN under the impact of interference in the absence of DL traffic was studied in [35]. The testbed and simulation results concluded that one of the two packets could be received if the headers of both packets did not collide. In contrast to previous works, [19] considers inter- and intra-SF interferences. The authors in [36] aimed to maximize the LoRaWAN network capacity by optimizing the number of EDs for a given SF. The numer-

ical results showed that the proposed method in [36] maximizes the LoRaWAN network capacity up to 700%, as compared to the equal number of EDs per SF strategies.

### 2.4.2 Link- and System-Based Approaches

The capacity of an LoRaWAN in terms of the maximum number of EDs that can communicate in a single and multi-cell scenario is analyzed in [37] under realistic traffic conditions in the simulation and the testbed. It is certain that increasing the network capacity in terms of the offered traffic in all the use cases can provide a satisfactory PSR. Furthermore, [37] shows that the PSR increases with the number of GWs. In the unconfirmed mode, the traffic load has a low affect on the SR, as the geometric coverage plays a significant part, resulting in an SR of 55% or 93% depending on the number of GWs. Furthermore, in [37], the intra-SF interference is limited to SF values of 7, 9, and 12.

The reliability and scalability of the LoRa (RS-LoRa) scheme aims to enhance the reliability and scalability of a LoRaWAN under an ideal network situation [38]. RS-LoRa works in two phases: In the first phase, GW groups the EDs within its coverage by obtaining the received signal strength indicator (RSSI) and SF on each channel. EDs get their SFs, transmit power, and a channel based on the RSSI in the second phase. This grouping based on the RSSI decreases collision by choosing a suitable SF and enhancing the network reliability, scalability, and capture effect. Another work presents a system-level simulation with heterogeneous traffic in [39]. The primary purpose of the work in [39] is to enhance the SR by allocating possibly the lowest SFs based on the SNR of the ED packet. Hence, the scheme in [39] decreases the ToA for each ED and reduces the probabilities of collision by suitable SF allocation. A similar approach called an adaptive spreading factor selection (ASFS) algorithm aims to allocate SFs to EDs in the presence of channel activity detection to improve the throughput of a single, and multi-hop LoRaWAN network [40]. The performance of the proposed SF allocation algorithm shows improved throughput in comparison with SX1272 and SX1301 chips.

On the other hand, EXplora-TS considers the heterogeneous traffic load, where EDs having a higher payload sizer are served based on priority. The performance of these two approaches has been compared to EXplora-AT, where results show a 21% increase. Furthermore, the authors in [41] further improved the performance of EXplora-AT and EXploRa-SF by considering the capture effect. EXplora-Capture (EXplora-C) in [41] equalizes the ToA of UL packets, keeping the balance regarding SF allocation in a single and multi-GW environment, and takes the capture effect into account. The performance of the EXplora-C approach has been compared to EXplora-AT and EXploRa-SF, where EXplora-C shows im-

proved results in terms of the data extraction rate. In particular, EXplora-C shows enhanced results of up to 38% on average over the legacy ADR mechanism.

EXPLoRa-SF assigns SFs to EDs based on the received signal strength indicator (RSSI), where the EDs should be above the minimum required sensitivity of each SF [42]. At the same time, EXPLoRa-AT guarantees ToA equalization for all EDs in the entire network in addition to EXPLoRa-SF by equally balancing the offered traffic [42]. Furthermore, EXPLoRa K-means (EXPLoRa-KM) in [43] locates congested areas with a high collision, increasing the SF to mitigate collision impact. Meanwhile, EXPLoRa-time symbol (EXPLoRa-TS) in [43] considers the diverse traffic load, prioritizing EDs with larger payload sizes. Finally, EXPLoRa-capture (EXPLoRa-C) [41] applies the load balancing and diversity requirements in terms of "sequential waterfilling" to improve the overall system capacity. [41–43] were evaluated through simulations using LoRaSim[1] and showed improved performance compared to the typical ADR.

To improve the power efficiency of ADR, a proposed ADR is presented in [44]. Firstly, it takes the average of the SNRs of M UL packets (i.e., M=20). Secondly, it takes the standard deviation of the SNRs of M UL packets. The performance of the proposed ADR shows better performance than ADR in terms of power efficiency. However, the proposed work in [28] completely ignores the slow convergence time of the ADR, which is affected by variable channel conditions [20, 24].

### 2.4.3 Mathematical Model-Based Approaches

Some mathematical models for LoRaWAN have been developed in the literature [33–37]. The authors in [45] aimed to analyze and evaluate the LoRaWAN channel access operation in terms of the PER and packet loss ratio (PLR) in a confirmed mode. The results in [45] reveal that PER and PLR increase with an increasing load in the network. The authors in [46] further enhanced the work presented in [45] by proposing a mathematical model based on retransmissions. The proposed model accurately estimates the PER based on the offered traffic. The proposed method was verified through simulation by finding the distribution of data rates probabilities. The simulation results show that the model accuracy is significantly improved by considering the retransmissions.

Furthermore, the model presented in [46] was enhanced by proposing MCS allocation to satisfy the different Quality of Service requirements of IoT applications. However, the reception paths at the GW and duty cycle limitations both at EDs and GW were neglected. To take into the reception paths and duty cycle

[1] https://www.lancaster.ac.uk/scc/sites/lora/lorasim.html
A discrete-event simulator based on SimPy for analyzing scalability and collisions in LoRa networks.

limitations, the authors proposed a mathematical model in [47]. The performance evaluation of the proposed model shows an improved packet success ratio when compared with [46].

### 2.4.4 Improvements in Typical ADR Approaches

In [48], an approach to avoiding unnecessary changes to the SF that occur at the NS-managed ADR is presented. Their method offers a congestion classifier, which determines whether to switch to a higher SF or adjust the backoff time to avoid massive congestion. The congestion classifier is based on the number of UL and DL packets. No congestion is shown if the number of DL packets received by the ED is equal to the number of UL packets. Otherwise, the SF is reduced because a higher SF is vulnerable to interference owing to a high time-on-air. When an ED fails to receive an ACK after *ADR_ACK_DELAY*, it chooses a long backoff time. By contrast, it increases the SF to extend the network scalability and coverage. The authors showed that their method reduces the delay because the ED maintains the SF and increases the backoff time when congestion occurs.

To improve the ADR performance, an ADR+ scheme was proposed in [21]. The ADR+ scheme slightly modifies the NS-managed ADR by taking the average SNR of the last $M$ packets received. Thus, the ADR+ plays a vital role in increasing the consistency and energy efficiency of EDs under variable channel conditions. ADR+ shows an improved performance in terms of the PSR and energy consumption when compared to a typical ADR.

In [49], the authors suggest another enhanced ADR with coding rate adaptation in the LoRaWAN under the unconfirmed mode of LoRaWAN. The primary aim is to improve the tradeoff between the PSR and energy consumption, which considers the coding rate and the capture effect, by taking the average of $M$ packets to fine-tune the link performance of the EDs. The method described in [49] outperforms a typical ADR in energy consumption and fairness.

### 2.4.5 Improvements in Convergence Period Approaches

A performance assessment of the convergence period under different configurable parameters was conducted in [20]. This study provides in-depth insight into the runtime performance of the ADR under variable channel conditions and additional network requirements by aiming to highlight limitations such as the convergence period. The simulation results showed that the ADR convergence period and energy consumption are primarily dependent on the link conditions and number of EDs. It was revealed that the ADR suffers from a high convergence period when the link quality degrades, and the EDs change their SF or TP to a higher value (such as SF = 12 and TP = 14 dBm) to recover their

connectivity with the GW. Furthermore, the convergence period is more sensitive to *ADR_ACK_DELAY* than to *ADR_ACK_LIMIT* (i.e., *ADR_ACK_DELAY* and *ADR_ACK_LIMIT* are equal to 32 and 64 UL packets in the ED-managed ADR, respectively). Their simulation results also revealed that the slow convergence rate of the ADR introduces a higher energy consumption and greater packet losses.

It was recently indicated that typical ADRs (ED- and NS-managed) suffer from convergence issues [50]. An ED-managed ADR is inefficient for lossy links, resulting in considerable time to converge to a constant and stable state. Meanwhile, the NS-managed ADR takes $M$ packets to alter the SF and TP, making it too time-consuming to determine a reliable configuration. Therefore, [50] suggests some changes (such as decreasing $M$ packets during SF and TP configuration adaptation) in both ED- and NS-managed ADRs for enhancement. NS-managed ADR controls the ED-managed ADR by computing the PSR of an individual ED before sending the DL packet (*LinkADRReq*) in response to *ADRACKReq*. Here, the PSR is compared to a predefined threshold (i.e., PSR<80%). NS sends the *LinkADRReq* MAC layer command for the ED containing the SF and TP if the condition holds. Indeed, it changes the SF and TP of the individual ED after five UL packets (in a typical ADR, this UL history is set to $M$ packets). The performance of both enhanced methods (ED- and NS-managed ADRs) has been compared to typical ADRs, where the results show improved outcomes in terms of the convergence period, energy consumption, and PSR. However, the performance evaluation of the enhanced methods is limited to static EDs and only a confirmed mode of communication. By contrast, mobility under intra-SF interference and different propagation loss models (such as log-distance and shadowing losses) are considered.

Similarly, [51] proposed two ADRs (at the NS side) using Gaussian and exponential moving average filters to improve the convergence period, energy consumption, and PSR of the ADR. The proposed methods were validated using a testbed and evaluated using ns-3 [52]. Further the work in [51] was extended in [53, 54]. [53] proposed two ADRs, namely, Linear Regression-ADR (LR-ADR) and Linear Regression +ADR (LR+ADR) at NS and ED sides, respectively. The proposed schemes were compared to G-ADR. The simulation results showed improved PSR.

Furthermore, [54] proposed Resource Management Adaptive Data Rate (RM-ADR) based on the number of remaining UL transmissions, transmitted to the NS in FHDR. In the RM-ADR, the NS is responsible for finding suitable SF and TP configurations. The RM-ADR was compared to the typical ADR and G-ADR. Their proposed method showed improved performance in PSR and convergence period.

### 2.4.6 Artificial Intelligence-Based Approaches

The scalability issue in LoRaWAN was studied for a health monitoring system using human activity recognition [55]. The accelerometer data were collected with labels and utilized by supervised machine learning approaches such as Linear Discriminant Analysis (LDA), Random Forest (RF), and K-Nearest Neighbor (KNN) for classification. In addition, the authors considered a cross-validation method while computing the feature vectors. As a result, the authors in [55] claimed an activity recognition accuracy of 94.44% by LDA, 84.72% by RF, and 98.61% by KNN.

Authors in [56] proposed a load balancing (for the downlink traffic) method by utilizing unsupervised, supervised, and Markov Decision Process (MDP) machine learning techniques. Their proposed methodology comprised of four primary stages, including pre-processing (i.e., cleaning of the data using min-max scaling method), pattern analysis (such as principal component analysis for data visualization and feature selection), classification (classifier selection), and decision-making model. Through simulation results with 5000 EDs in a multi-cell environment, the authors in [56] achieved 50% and 20% improved PSR and energy consumption, respectively.

The collision problem was resolved by employing a decision tree classifier (DTC) and support vector machine (SVM) to predict accurate SF for the subsequent transmission in an unconfirmed mode of LoRaWAN [57]. First, the dataset was generated using a random SF assignment approach, where the packets were classified as interfered, successful, and under sensitivity. Then, after the DTC and SVM classifiers training, simulation was executed to predict the optimal SF. When the trained model classified a packet as interfered, it increased the SF, while no changes were suggested when a packet was classified as successful. Lastly, when the trained model classified a packet as unsuccessful at the GW, the SF was decreased.

Predicting the LoRaWAN behavior using machine learning was presented in [58]. Their proposed work was divided into two parts: unsupervised learning and prediction. Unsupervised learning was utilized for profiling EDs (i.e., clustering) through a well-known "K-Means" method. To perform profiling of the EDs, authors in [58] considered two GWs within the range of the transmitting EDs. Their profiling method aimed to group the EDs with similar transmission characteristics (e.g., the same SF and same packet size, etc.). The DTC and LSTM models were used to predict traffic patterns and showed improved performance. However, the unsupervised clustering technique (i.e., K-Means) although is desirable for classification in IoT due to its simplicity. However, it would be hard to implement concerning the number of clusters required in such a dynamic environment of the LoRaWAN. Hence, the optimal cluster selection and accuracy

analysis are highly application-specific in the grouping process using K-Means.

Paper [59] proposed a regression approach to predict the collision using extended Kalman filter-based (EKF) LSTM. The authors used the LSTM-EKF model as the backbone based on a pre-trained conventional LSTM model. The primary aim was to predict the future collision, where the LSTM-EKF model was compared to the offline traditional LSTM model. The dataset was generated using the LoRaSim simulator [60]. Results showed that LSTM-EKF produced better results in terms of future collision prediction when compared to conventional LSTM. However, no proactive solution was proposed to alleviate the collision by allocating a suitable DR to EDs.

## 2.5 Summary

This chapter presented the difference between LoRa and LoRaWAN and the ADR approaches in both confirmed and unconfirmed modes. Furthermore, existing approaches related to the resource assignment and enhancement to the typical ADR approaches were presented in this chapter. Many of the existing solutions are based on traditional approaches. However, recently, researchers have been moving to solve the resource allocation issue in the LoRaWAN by using AI methods. As a result, the existing AI solutions show improved performance compared to the traditional approaches.

# Chapter 3
# Network Model and Problem Formulation

Many factors affect the performance of LoRaWAN, depending on the scenario and underlying propagation environment. This chapter considers some assumptions and simplifications to acquire a reasonable model, leading to computationally feasible simulations.

This chapter is organized as follows: Section 3.1 presents the assumptions and constraints considered in the network model deployed in the network simulator (ns-3). Section 3.2 highlights the key performance indicators utilized throughout this dissertation for performance measurement of the proposed paradigms. Section 3.3 presents the network model. Section 3.4 highlights the issues with ADR and BADR of LoRaWAN in static and mobility scenarios, while last Section 3.5 presents some concluding remarks.

## 3.1 Assumptions and Constraints

In this section, some important constraints of the LoRaWAN considered in the dissertation are highlighted.

### 3.1.1 Class *A* End Devices

This dissertation considers *Class A* EDs, where these EDs randomly choose UL channels using the ALOHA channel access method. *Class A* EDs deal with sensors and are primarily designed for LPWAN and IoT applications due to their ultra-low energy consumption and bi-directional communication. EDs in *Class A*, transmits UL packet to GW using six SFs $\in$ [7, 8, 9, 10, 11, 12].

### 3.1.2 Frequency Region

The EDs follow the European frequency region (i.e., EU-868 MHz) with three mandatory channels, that is, 868.1, 868.3, 868.5 in MHz. The reception paths at GW for the three mandatory channels are shown in Table 3.1 [61]. Furthermore, these reception paths are aligned according to the *SX*1301 datasheet to demodulate eight packets [16] concurrently.

### 3.1.3 Duty Cycle Constraints

The duty cycle (DC) is defined as the ratio of time an ED device is "ON" over one hour, represented as a percentage. These restrictions apply to all EDs involved in communication, except those with listen before talk (LBT) capability. Table 3.2

Table 3.1: Reception paths distribution over the three mandatory channels in the EU region at GW.

| Channel | Frequency [MHz] | Distribution of receive paths |
|---|---|---|
| 1 | 868.1 | 3 |
| 2 | 868.3 | 3 |
| 3 | 868.5 | 2 |

shows how a DC limitation adheres to a maximum ToA and a minimum allowable delay time between subsequent packet transmissions.

Table 3.2: Duty cycle constraints.

| Duty cycle | Max ON time per hour | Max ON time | Min OFF time |
|---|---|---|---|
| $\leq 1.0\%$ | 36 seconds | 3.6 seconds | 1.8 seconds |
| $\leq 10\%$ | 360 seconds | 36 seconds | 3.6 seconds |

## 3.2 Key Performance Indicators Utilized in Dissertation

This section presents key performance indicators, including packet success and loss ratios (PSR and PLRs), convergence period, and energy consumption.

### 3.2.1 Uplink Packet Outcomes

The transmission of the UL packet can succeed or fail during communication for a variety of reasons, which are explained below.

1. **PSR**: When the NS gets the UL packet (within the $Tx_{limit}$ = 8 available transmission attempts). During PSR calculation, this study does not count retransmitted packets as new packets.

2. **PLR-I (I**nterference): It is calculated when multiple packets with the same or different SFs (i.e., Inter- and intra-SF interferences [18, 27]) occur with one another with no external interference from other technologies (e.g., IEEE 802.15.4, Wi-Fi, cellular etc.) is assumed, as described in [18, 61].

3. **PLR-R (R**eception paths): When the reception paths employed at the GW are busy in receiving incoming UL packets from the ED.

4. **PLR-S (S**ensitivity): It is measured when an UL packet arrives at the GW under the required sensitivity threshold (thresholds values at GW ($S_g$) and ED ($S_e$) are mentioned in Table 2.1 for each SF).

5. **PLR-T (T**ransmission priority): PLR-T occurs when an ongoing reception of UL packet or incoming UL packet arriving at the GW is interrupted by an ACK transmission [62].

#### 3.2.2 Convergence period

Time required by the ED to realize a stable SF and PSR. The convergence period is primarily dependent on the initial SF (which is set to 12 in the ADR), number of EDs, and interval of the UL packet [20, 50, 51].

#### 3.2.3 Energy consumption

Energy consumed by the EDs divided by the total number of successful receptions (in the confirmed mode, a packet is termed successful when it receives a corresponding ACK from the NS [63]).

### 3.3 Network Model

The network model utizilized in this dissertation is comprised of channel and its performance models.

#### 3.3.1 Channel Model

The channel model is comprised of link measurement, log-distance propagation loss, building penetration loss, and correlated shadowing loss models.

##### 3.3.1.1 Link measurement model

The link measurement model is mainly based on [61]. It considers the impact of propagation on signal strength, small-scale fading and similar influences. To estimate the received power ($P_{rx}$) at the GW is given by

$$P_{rx} = \frac{P_{tx} \times G_{ED} \times G_{GW}}{L} e^{\xi}, \tag{3.3.1}$$

where $G_{ED}$ and $G_{GW}$ represent the ED and GW antenna gains, respectively, and $P_{rx}$ is the transmit power, $L$ is the path loss, $e^{\xi}$ is the log-normal shadowing component, i.e., $\xi \sim \mathrm{N}(0, \sigma^2)$, where $\mu$=0 which is the mean captured in the $L$, and $\alpha$ represents the depth of shadowing, which is the logarithm standard deviation. Its value is dependent on the condition, i.e., $4 < \alpha < 12$. It shows that the signal strength varies owing to the objects hindering the propagation path between the ED and GW.

Furthermore, $e^{\xi}$ is a factor modeling the shadowing via a lognormal random variable (or log-distance path loss) with $\xi \sim N(0, \sigma^2)$. Writing (3.3.1) in the logarithmic domain, with $10\xi log_{10}e = 4.34\xi$ , it yeilds

$$P_{rx} = P_{tx} + G_{ED} + G_{GW} - L + 4.34\xi. \tag{3.3.2}$$

The path loss $L$ in $dB$ is the combination of both propagation loss ($L_{prl}$) and building penetration loss ($L_{bpl}$). $L_{prl}$ depends on the distance between ED and GW, while $L_{bpl}$ represents attenuation due to building walls, this yield

$$L = L_{prl} + L_{bpl}, \tag{3.3.3}$$

In (3.3.3), $L$, $L_{prl}$, and $L_{bpl}$ are computed in $dB$, respectively.

#### 3.3.1.2 Log-distance path loss model

The log-distance path loss model is presented in (3.3.4).

$$L_{prl(LOG)} = 40 \times (1 - 4 \times 10^{-3} h) log_{10}(R) - 18 log_{10} h + 21 log_{10}(f) + 80, \tag{3.3.4}$$

where $d$ in $km$ is the distance; $h$ is the height of antenna in $m$ mounted at GW, and $f$ represents the frequency measured in $MHz$. As an example, for frequency 868 MHz and a GW antenna of 15 m height, the $L_{prl}$ is computed using (3.3.5)

$$L_{prl(LOG)} = 120.5 + 10 \times 3.76 log_{10} R. \tag{3.3.5}$$

Moreover, the path loss exponent ($\alpha$) is another model parameter affecting system performance. Typically, $\alpha$ is known; however, mostly, that is not the case. In this dissertation, the value of $\alpha$ = 3.76 is computed concerning 15 $m$ of the antenna height, as shown in (3.3.6)

$$L_{prl(LOG)} = 120.5 + 10 \times 3.76 log_{10} R + LogF. \tag{3.3.6}$$

#### 3.3.1.3 Building penetration loss model

A building penetration loss model based on COST 231 "non-line-of-sight" (NLOS) is presented in (3.3.7).

$$L_{bpl(LOG)} = L_{ew} + max(L_{in,LOS}, L_{in,NLOS}) - G_{fh}, \tag{3.3.7}$$

where $L_{ew}$ is the external wall penetration loss caused by the external walls of the buildings. $L_{in,LOS}$ and $L_{(in,NLOS)}$ are computed using equations (3.3.8) and (3.3.9), respectively.

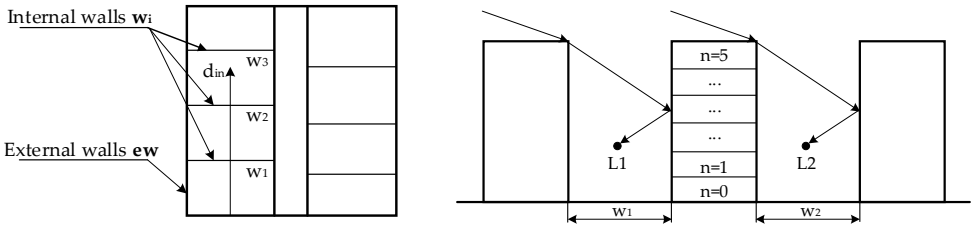


Figure 3.1: Building penetration: **(a)** top view of the building and model parameters for the LOS, and **(b)** side view of the building for NLOS.

$$L_{in,LOS} = l_{wi} \times k_w, \tag{3.3.8}$$

$$L_{(in,NLOS)} = D \times d_{in}, \tag{3.3.9}$$

In (3.3.8), $l_{wi}$ represents the loss of signal strength in the $i^{th}$ internal wall that is uniformly distributed between 4 and 10 dB (depending on the wall materials); and $k_w$ is the number of internal walls separating the ED from the GW. For $k_w = 3$, 15% of the EDs are assumed, while the rest of the EDs are equally distributed among [0,1,2]. In (3.3.9), $D$ is the penetration distance coefficient (i.e., 0.6 dB/m); and $d_{in}$ is uniformly distributed between [0,15] m range. $G_{fh}$ is the floor gain, presented by (3.3.10) and (3.3.11), and shown in Figure 3.1.

$$G_{fh} = n \times G_n, \tag{3.3.10}$$

$$G_{fh} = n \times G_h, \tag{3.3.11}$$

where $G_n$ is the gain of floor height (with an attenuation of 1.5 to 2 dB/floor and applicable to 6 m); $G_h$ is the height gain (with an attenuation of 1.1 to 1.6 dB/m) and suitable for 4–5 m), and $n$ is the number of the floor. This study takes into account (3.3.10) case because (3.3.11) is only appropriate at a frequency of 1800 MHz.

#### 3.3.1.4 Correlated shadowing model

The correlated shadowing generation model is mainly based on the decaying exponential of distance (i.e., distance-only model) [61].

$$P_{rx(i,j)}(d_{i,j}) = e^{-(\frac{d_{i,j}}{d_0})}, \tag{3.3.12}$$

where $P_{rx(i,j)}$ is the measured received power at $ED_j$ transmitted by $ED_i$, $d_{(i,j)}$ is the distance among two EDs (shadowing correlation), $d_0$ is a decorrelation distance parameter, which is tunable and always greater than zero ($d_0$ is set to 110 m [64]). The shadowing values of EDs which are not closely positioned on a vertex of the grid are interpolated using the exponential covariance function (covariance is set to 6 dB [62]). Also, correlated shadowing in wireless communication is divided into two types, and its implementation details are described in [61]:

1. When an ED transmits a packet to a GW, it is anticipated that the shadowing experienced by the GW is correlated with shadowing disturbing any other ED, which is "near" to it. This phenomenon is the $d_{(i,j)}$ and demonstrated with an exponential function.

2. If two EDs transmit and are near to each other, the shadowing values are expected to be correlated at the GW. This consequence is the site-to-site cross-correlation.

This model captures the first case adequately, and to express the fact that a GW "sees" two correlated shadowing values from adjacent EDs, the same shadowing map for every likely point in the grid is used. It is because nearby links are frequently affected by similar shadowers; link losses can be correlated.

### 3.3.2 Channel Performance Model

The link performance model includes receiver (i.e., GW) sensitivity and interference models.

#### 3.3.2.1 Receiver sensitivity

Table 2.1 shows the required SF threshold sensitivities [16, 17]. For both the EDs and GW, the sensitivity decreases with an increasing SF. An ED can detect a packet if the $P_{rx}$ is above the sensitivity level. In this dissertation, it is assumed that the $P_{rx}$ of a packet is constant during the whole experimental period. If the power is sufficient to start the decoding process, a packet is assumed to be decodable till the end of the reception. Lastly, it is assumed that if two weak signals from the EDs arrive concurrently at the GW, they cannot be perceived as decodable even if the sum of their powers is above the sensitivity; this is because the signals interfere.

#### 3.3.2.2 Interference model

In this dissertation, both Intra- and Inter-SF interferences caused due to the collision of multiple packets with the same and different SF over the same channel are presented. Furthermore, in this dissertation, external interference from other wireless technologies is not considered. Based on these assumptions, the study of interference focuses on how transmissions performed by different EDs, at different transmit power, and various SFs impact each other. To continue with interference among Intra- and Inter-SF interferences, a Signal to Interference Ratio (SIR) threshold matrix in [13] is shown in (3.3.13):

$$\beta_{(i,j)} = \begin{bmatrix} 6 & -16 & -18 & -19 & -19 & -19 \\ -24 & 6 & -20 & -22 & -22 & -22 \\ -27 & -27 & 6 & -23 & -25 & -25 \\ -30 & -30 & -30 & 6 & -26 & -28 \\ -33 & -33 & -33 & -33 & 6 & -29 \\ -36 & -36 & -36 & -36 & -36 & 6 \end{bmatrix} \tag{3.3.13}$$

The elements in $\beta_{i,j}$ represent the SIR margin (in dB), when a packet $x$ transmitted with $SF_{(i)} = 10$, and another packet $y$ transmitted with $SF_{(j)} = 10$ can be correctly decoded when the SIR is greater than $\beta_{i,j}$, as shown in Figure 3.2. The SIR is computed in (3.3.14)

$$SIR_{(x,y)} = \frac{P_{rc,0}}{\sum_{k \in ly} P_{rc,k}}, \tag{3.3.14}$$

where in (3.3.14), $P_{rc,0}$ is a packet under observation, which is received at the GW with sufficient power, $k$ is the interfering packet and $ly$ are the list of interfering packets.

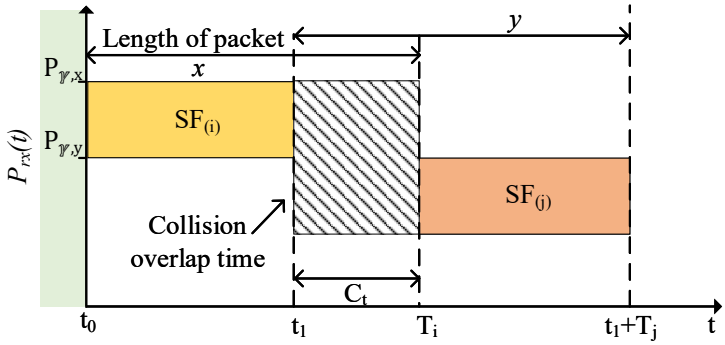


Figure 3.2: Overlap time ($C_t$) of the two packets arriving at the GW (as an example with same SF = 10).

Packet under observation ($P_{rc,0}$) is received correctly if the SIR is larger than the threshold $\beta_{(i,j)}$. In contrast, a packet can be considered lost.

## 3.4 Problem Formulation

Resource management of LoRa-enabled devices deployed on a large scale is challenging due to the underlying propagation conditions. LoRaWAN supports an energy-efficient ADR mechanism to manage the static device resources (i.e., SF and TP). Semtech recommends using BADR for mobile applications, such as pet-tracking. However, due to the sudden changes in the propagation environment, both ADRs cannot provide any appropriate measures to predict and consider evasive measures to alleviate the massive packet loss that is caused due to the inefficient SF adapted by the devices. Issues in both ADRs are illustrated in the rest of this section.

### 3.4.1 Single mobile ED

Fig. 3.3 shows the trajectory of a mobile ED, received power, and distance from the GW with a UL interval of 6 packets/h as suggested by the BADR for a pet-tracking application [11]. Successful packet reception is mainly based on the GW sensitivity corresponding to each SF. A packet that arrives with sufficient power and exceeds the required sensitivity of each SF can be successfully decoded and received. These required SF sensitivities are highlighted in Table 2.1, where $S_g$ and $S_e$ denote the sensitivities defined for each SF at the GW and ED, respectively.

In Fig. 3.3, the received power for every UL packet is shown in a circle. Fig. 3.3 (a) shows that 36 packets are transmitted toward the GW, and 29 packets are received (PSR of 80%). The circles with red crosses denote PLR-S at the GW with an SF of 7 and 10 when arriving under the required SF sensitivity (the total packet loss recorded was 7). Simultaneously, Fig. 3.3 (b) shows a similar trajectory for a mobile ED employing the ADR. In Fig. 3.3 (b), a circle represented with a red cross shows a single packet loss recorded with an SF of 8 (the receiver sensitivity for an SF of 8 is -132.5 dBm; however, the packet arrived with an insufficient power of –134.5 dBm).

The primary aim when considering BADR is to lower the energy consumption, which is realized as shown in Fig. 3.4. It is clear that the energy consumption of a mobile ED employing the ADR and an SF of 12 with respective rates of 48.64% and 69.51% is higher than that in the case of the BADR. This is because the energy consumption in LoRa is mainly dependent on the SF, TP, ToA, and retransmissions [65, 66].

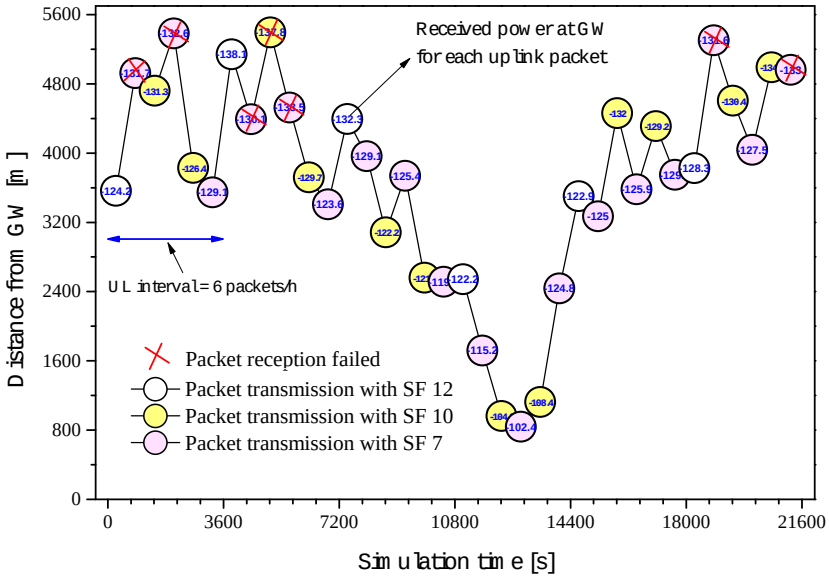


(a) BADR

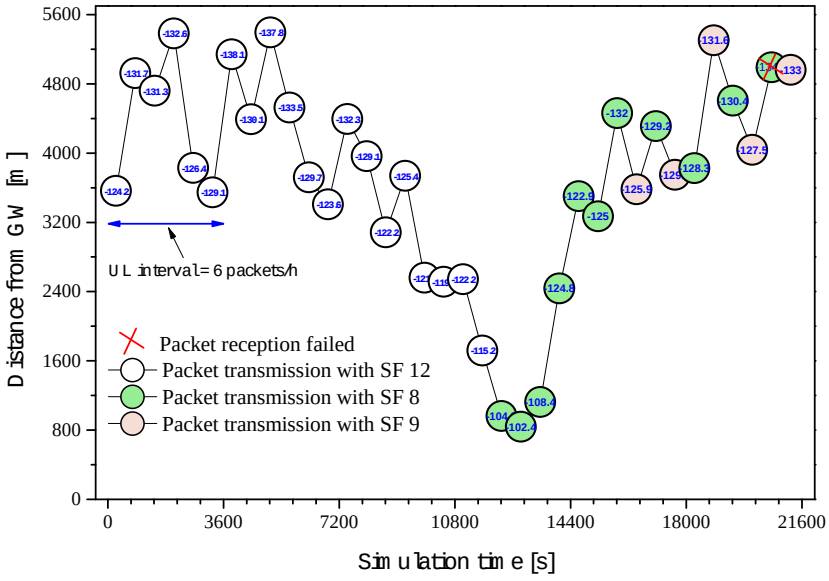


(b) ADR (NS side)

Figure 3.3: Trajectory and received power at the GW of a single mobile ED during 6 h of simulation time.

### 3.4.2 Massive mobile EDs

The performance evaluation for the BADR under massive ED ($N$) conditions is presented in Fig. 3.5. As shown in Fig. 3.5 (a), the BADR underwent PLR-S

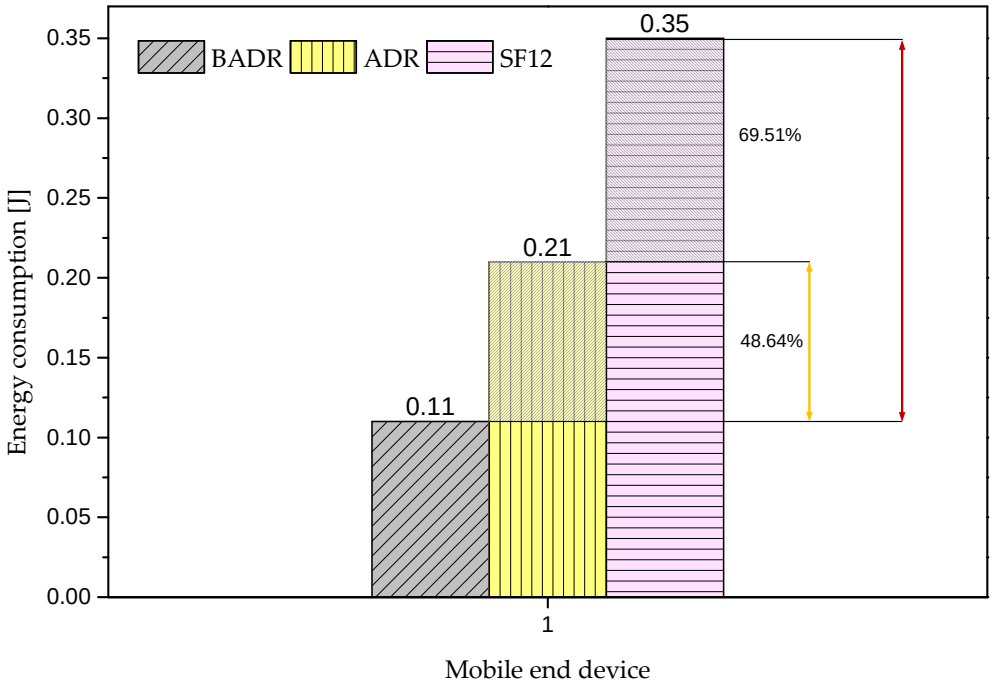


Figure 3.4: Energy consumption measured at a single mobile ED during 6 h of simulation time.

because the packets arrived with insufficient power at the GW (in the cases an SF of 7 and 10) under the condition of 100 EDs. The overall fractions of the PSR and PLRs for the other EDs are shown in Fig. 3.5 (b).

Similarly, in Fig. 3.6 (a), EDs employing the ADR underwent PLR-I for the initial 3 h owing to a higher SF (e.g., SF = 12), thereby resulting in a high ToA. The ADR at the NS side changed the SF and TP after interpreting the UL history of $M$ packets. However, the ED movement could change the underlying environment radically. Thus, the recent parameters can potentially be unsuitable for the successful delivery of a packet to a GW, thereby leading to an increase in the PLR-S as shown in Fig. 3.6 (a). Thus, retransmissions from the EDs are increased, which in turn restrict the scalability of a LoRaWAN network [67].

The average energy consumption, as shown in Fig. 3.7, reveals that the BADR is more energy-efficient when compared to the ADR and a static SF of 12. This higher energy consumption in the case of the ADR (e.g., with a higher SF of $>=$ 10) and a static SF of 12 results from the high ToA [68].

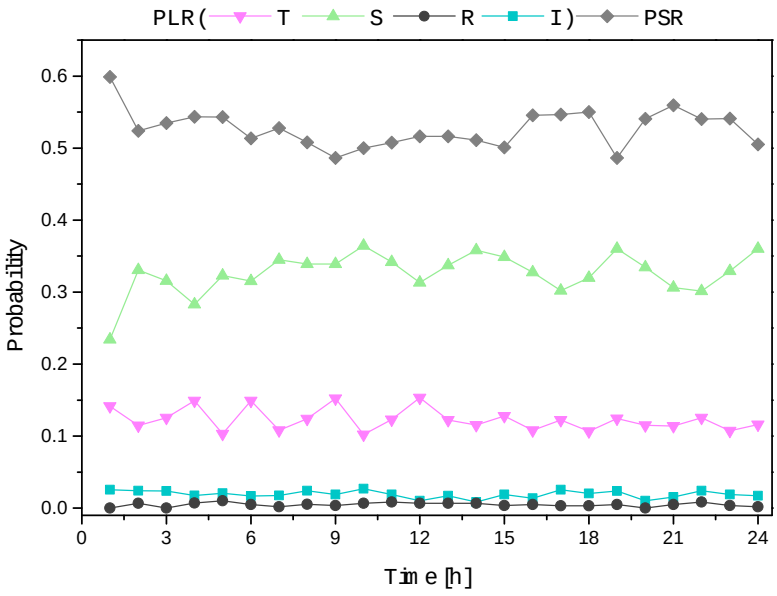


(a) in the case of $N$ of 100

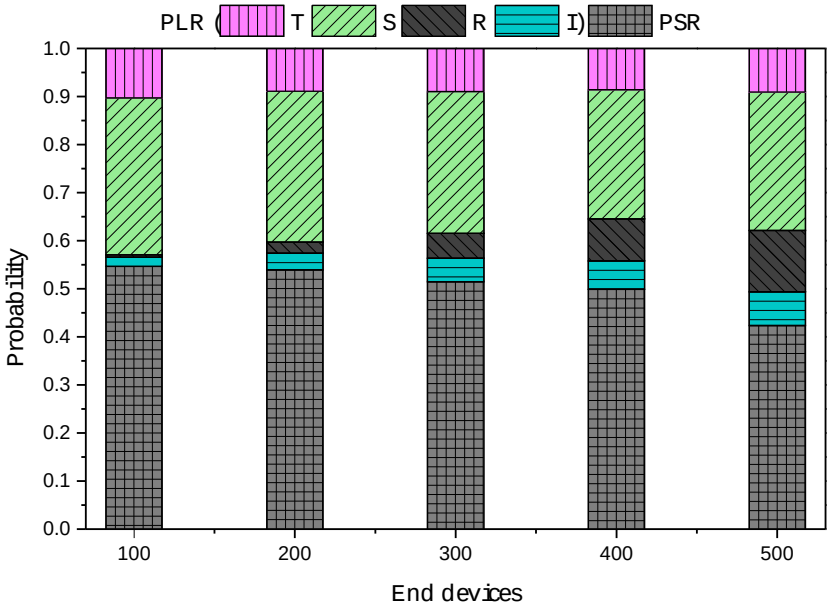


(b) in the case of various $N$

Figure 3.5: Average PSR and PLRs for the BADR during 1-day experiment.

### 3.4.3 Findings in BADR and ADR

Based on the evaluation of the BADR and ADR, the following conclusions and issues concerning them are elaborated:

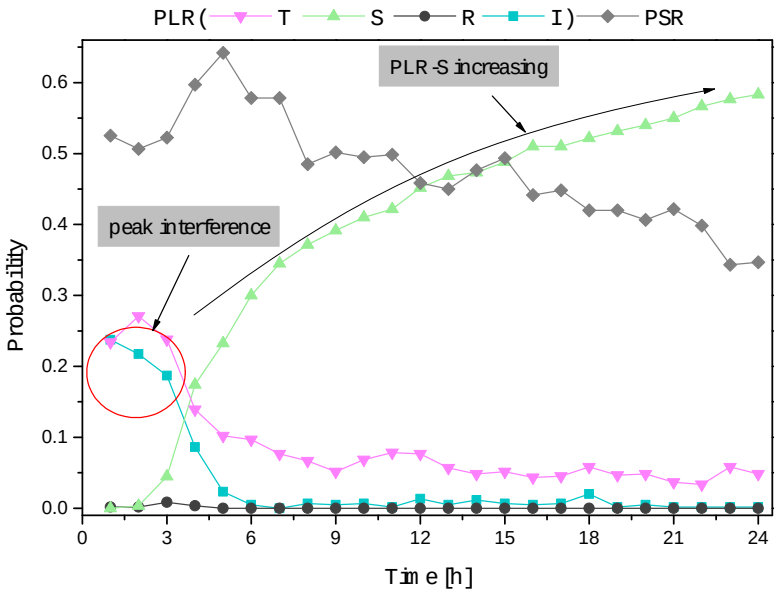


(a) in the case of $N$ of 100

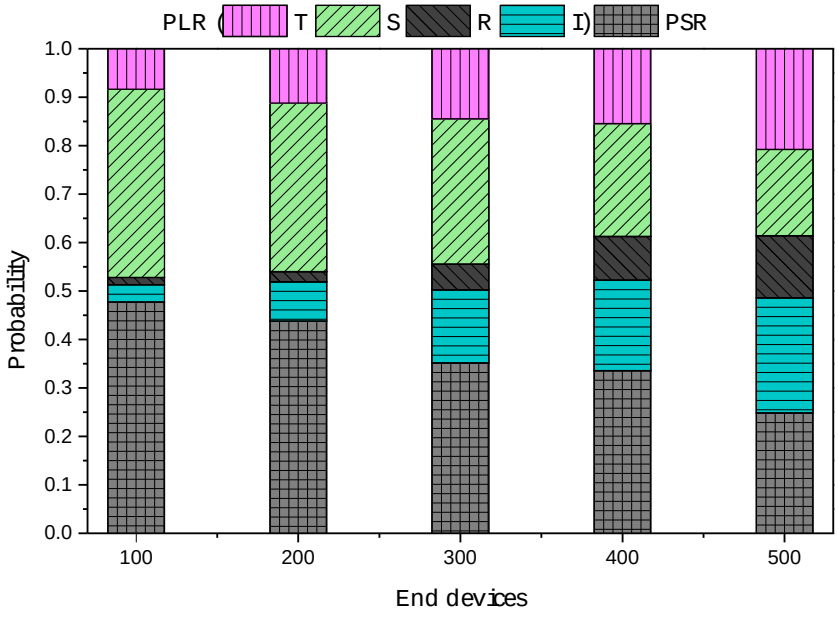


(b) in the case of various $N$

Figure 3.6: Average PSR and PLRs for ADR during 1-day experiment.

- **BADR**: It was observed that BADR underwent PLR-S because the ED packets arrived at the GW with insufficient power, resulting in massive packet loss. This situation occurs when the ED moves around the GW and

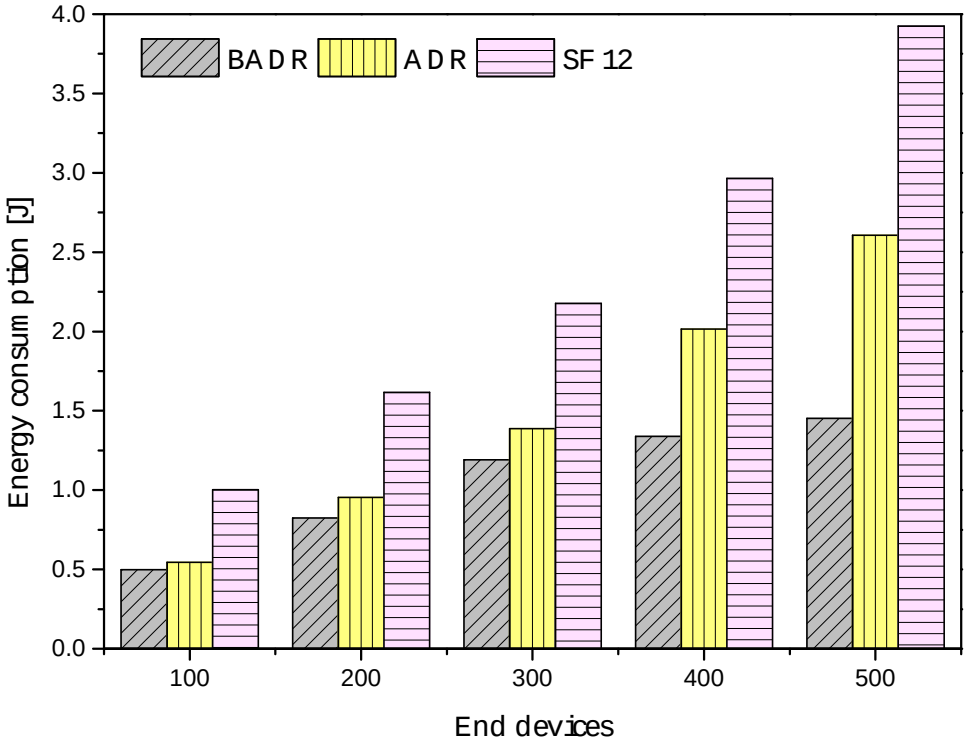


Figure 3.7: Average energy consumption of BADR, ADR, and SF = 12 during a 1-d experiment.

transmits a packet arbitrarily using an SF (i.e., between 7, 10, and 12). For example, an ED, far from the GW transmitting a packet with an SF of 7, might not be received at the GW due to low signal strength. As a result, the ED packet is lost, and retransmission occurs. Hence, this leads to a significant PLR-S and increases energy consumption.

- **ADR**: This dissertation followed the ADR recommended by the LoRa server [25, 26]. The simulation analysis revealed that ADRs were associated with different PLRs, such as PLR-I and PLR-S. Furthermore, it was revealed that the ADR involved significant energy consumption owing to high SF, TP, ToA, and retransmission parameters [66]. Apart from these identified issues, the authors in [50], and [69] claimed that the ADR involved a considerable convergence period because of the time-consuming process of changing the SF and TP values when using the ADR method.

To resolve the issues mentioned above concerning the BADR and ADR caused owing to the inefficient use of SF and TP, this dissertation presents the three

proposed resource allocation paradigms: reactive, proactive, and hybrid.

## 3.5 Summary

This chapter presented assumptions and constraints, key performance indicators, and network models. These models are utilized in the subsequent chapters of the dissertation to model the LoRaWAN network correctly in ns-3. Furthermore, the issues with ADR and BADR were highlighted under static and mobility scenarios. The identified issues are resolved using reactive, proactive, and hybrid paradigms in the subsequent chapters of the dissertation.

# Chapter 4
# Reactive Resource Allocation

A reactive paradigm is based on responding to events (such as collision, interference, and channel variations) after they have happened in the LoRaWAN network. Reactive resource allocation include “Channel-Aware Spreading Factor Allocation (C-ASFA)", “Gaussian- and Exponential Moving Average ADR (G-ADR and EMA-ADR)," as shown in Figure 4.1.

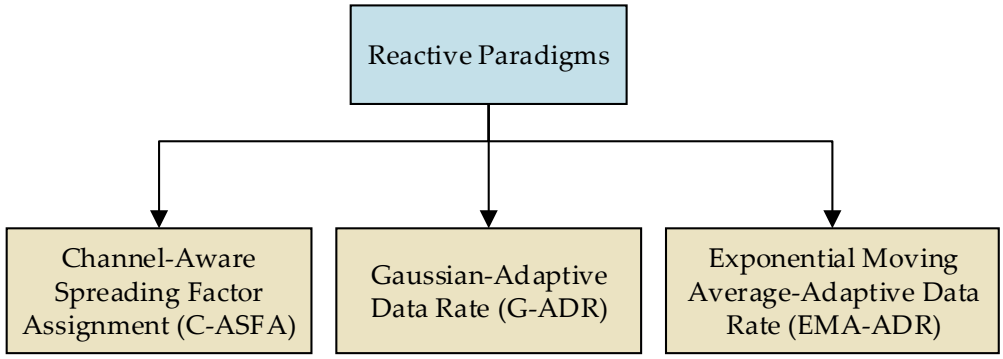


Figure 4.1: Reactive resource allocation paradigms.

The remaining of this chapter is structured as follows: Section 4.1 presents the proposed C-ASFA. Section 4.2 describes the proposed G-ADR. Section 4.3 highlights the proposed EMA-ADR, while Section 4.4 concludes this chapter.

## 4.1 Channel-Adaptive Spreading Factor Allocation

In a massive LoRaWAN network, only incrementing the SF can create a situation where most of the EDs switch their SF to higher values, resulting in a high ToA and hence, a collision possibility [10]. Besides, the UL transmission becomes a bottleneck for dense LoRaWAN deployments, wherein the packet loss rate increases with the high traffic load situation. As a result, the power depletion of each ED causes a reduction of their battery lifetimes. The proposed channel-adaptive spreading factor allocation (C-ASFA) approach comprises two phases: increment SF in the case of ACK failure and decrement SF when ACK is successfully received.

### 4.1.1 Increment SF

The proposed C-ASFA is based on a typical SF management scheme [2, 37], which is triggered after the retransmission is initiated from the ED. When ACK

is not received in either of the *RXs* by the ED, it increases SF for the next UL packet. If $ReTx\_Left\_CNT$ is a multiple of two, the proposed C-ASFA increases the SF to a higher value to avoid further packet loss. However, in the proposed C-ASFA, if any changes are detected to the SF, a counter, denoted as $SF\_CHANGE\_TRACK$, keeps a count of the SF change.

### 4.1.2 Decrement SF

On the other hand, when ED receives ACK successfully, the proposed C-ASFA increments a counter, $ACK\_CNT$. If $ACK\_CNT$ reaches α, the network reliability is satisfied. Furthermore, the $SF\_CHANGE\_TRACK$ value is verified if greater than zero. It shows that SF is higher than seven ($Min_{SF} < \text{SF} \leq Max_{SF}$). Therefore, it can be decremented, and the proposed C-ASFA lowers the SF further to decrease the ToA when the channel is determined to be stable. The detailed working of the proposed C-ASFA is presented in Algorithm 4.1.

## 4.2 Gaussian-Based Adaptive Data Rate

This section presents the scope and working procedure of the proposed Gaussian-Based Adaptive Data Rate (G-ADR).

### 4.2.1 Scope of the Proposed G-ADR

The signal strength received at the GW can be thought of as a Gaussian distribution [70]. For example, It is shown through real-time experiments, and computer simulations that the SNR received at the NS follow a Gaussian distribution using SF 7 and SF 12, as shown in Figure 4.2 (a) and 4.2 (b), respectively. Therefore, a Gaussian filter can be utilized to estimate the value of the SNR to accurately find SF, TP, or both because these parameters are dependent on the SNR.

### 4.2.2 Working Procedure of the Proposed G-ADR

The steps involved in the proposed G-ADR scheme are as follows:

1. When the NS receives an UL packet with the ACK bit enabled in the frame header of the *ADRACKReq* MAC command, the NS starts tracking the SNR of the $M$ received packets. The G-ADR algorithm is initiated by computing the mean ($\mu$) and variance ($\sigma$) using (4.2.1) and (4.2.2) [71], respectively.

$$\mu = \frac{1}{M}\sum_{i=0}^{M} SNR_i, \tag{4.2.1}$$

**Algorithm 4.1:** Channel-adaptive SF allocation approach.

**Input :** SF = 7∼12, $m$ = 8, ED = $i \sim N$, $ACK\_CNT$ = 32, $SF\_CHANGE\_TRACK$ = 6, $\alpha$ = 6 ($ACK\_CNT$ threshold)
**Output :** increase SF

```
At each uplink packet
if (is CON_UL ?) then
    ▷ it is a confirmed uplink transmission
  if (is ACK failed ?) then
      ▷ it is a confirmed uplink retransmission
    if (is ReTx_CNT(rem) %2 == 0 ?) then
      SF = SF + 1
      SF_CHANGE_TRACK ++
    else
      Retransmit with current SF
    end
  else
    ACK_CNT ++
    if (is ACK_CNT % α == 0 ?) then
      if (is SF_CHANGE_TRACK > 0 ?) then
        SF_CHANGE_TRACK -
        SF = SF − 1
      end
      ACK_CNT = 0
    end
    Transmit with current SF        ▷ ACK received
  end
else
  Transmit unconfirmed uplink packet      ▷ it is
   unconfirmed uplink transmission
end
getRandomChannel() transmitPacket()     ▷ ED i transmits UL
 packet
```

$$\sigma^2 = \frac{1}{M-1}\sum_{i=0}^{M}(SNR_i - \mu)^2, \tag{4.2.2}$$

where $i$ is the number of packets.

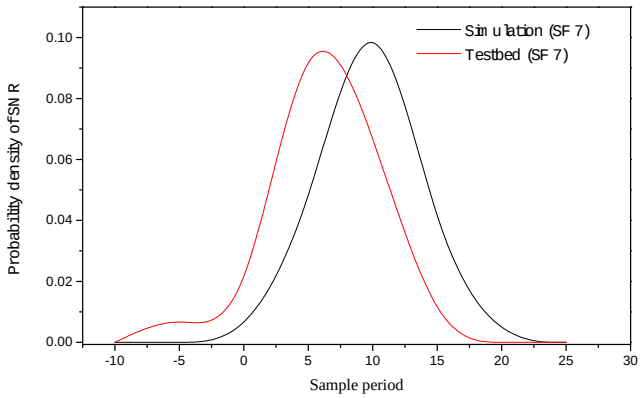


(a) PDF of SNR using SF7

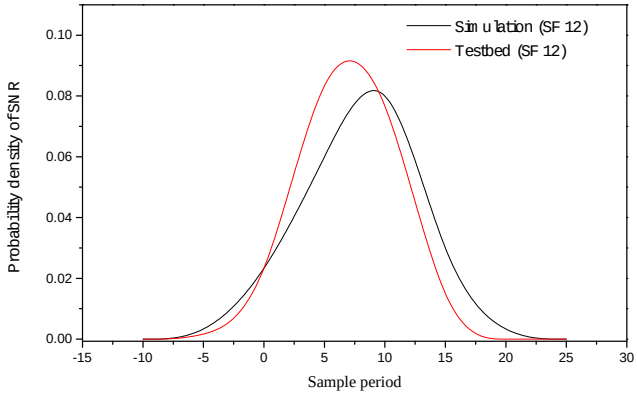


(b) PDF of SNR using SF12

(c) Deployment of two EDs with SF7 and SF12

Figure 4.2: The PDF of the SNR of *M* packets received at the network server using real-time experiment and computer simulation.

**Algorithm 4.2:** The proposed G-ADR scheme.

**Input :** TP = 2∼14, SF = 7∼12, $M$ = 20, $SNR_{req}$, $device_{margin}$
**Output:** SF and TP

Executed when NS receives $M$ UL packets
a. mean of the $SNR$ of $M$ received packets
b. Variance ($\sigma^2$)
c. Standard deviation ($\sigma$)
d. $LowPassFilter$ (LPF) = ($\mu$ - $\sigma$) and $HighPassFilter$ (HPF) = ($\mu$ + $\sigma$)
**for** $i \leftarrow 0$ **to** $M$ **do**
    $SNR$ = $getSNR(i)$
    **if** ($SNR \geq LPF$ and $SNR \leq HPF$ ) **then**
        insert $SNR$ into $SNRlist$
    **end**
**end**
**for** $i \leftarrow 0$ **to** $SNRlist$ **do**
    $Sum$
**end**
$SNR_m$ = $Sum$/ Size of $SNRlist$
▷ Network server LoRaWAN ADR
1. $SNR_{req}$ = demodulation $floor$ (current SF/DR)
2. $device_{margin}$ = 10 ▷ LoRaWAN default
3. $SNR_{margin}$ = ($SNR_m$ − $SNR_{req}$ − $device_{margin}$)
4. $steps$ = $int$ ($SNR_{margin}$/3)
**while** ($steps > 0$ and $SF > SF_{min}$) **do**
    $SF$ = $SF$ − 1
    $steps$ = $steps$ − 1
**end**
**while** ($steps > 0$ and $TP > TP_{min}$) **do**
    $TP$ = $TP$ − 2
    $steps$ = $steps$ − 1
**end**
**while** ($steps < 0$ and $TP < TP_{max}$) **do**
    $TP$ = $TP$ + 2
    $steps$ = $steps$ + 1
**end**
NS transmits $LinkADRReq$

Now, the probability density function (PDF) is expressed as follows: [71]

$$f(SNR) = \frac{1}{\sigma\sqrt{2\pi}} e \frac{-(SNR-\mu)^2}{\sigma^2}. \tag{4.2.3}$$

2. The proposed G-ADR accepts the centralized SNR values that lie within the effective range of $\mu + \sigma$ and $\mu$ - $\sigma$. The SNR value is estimated by averaging the values that are within the effective range.

3. Finally, the G-ADR obtains the SNR required ($SNR_{req}$, a demodulation threshold based on the current DR, as shown in Table 2.1) and computes the SNR margin ($SNR_{margin}$) and $N_{step}$ using (4.2.4) and (4.2.5) [20], respectively.

$$SNR_{margin} = SNR_m - SNR_{req}(DR) - margin_{dBm}, \tag{4.2.4}$$

$$N_{step} = int\left(\frac{SNR_{margin}}{3}\right). \tag{4.2.5}$$

In (4.2.5), $N_{step}$ represents the number of times the algorithm is executed [20]. Furthermore, the detailed operation of the G-ADR method is described in Algorithm 4.2.

## 4.3 Exponential Moving Average-Based Adaptive Data Rate

The scope and working procedure of the proposed Exponential Moving Average-based Adaptive Data Rate (EMA-ADR) is presented in this section.

### 4.3.1 Scope of the Proposed EMA-ADR

In general, the SNR varies over time, even in a fixed environment, resulting in an inaccurate SF and TP configuration [24]. The reasons why the SNR shows such high variability in space and time include various noise factors, fading, interference, and attenuation. The EMA for time-series data can be computed iteratively as follows:

$$S_t = \begin{cases} Y_1, & t = 1 \\ \delta.Y_t + (1 - \delta).\, S_{t-1}, & t > 1 \end{cases}. \tag{4.3.1}$$

In (4.3.1), $Y_t$ represents the current SNR value at time $t$, $S_t$ denotes the value of the EMA at any time $t$, and $\delta$ is a smoothing factor ($0 < \delta < 1$). Note that a larger value of $\delta$ reduces the level of smoothing, whereas a value of $\delta$ close to zero has a greater smoothing effect and is less responsive to recent SNR observations.

Based on the assumption, an experiment was conducted by using EMA filter-based smoothing of the SNR for several packets received at the NS through a computer simulation, as shown in Figure 4.3. It can be seen that the smoothing process reduced the spikes of the raw SNR values. Therefore, the EMA filter can be utilized to resist the rapid changes occurring in the SNR of $M$ packets owing to the mobility of the EDs.

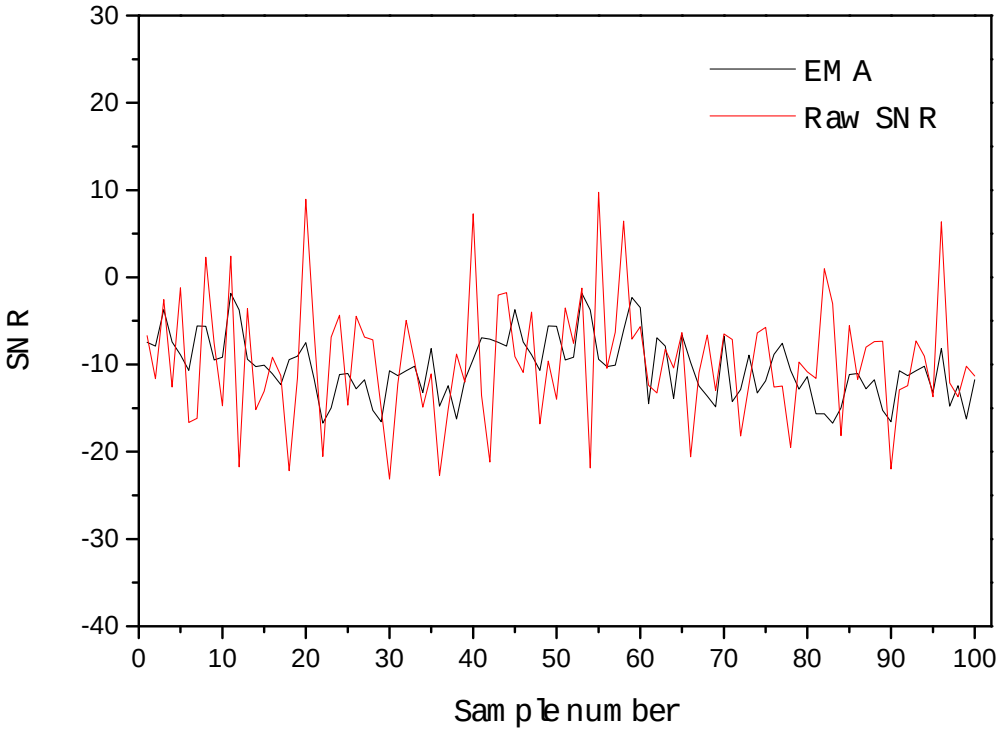


Figure 4.3: Example of smoothed SNR using EMA filter generated at ns-3.

### 4.3.2 Working Procedure of the Proposed EMA-ADR

The steps involved in the proposed G-ADR scheme are as follows:

1. When the NS receives the first two UL packets, the EMA-ADR is commenced.

2. The EMA starts smoothing the SNR values using (4.3.1). In this work, the value of $\delta = 0.7$ is chosen owing to ED mobility ( [72] uses $\delta = 0.5$ for indoor positioning).

3. The rest of the EMA-ADR operation is similar to G-ADR as shown in Algorithm 4.3.

## 4.4 Summary

This chapter presented proposed reactive paradigms: C-ASFA, G-ADR, and EMA-ADR. Reactive paradigms are responsible for dealing with SF and TP allocation

**Algorithm 4.3:** The proposed EMA-ADR scheme.

**Input :** TP = 2∼14, SF = 7∼12, $M = 20$, $\delta = 0.7$, $SNR_{req}$, $device_{margin}$
**Output:** SF and TP

Executed when NS receives two uplink packets
**for** $i \leftarrow 0$ ***to*** $SNRlist$ **do**
  $SNR_m$ = using (4.3.1)
**end**
▷ Network server LoRaWAN ADR
1. $SNR_{req}$ = demodulation $floor$ (current SF/DR)
2. $device_{margin}$ = 10 ▷ LoRaWAN default
3. $SNR_{margin}$ = ($SNR_m$ − $SNR_{req}$ − $device_{margin}$)
4. $steps$ = $int$ ($SNR_{margin}$/3)
**while** ($steps > 0$ and $SF > SF_{min}$) **do**
  $SF = SF - 1$
  $steps = steps - 1$
**end**
**while** ($steps > 0$ and $TP > TP_{min}$) **do**
  $TP = TP - 2$
  $steps = steps - 1$
**end**
**while** ($steps < 0$ and $TP < TP_{max}$) **do**
  $TP = TP + 2$
  $steps = steps + 1$
**end**
NS transmits *LinkADRReq*

to EDs when NS observes issues. These approaches are implemented at the NS side and activated when NS receives 20 UL packets from ED. After efficient SF and TP parameters identification, NS transmits them in a downlink *LinkADRReq* MAC command to the concerned ED. Upon the reception of *LinkADRReq*, the ED adapts the recommended transmission parameters and transmits UL packets.

# Chapter 5
# Proactive Resource Allocation

A proactive approach eliminates the issues in the LoRaWAN network before they occur (e.g., collision and packets arriving under the required SF sensitivity due to propagation environment). Reactive resource allocation include the “Mobility-Aware Spreading Factor Allocation (M-ASFA)", “Retransmission Assisted Resource Management (R-ARM)," and Artificial Intelligence-Empowered Resource Allocation Framework (AI-ERA), as shown in Figure 5.1.

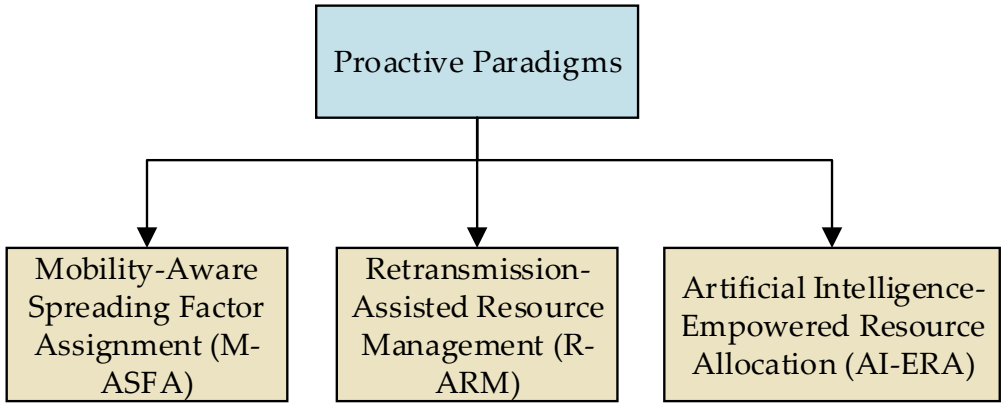


Figure 5.1: Proactive resource allocation paradigms.

The remaining of this chapter is structured as follows: Section 5.1 presents the proposed M-ASFA. Section 5.2 describes the proposed R-ARM. Section 5.3 highlights the proposed AI-ERA framework, while Section 5.4 concludes this chapter.

## 5.1 The Mobility-Aware Spreading Factor Allocation

The M-ASFA consists of two phases: (1) an initial SF allocation with traffic heterogeneity and (2) a mobility-aware SF Assignment (M-ASFA) to mobile EDs.

### 5.1.1 Initial SF Allocation with Traffic Heterogeneity

The SF assignment during the initial deployment is primarily based on [61]. First, the $P_{rx}$ is computed for each UL transmission at the GW by assuming a time-independent and symmetric link. Here, the channel uses the same path loss model for UL and DL transmissions. Second, the lowest SF is allocated to the ED based on the $P_{rx}$ that would be above the GW sensitivity ($S_g$). The $S_g$ values for each SF

**Algorithm 5.1:** Initial SF allocation with traffic heterogeneity in the proposed M-ASFA.

**Input :** $S_g$ = GW-sensitivity for each SF, SF = 7∼12, EDs = $i$∼$N$
**Output:** Assignment of SF to static and mobile EDs

```
for i ← 0 to N do
    P_rx(i) = getRxPower()    ▷ P_rx at GW (i.e., a GW would
     receive from ED)
    if (P_rx(i) > S_g) then
        i = getSpreadingFactor()
        PL_i = getPacketLength()
        if (PL_i < PL_th) then
            No variation in SF of ED i
        else
            i = getHighestSpreadingFactor()
            ▷ highest permissible SF, which can still
             support the specified PL
        end
    else
        i = SF 12                ▷ EDs are out of range
    end
end
```

are presented in Table 2.1. This allocation method minimizes the ToA and reduces the probability of collisions. However, a typical initial SF assignment approach shown in [61] is not suitable for a scenario where EDs have heterogeneous traffic with different PL, reliability, and mobility requirements. Thus, a third step (i.e., traffic heterogeneity) is added to restrict the biased SF allocation to the EDs based on the PL. If the condition holds (i.e., $PL_{N_i} < PL_{th}$; $PL_{th}$ [73]), ED can transmit a UL packet with a specified PL. Otherwise, the proposed scheme assigns a suitable SF to support the stated PL. The detailed procedure of the proposed method is shown in Algorithm 5.1.

### 5.1.2 Mobility-Aware SF Assignment Scheme

The working of the M-ASFA is described in Algorithm 5.2. The M-ASFA executes before an ED initiates a UL packet transmission at the ED side. At the time of UL packet transmission, M-ASFA verifies the ED status (i.e., whether the ED is mobile or static) by determining the distance between the current ($x_2$, $y_2$) and previous ($x_1$, $y_1$) positions of an ED (i.e., $d_0$), as shown in Fig. 5.2.

When $d_0$ is known, the M-ASFA scheme verifies the condition by compar-

**Algorithm 5.2:** Mobility-aware SF assignment in the proposed M-ASFA scheme.

**Input :** $S_g$ = GW-sensi-tivity for each SF, SF = 7∼12
**Output :** Allocating new SF to mobile EDs before transmission and retransmission

```
At each uplink packet
compute d_0
if (d_0 ≥ α) then
    ▷ ED i is mobile
    compute P_rx at GW for each transmitting ED
    P_rx(i) = getRxPower()
    if (P_rx(i) > S_g) then
        i = getSpreadingFactor()
        PL_i = getPacketLength()
        if (PL_i < PL_th) then
            No variation in SF of ED i
        else
            i = getHighestSpreadingFactor()
        end
    else
        i = SF 12
    end
else
    No variation in SF of ED i      ▷ ED i is static
end
getRandomChannel()    ▷ ED i obtains a random channel from among R
R = number of available channels  ▷ R = 3 (default channels in the EU region)
channels = [1,...,R]              ▷ shuffle channels
transmitPacket()              ▷ ED i transmits UL packet
```

ing $d_0$ with a pre-defined threshold (i.e., $\alpha$=10 meters). The proposed M-ASFA scheme considers the value of $\alpha$ as 10 m because the received signal strength remains unaltered up to 40 m [74]. Therefore, this results in two alternative conditions.

1. Condition 1: ($d_0 \geq \alpha$): If the condition holds, it verifies that the ED is mobile. Subsequently, M-ASFA measures $P_{rx}$ at the GW and allocates a suitable SF such that $P_{rx}$ is higher than $S_g$, and the newly assigned SF can

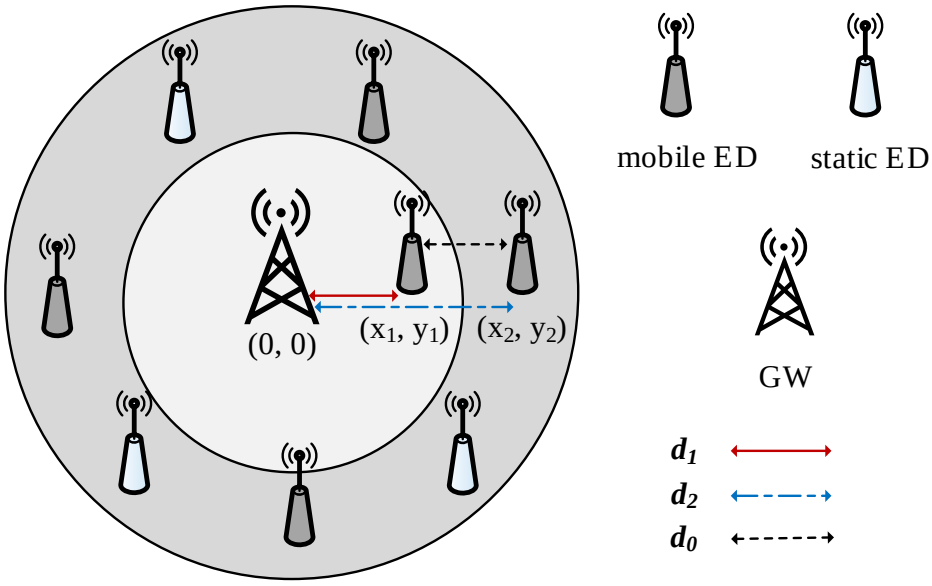


Figure 5.2: Detection of ED movement in the proposed M-ASFA scheme.

support the specified PL. After the SF selection, ED picks a random channel (from among the three available channels in the EU region) and transmits a UL packet (either confirmed or unconfirmed).

2. Condition 2: ($d_0 < \alpha$): The ED is considered static in this condition. Therefore, static EDs transmit their UL packet with a previously allocated SF.

## 5.2 Retransmission-Assisted Resource Management ADR

A detailed overview of the proposed R-ARM ADR operating on the ED and NS sides is presented in this section.

### 5.2.1 R-ARM at ED side

Algorithm 5.3 shows the detailed mechanism of the proposed R-ARM approach on the ED side. The R-ARM is triggered at every UL packet transmission via verification of the status of each packet (i.e., a confirmed or an unconfirmed transmission) with either message type (*mType*) or *ADRACKREq* bit in the frame header (FHDR). The proposed R-ARM uses *mType*, which was selected during the ED deployment time by setting it as *CONFIRMED_DATA_UP* (for confirmed traffic) or *UNCONFIRMED_DATA_UP* (for unconfirmed traffic) in the LoRaWAN *MAC* header. When *mType* holds, the confirmed mode is verified such that the UL

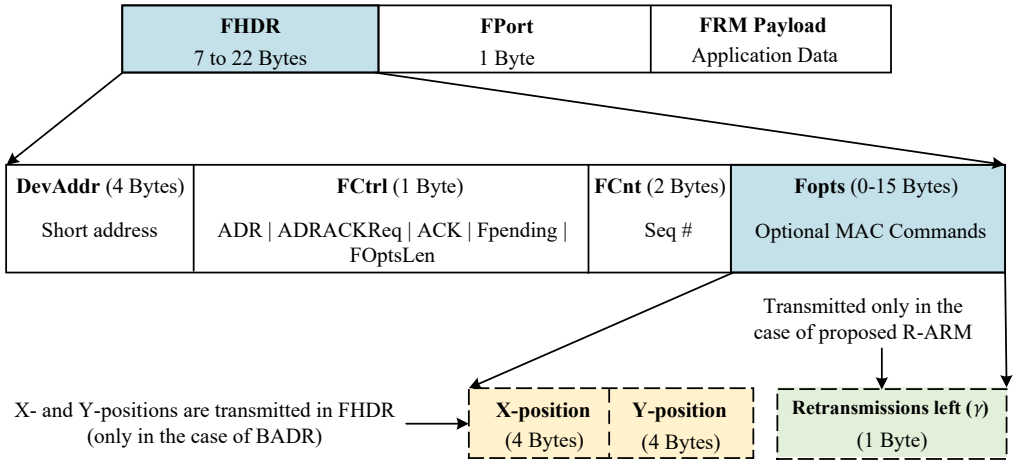


Figure 5.3: Modified frame header (FHDR) of the LoRa message for the proposed R-ARM and BADR.

packet requires an ACK from the NS. Furthermore, the R-ARM implemented on the ED side analyzes whether the ongoing packet is a new transmission or retransmission. This step can be verified in two ways:

(i) If the frame count ($F_{Cnt}$) contained in the LoRa message frames of the ongoing packet and the previously transmitted packet is identical, then R-ARM considers the current packet as a retransmission. Here, $F_{Cnt}$ is a 2-byte field in the FHDR, which shows the sequence number of the transmitting packet as shown in Fig. 5.3.

(ii) A new transmission or retransmission can be verified by checking for an ACK reception in the receive windows.

The proposed R-ARM utilizes $F_{Cnt}$ to determine retransmissions conducted ($Rxs_{Cnt}$) at the ED. When packet retransmission is confirmed, $Rxs_{Cnt}$ is incremented each time. This aids in identifying the number of remaining retransmissions ($\gamma$). When $\gamma$ is a multiple of 2, R-ARM computes the $P_{rx}$ by considering the impact of the propagation loss and small-scale fading using an approach similar to that presented in [18].

When $P_{rx}$ is obtained, it is compared with the GW sensitivity thresholds ($S_g$) as defined in Table 2.1. The R-ARM approach assigns the lowest possible SF (satisfying $P_{rx} > S_g$) through the $SetSF(index)$ function, where $index$ denotes the number of SF. Under this scenario, when stating the $S_g$ threshold values, the SF 9 can be extremely low, whereas the GW can still receive a packet from the mobile

ED when transmitted using an SF $\in [10, 11, 12]$. The R-ARM method selects the lowest value (i.e., SF = 9) to minimize the ToA. Higher SFs are vulnerable to interference owing to a higher ToA [29, 31–33, 75].

Next, to prevent a massive packet loss given retransmissions of mobile EDs, $\gamma$ was compared to a threshold $\alpha$ (i.e., $\alpha = 4$). When $\gamma$ and the SF are lower than $\alpha$ and 12, respectively, the R-ARM increases the SF and allocates the TP. In this study, R-ARM assumes the threshold value of $\alpha$ as four because retransmission significantly increases energy consumption [76, 77]. When the ED receives an ACK in any two receive windows, the ED continues transmission with the previous SF set via the NS. Finally, $\gamma$ is encapsulated in the FHDR and transmitted to the NS as shown in Fig. 5.3.

However, encapsulating $\gamma$ in the FHDR can add 1 byte to the payload, thereby increasing ToA, i.e., SF7 = 25.86, SF8 = 51.71, SF9 = 103.42, SF10 = 206.85, SF11 = 413.70, and SF12 = 827.39 (in ms). It is noted that the BADR shares mobile ED positions with the NS [11] as shown in Fig. 5.3. By sending ED positions (in this study, the ED positions consist of 8 bytes, and the PHY/MAC header size is 9 bytes), the ToA and transmission energy can be significantly increased. However, the proposed R-ARM omits sending ED positions to the NS to decrease the ToA and extra energy consumption. Additionally, any energy-demanding localization, such as a global positioning system (GPS), is not required.

### 5.2.2 R-ARM at NS side

Algorithm 5.4 presents the detailed mechanism of the proposed R-ARM approach on the NS side.

When the NS receives a UL packet wherein *ADRACKReq* bit is enabled in the FHDR, the typical ADR of LoRaWAN on the NS side is executed by considering the maximum SNR value among the $M$ packets to determine $NS_{SF}$ and $NS_{TP}$ parameters (line 3).

To further optimize SF and TP parameters, R-ARM recommends using two Gaussian thresholds: low Gaussian and high Gaussian filter thresholds ($LGT$ and $HGT$). These thresholds are dependent on two parameters: the mean ($\mu$) and standard deviation ($\sigma$) of $P_{rx}$ [51]. The R-ARM uses $P_{rx}$ values that lie within the effective range of $\mu + \sigma$ and $\mu$ - $\sigma$. The $P_{rx}$ associated with each received packet at the NS is compared with thresholds of $LGT$ and $HGT$, the resultant values of $P_{rx}$ are stored in the received power list (*RxPwList*), and the average value is computed (lines 9-17).

Furthermore, to prevent unnecessary retransmissions from mobile EDs, R-ARM extracts $\gamma$ from the FHDR and compares it to a threshold $\alpha$. When the $\gamma$ condition holds (i.e., $\gamma < \alpha$), R-ARM compares $P_{rx}$ to each value contained in $S_g$, thereby resulting in the assignment of a suitable SF (such that $P_{rx} > S_g$) (lines 18-

**Algorithm 5.3:** Proposed ED-side R-ARM approach.

**Input :** ED = i∼N, index = SF 7∼ SF 12, $\alpha = 4$, $S_g$ = Table 2.1, $Tx_{limit} = 8$, $TP = 14$ dBm
**Output :** Spreading factor (SF) and transmit power (TP)

1 At each uplink transmission
2 **if** $(mType == CONFIRMED\_DATA\_UP)$ **then**
3 ▷ it is a confirmed uplink transmission
4 **if** $(Rxs_{Cnt} > 0)$ **then**
5 ▷ it is a retransmission
6 ▷ R-ARM finds number of retransmissions left ($\gamma$)
7 $\gamma = (Tx_{limit} - Rxs_{Cnt})$
8 **if** $(\gamma \ \%2 == 0)$ **then**
9 ▷ R-ARM computes $P_{rx}$ as in [18]
10 **if** $(P_{rx(i)} > S_g)$ **then**
11 $i_{SF} = SetSF(index)$
12 ▷ ED $i$ transmits UL packet with the assigned SF
13 **end**
14 **else**
15 **if** $(\gamma < \alpha$ *and* $SF < 12)$ **then**
16 $i_{SF} = i_{SF} + 1$
17 $i_{TP} = 14$ dBm
18 **end**
19 **end**
20 **else**
21 *continue* transmission with current $SF$ ▷ ACK is received
22 **end**
23 **else**
24 *continue* transmission when $mType =$ $UNCONFIRMED\_DATA\_UP$
25 ▷ it is unconfirmed uplink transmission
26 **end**
27 include $\gamma$ in FHDR (as shown in Fig. 5.3)

22). At this stage, R-ARM indicates a satisfactory SF for an ED of $i$ ($i_{SF}$), which is compared to the $NS_{SF}$ determined by the typical ADR in the same interval (lines 23-25). When this condition is true, the ED transmits the next packet with

**Algorithm 5.4:** Proposed NS-side R-ARM approach.

**Input :** ED = $i \sim N$, index = SF 7 $\sim$ SF 12, $\alpha = 4$, $S_g$ = Table 2.1, $TP$ = 2$\sim$14 dBm, $M = 20$

**Output :** SF and TP

1 At each uplink packet reception
2 **if** *(ADR == enabled)* **then**
3 ▷ typical ADR finds $NS_{SF}$ & $NS_{TP}$
4 // R-ARM computes the following:
5 a. Standard deviation ($\sigma$),
6 b. $LGT = (\mu - \sigma)$,
7 c. $HGT = (\mu + \sigma)$,
8 d. and $P_{rx}$.
9 **for** $j \leftarrow 0$ **to** $M$ **do**
10 **if** $(P_{rx} > LGT$ and $P_{rx} < HGT)$ **then**
11 $RxPwList.push\_back\,(P_{rx})$
12 ▷ *RxPwList* is a list, which contains $P_{rx}$ values after applying Gaussian filters
13 **end**
14 **end**
15 // computing average
16 $P_{rx}$ = *Sum* for all element values in *RxPwList* / *RxPwList*.size()
17 ▷ *RxPwList*.size() returns the number of elements present in *RxPwList* list
18 ▷ extract $\gamma$ from FHDR
19 **if** $(\gamma < \alpha)$ **then**
20 **if** $(P_{rx(i)} > S_g)$ **then**
21 $i_{SF} = SetSF(index)$
22 **end**
23 **if** $(i_{SF} > NS_{SF})$ **then**
24 transmit *SF* to ED $i$
25 **end**
26 **end**
27 transmit $NS_{SF}$ and $NS_{TP}$ to ED $i$
28 **end**
29 NS transmits *LinkADRReq* MAC command

newly identified parameters via R-ARM (i.e., $i_{SF}$). Otherwise, the ED sends the next transmission with $NS_{SF}$ and $NS_{TP}$ (line 27).

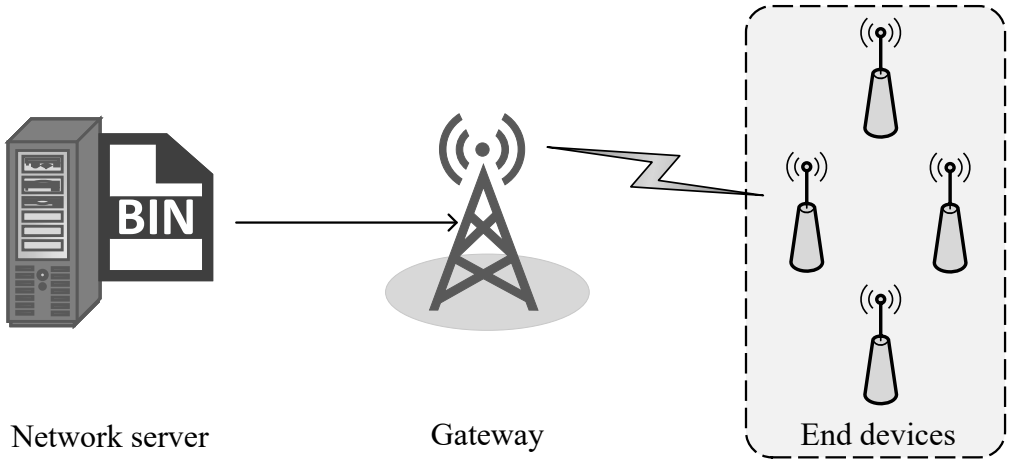


Figure 5.4: An example of the firmware update over the air (FUOTA) process in LoRaWAN.

When the R-ARM execution is completed, the *LinkADRReq* MAC command is transmitted to the concerned ED as unconfirmed (line 29). The unconfirmed transmission of the MAC command suggests that the NS does not require an ACK notification from the ED to lower the overhead and energy consumption.

### 5.2.3 Integration of R-ARM in LoRaWAN

Typically, to integrate the proposed R-ARM ADR on the ED in a real LoRaWAN network, a firmware update process is required using a wired connection such as serial communication. However, LoRaWAN comprises a large number of EDs, which makes the firmware update process more challenging. Therefore, firmware update over the air (FUOTA) can be utilized to update the firmware of the target ED as shown in Fig. 5.4. The FUOTA is recommended by the STM, which is a LoRa Mote maker [78, 79].

## 5.3 Design of the Proposed Artificial Intelligence-Empowered Resource Allocation Framework

### 5.3.1 Scope of the Proposed AI-ERA Framework

In general, AI is a computational paradigm that provides systems with intelligence, teaching them to operate, respond, and learn the same way as humans. ML is an AI technique that enables artificial processes to learn from data and

make decisions without being explicitly programmed. Additionally, ML performance does not scale linearly with increasing data in volume and plateaus quite quickly [80]. Furthermore, ML algorithms occasionally require storing all data in memory, computationally impracticable in big data scenarios. Deep neural network (DNN) is a class of AI algorithms modeled after biological nerve systems that perform representation learning through multi-layer transformations. They generate output at each time step via recurrent connections between hidden units [80]. The DNN is an Artificial Neural Network (ANN) approach, which addresses these concerns that is effective in a variety of applications [81]. A significant benefit of DNN is its ability to extract high-level characteristics automatically from data with a complicated structure and internal relationships [82].

Furthermore, DNN is capable of dealing with enormous volumes of data [83–87]. Wireless networks rapidly generate massive amounts of data (e.g., traffic series with periodicities such as daily and weekly, traffic with different data rates under different environments, channel variations, etc.). Due to the growing number of AI applications in mobile and wireless networking [82], the crossovers between these domains construct the scope of the proposed AI-ERA framework for resource allocation to IoT applications.

### 5.3.2 AI-ERA Framework: Offline Mode

The offline mode of the proposed AI-ERA consists of two phases: preparation and learning, as shown in Fig. 5.5.

#### 5.3.2.1 Preparations Phase

In this phase, a raw dataset is generated by utilizing LoRaWAN module[1] in the ns-3 simulator. For example, to generate the training dataset shown in Fig. 5.5, transmission was made between GW and EDs for ten days of simulation time, where ED transmits 6 UL packets periodically every hour with SF7 to SF12 in a group, $G \in \{UL_1, ..., UL_6\}$ in a confirmed mode without a retransmission mechanism. As an example shown in Fig. 5.6 (a), ACK failure is represented with "0," and successful ACK reception for each corresponding $UL$ packet is marked with "1" (in a confirmed mode, a $UL$ packet is considered successful if ED receives ACK). Furthermore, the UL transmissions generated in $G_1 \sim G_6$ are from the same location and ED. The primary aim is to find the best SF based on the propagation environment.

[1] https://github.com/signetlabdei/lorawan

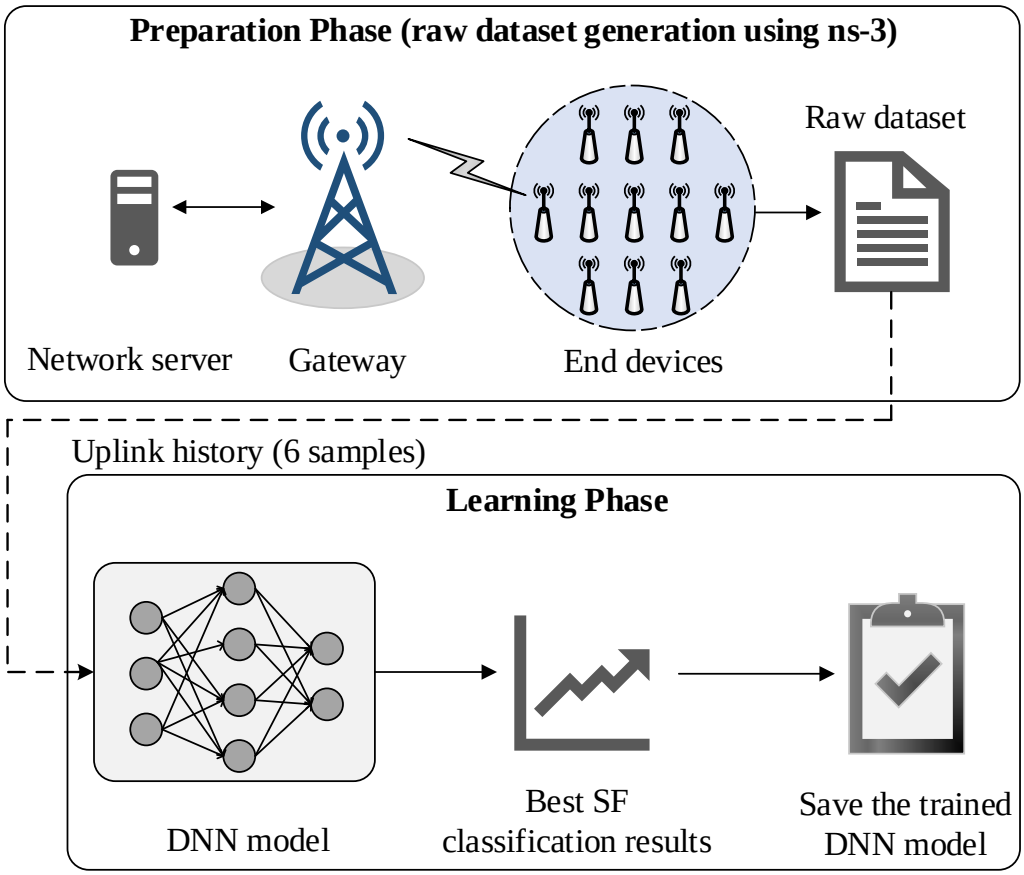


Figure 5.5: Representation of offline mode for the proposed AI-ERA framework.

#### 5.3.2.2 Best SF Selection

Based on the successful ACK reception, the lowest and best SF is chosen among every $G$. For instance, SF9 and SF 11 are selected from $G_1$ and $G_6$, respectively, as shown in Fig. 5.6 (a). However, in the case of ACK failure in any $G$, SF12 is assumed. Once the best SF is selected from each $G$, a total of 6 input samples with essential features, including X- and Y-coordinates, received power ($P_{rx}$), and SNR is given as input to the DNN model, as shown in Fig. 5.6 (b).

#### 5.3.2.3 Learning Phase

Once the preparation phase is completed, the learning phase is initiated, which is further elaborated in Fig. 5.7. Once the dataset is pre-processed according to the required UL history as input for the DNN model, it is divided into training (80%), validation (10%), and testing (10%). To properly train the DNN model,

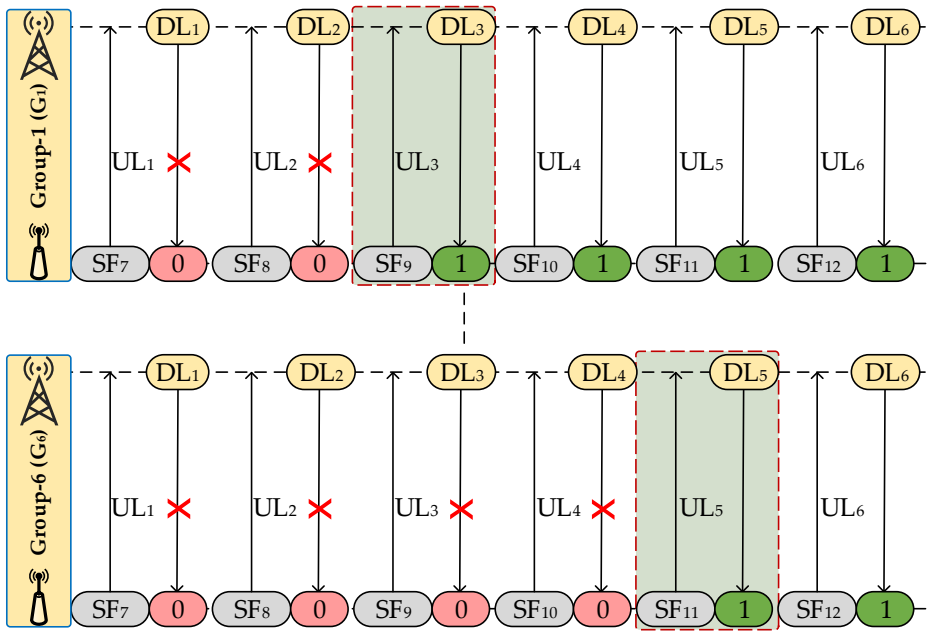


(a)

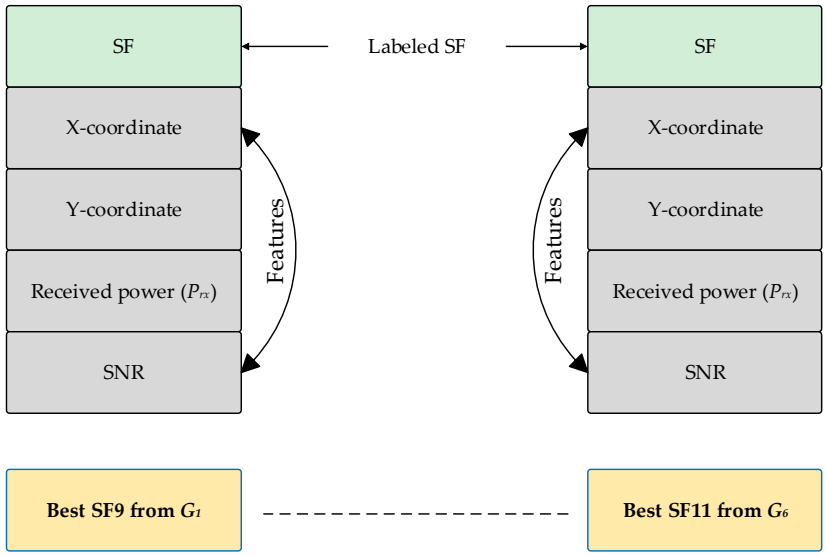


(b)

Figure 5.6: Input features and data labeling: (a) best SF selection based on successful ACK among 6 groups, and (b) input sequence with features including X- and Y-coordinates, $P_{rx}$, SNR and labeled SF.

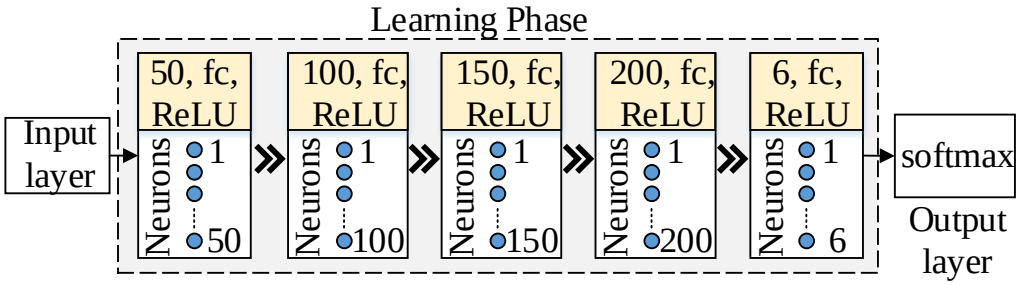


Figure 5.7: Learning phase of DNN model.

the proposed method utilizes 5 fully connected layers via the *ReLu* to update the weight and biases. Finally, $softmax$ is utilized at the output layer, responsible for the classification of SFs. In multi-class classification issues, the $softmax$ activation function is typically used at the last layer of a deep learning model to map the outputs to a list of probabilities S = ($S_1$, $S_2$,..., $S_K$) overall available classes, mathematically represented as [88]

$$S_k = \sigma(z)_k = \frac{e^{zk}}{\sum_{j=1}^{K} e^{zk}} \quad \text{for k = 1, 2,..., K,} \tag{5.3.1}$$

where $K$ is the number of classes, $S_k$ is the probability of the k-th class, and z = ($z_1$, $z_2$,..., $z_K$) represents the output of the layer before softmax activation function.

Furthermore, the DNN model during the training process is validated after every $10^{th}$ epoch and tested with 10% unknown UL history to evaluate the model accuracy. This pre-trained DNN structure with the best hyperparameters is further utilized as a backbone to suggest the best SF in the online mode.

### 5.3.3 AI-ERA Framework: Online Mode

Online mode refers to the process of classifying an appropriate SF with new data without updating the model weights. The online mode is divided into two phases: preparation and execution, as shown in Fig. 5.8.

1. **Preparation Phase:** This phase is responsible for managing the data required for the pre-trained DNN model (e.g., required features with a sequence of size 6 for each ED during communication). When ns-3 is executed, EDs (e.g., static or mobile) transmit UL packets toward GW. The input sequence of size 6 is gathered with required features (i.e., X-, Y-coordinates, $P_{rx}$, and SNR) at the time of UL packet without prior knowledge of ACK status.

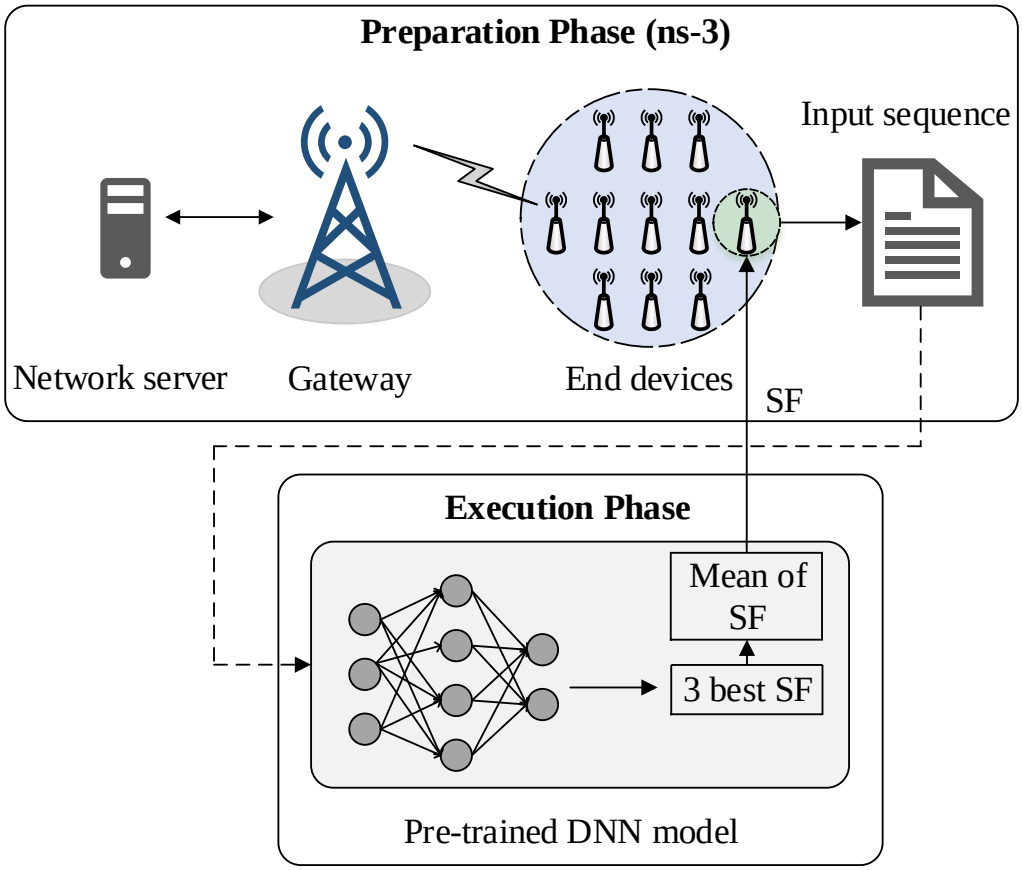


Figure 5.8: Representation of online mode for the proposed AI-ERA framework.

2. **Execution Phase:**

   When the sequence length reaches 6 for a particular ED, the execution phase is commenced. The proposed AI-ERA waits only for the first 6 packets and then uses a sliding window afterward. At this stage, the input size with required features is fed as input into the pre-trained DNN model to classify a suitable SF for the subsequent UL transmissions. Once the pre-trained DNN model classifies the SF, an ED (e.g., static or mobile) transmits a UL packet with this new SF to the GW. Finally, the GW forwards the received data to the NS for further processing, as shown in Fig. 5.8.

### 5.3.4 Computational Complexity of the Proposed Deep Learning Model

The proposed AI-ERA framework is implemented at the ED side. It can also be deployed at the NS side; however, it will significantly increase the convergence

period since it should wait for $M$ (i.e., $M = 20$) UL packets received at the NS to be activated. Therefore, the proposed AI-ERA framework was deployed at the ED side to proactively classify a suitable SF before each UL transmission, starting it as soon $M$ reaches 20, increasing the probability of successful transmission with classified SF. During the initial deployment, the AI-ERA framework utilizes SF of 12, which has the highest ToA. With this high ToA, SF 12 is vulnerable to high interference. The PLR at the GW increases the time to receive $M$ packets at the NS. Therefore, causing a convergence period (time required to reach a stable SF and PSR). However, the choice of employing the AI-ERA framework at the ED side can lead to excessive computational resources. Therefore, it can be a compromise between the attained performance (e.g., enhanced PSR, ultra-low energy consumption, and low convergence period) and computational cost.

## 5.4 Summary

This chapter presented three proactive paradigms, including M-SFA, R-ARM, and AI-ERA framework, to deal with SF and TP allocation. Proactive paradigms can resolve the SF and TP allocation problem more efficiently by resolving the issues caused due to inefficient SF/TP in the network. Furthermore, the proactive paradigms know the problem with SF and TP used by the ED. Therefore, proactive approaches proactively allocate new SF/TP parameters to ED before a problem occurs in the network, such as collision, interference, and/or packets arriving under the required sensitivity at the GW.

# Chapter 6
# Hybrid Resource Allocation

The primary aim of the hybrid paradigm is to fulfill the requirements of both static and mobile EDs simultaneously. Therefore, a hybrid adaptive data rate was proposed to dynamically assign physical layer resources to static and mobile EDs.

## 6.1 Hybrid Adaptive Data Rate

The operation procedure of the proposed HADR is shown in Fig. 6.1. There are two primary steps involved in the proposed HADR: computing the distance between previous and current locations of the ED ($d_0$) and ADR selection based on the ED status (i.e., static or mobile).

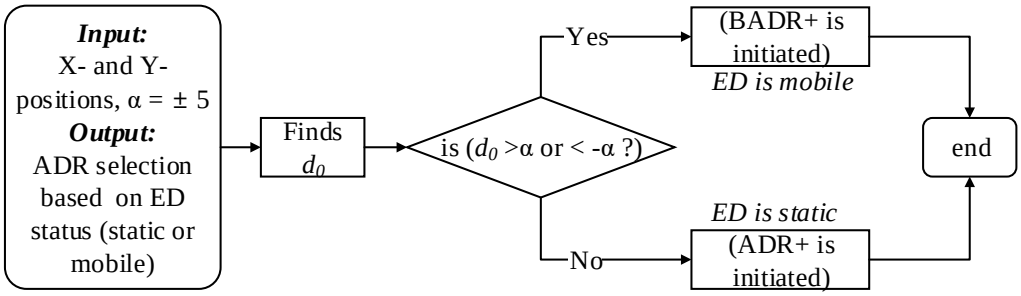


Figure 6.1: Operation procedure of the proposed hybrid adaptive data rate.

### 6.1.1 Computing $d_0$

HADR checks by whether the ED involved in communication is static or mobile at each UL packet transmission time. This step verifies the ED status (i.e., $d_0$), which is determined by finding the distance between the previous ($x_1$, $y_1$) and current ($x_2$, $y_2$) positions of an ED. The proposed HADR chooses a threshold of $\alpha = 5$ m because the received signal strength remains unchanged up to 40 m [66].

### 6.1.2 ADR Selection

Based on the $d_0$, HADR selects an appropriate ADR for the ED. When an ED is classified as mobile, BADR+ is initiated at the UL transmission ($TX$), as shown in Algorithm 6.1. The BADR+ is a slightly changed variant, where the ED transmits packets sequentially (i.e., [SF7∼SF12]), as shown in 6.2. To resolve the retransmission issue of the BADR, HADR utilizes a similar method, as shown in [22].

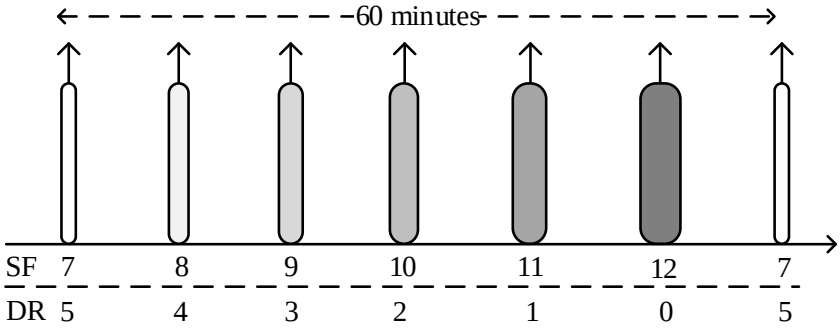


Figure 6.2: Operation procedure of the proposed BADR+.

**Algorithm 6.1:** BADR+ at the end device.

**Input :** SF = 7∼ 12, $\beta = 2$, $Tx_{limit} = 8$, $TP = 14$ dBm
**Output:** SF and TP

```
At each uplink transmission
if (TX == True) then
    // starting SF = 7
    Assign SF sequentially (see Fig. 6.2) instead
     of [12, 10, 7]
else
    // retransmission method
    if (ReTx_CNT % β == 0 and SF < 12) then
        SF = SF + 1
        TP = 14
    else
        continue transmission with current SF
    end
end
```

When ED fails to receive ACK, a retransmission counter ($ReTx\_CNT$) is incremented. If $ReTx\_CNT$ is a multiple of $\beta$ (i.e., $\beta = 2$) SF is increased by 1 to regain connectivity [22].

In the case of static ED, the ADR+ manages both SF and TP (ADR is defined by The Things Network (TTN) [50]), as shown in Algorithm 6.2. However, the ADR was slightly modified by taking the average ($AVG$) of $M$ UL packets to smooth the SNR, which helps in identifying an efficient SF and TP.

**Algorithm 6.2:** ADR+ at the network server.

**Input :** SF = 7∼ 12, TP = 2∼14 dBm, $M = 20$
**Output:** SF and TP

At each UL packet reception
**if** *(ACK == enabled)* **then**
  // confirmed mode
  1. $SNR_m$ = AVG(SNR of last $M$ UL packets)
  2. $SNR_{req}$ = demodulation $floor$ (current DR/SF)
  3. $SNR_{margin}$ = ($SNR_m$ − $SNR_{req}$ − $device_{margin}$)
  4. $N_{step}$ = $int$ ($SNR_{margin}$/3)
  **while** *($N_{step}$ > 0 and SF > 7)* **do**
    SF −= 1 and $N_{step}$ −= 1
  **end**
  **while** *($N_{step}$ > 0 and TP > 2)* **do**
    TP −= 2 and $N_{step}$ −= 1
  **end**
  **while** *($N_{step}$ < 0 and TP < 14)* **do**
    TP += 2 and $N_{step}$ += 1
  **end**
**end**

## 6.2 Summary

This chapter presented a hybrid ADR to simultaneously allocate resource parameters to both static and mobile devices. The proposed HADR is implemented at the ED side. When the HADR determines the ED status (i.e., static or mobile), appropriate ADR is executed.

# Chapter 7
# Experimental Results

In this chapter, the performance of reactive, proactive, and hybrid paradigms are assessed comprehensively compared to state-of-the-art approaches. In this dissertation, network simulator 3 (ns-3) is utilized. In addition, the module utilized in this dissertation was the LoRaWAN[1] by adding: (1) mobility environment, (2) confirmed mode, (2) typical ADR and blind ADR protocols of LoRaWAN, (3) LoRa modified FHDR for tracking application by including the X- and Y-coordinates [11], and (4) the proposed reactive, proactive, and hybrid approaches.

The remainder of this chapter is organized as follows: Section 7.1 presents the considered application along with key requirements. Section 7.2 describes the simulation environment. Section 7.3 presents the performance of the reactive approaches, comprising C-ASFA, G-ADR, and EMA-ADR. Section 7.4 evaluates the proactive approaches, containing M-ASFA, R-ARM, and AI-ERA. Section 7.5 presents the performance evaluation of the hybrid adaptive data rate approach. Finally, the last Section 7.6 presents some concluding remarks.

## 7.1 Application Scenario

This dissertation considers two IoT applications: smart grid (metering) [89–91], livestock, and industrial asset tracking [92,93], suggested by Semtech and GSMA-3GPP, respectively. A packet size of 30 bytes for electrical metering and industrial asset tracking (both static and mobile) is considered in simulation, as shown in Table 7.1. In the case of electrical metering, transmitting location information in FHDR is not required. However, for industrial asset tracking, location information needs to be sent in FHDR for tracking and monitoring purposes. Therefore, the packet size of industrial asset tracking (i.e., 30 bytes) includes 8 bytes of location information (i.e., X- and Y-coordinates are of size 8 bytes). Therefore, to transmit location information of the ED, LoRa FHDR was modified, as shown in Fig. 5.3.

Table 7.1: Applications requirements.

| Application | Suggested by | Uplink interval | Packet size | Mode |
|---|---|---|---|---|
| Smart grid (metering) | Semtech [11] | 24 [per day] | 30 [bytes] | confirmed |
| Industrial asset tracking | GSMA-3GPP [93] | 24 [per day] | 30 [bytes] | confirmed |

[1] https://github.com/signetlabdei/lorawan

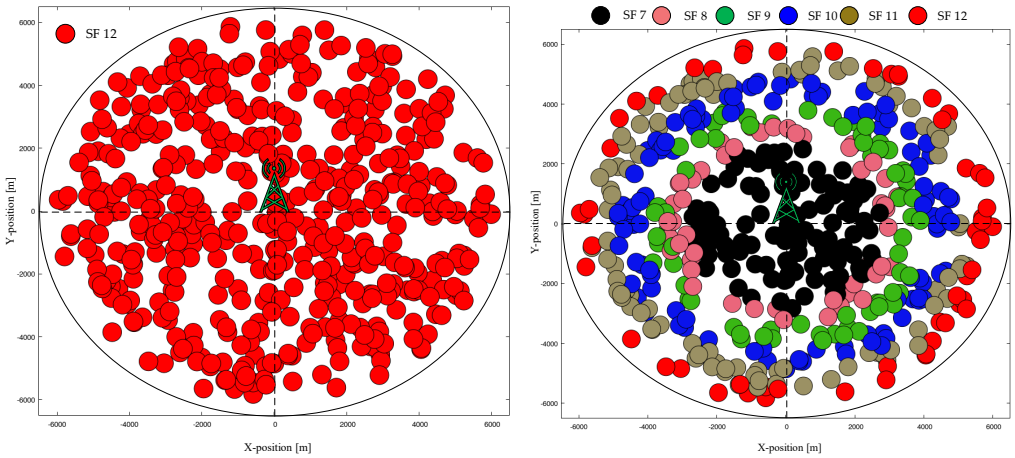


(a) Starting SF = 12 (b) Starting SF = I-SFA

Figure 7.1: Initial network topology in the case of static EDs with N = 500.

## 7.2 Simulation Environment

This study considers both confirmed and unconfirmed modes in a single GW scenario. The EDs are randomly deployed in a radius of 5 km. Under mobility scenarios, EDs employ a random walk 2-D mobility model [94]. The study also considers the random walk 2-D mobility model because the applications (i.e., industrial asset tracking) utilized in this dissertation are nomadic [93] in nature, where the ED does not follow a pre-defined mobility path and ED always randomly changes direction. During the initial deployment, SF = 12 is assigned to the EDs as the initial SF in all schemes [50]. In some cases, the SFs to EDs are assigned using initial-SF allocation (I-SFA), in the case of only the proposed methods (G- and EMA-ADRs). The I-SFA method allocates SF during the initial deployment based on the GW SF sensitivity thresholds, as defined in Table 2.1. The initial simulation environments with SF = 12 and I-SFA deployment are shown in Figures 7.1 (a) and 7.1 (b), respectively. The other parameters utilized in the simulation are listed in Table 7.2.

## 7.3 Experimental Analysis of Reactive Resource Allocation

This section presents the analysis of the C-ASFA, G-ADR, and EMA-ADR.

Table 7.2: Simulation parameters.

| Parameter | Description and Value |
|---|---|
| Path loss exponent | 3.76 |
| Path loss model | log-distance |
| ED movement speed [m] | 0.1∼1.0 ( [51, 66]) |
| Mobility model | random walk 2-D ( [51, 66]) |
| Frequency region | EU-868 |
| UL channels | [868.1, 868.3, 868.5] in MHz<br>with 125 kHz bandwidth |
| DL channel | 869.525 MHz<br>For receive window 2 and DR0 only |

### 7.3.1 Analysis of C-ASFA

Figure 6 presents the performance analysis of the typical and proposed channel-adaptive SF schemes. As shown in Figures 6 (a) and (b), the SR generally decreases with many EDs joining the network in both schemes. Therefore, when an ED does not receive an ACK, it transmits at low data rates after a few retransmissions. Owing to the higher ToA, the collision probability increases. When a packet collision happens, the two EDs involved in the collision schedule a retransmission time imposed by the duty cycle restriction. In a massive LoRaWAN network, a higher traffic load increases the chances of collision probability, and most of the RW is missed due to the duty cycle limitations [8,38]. As a result, more EDs with the SF management scheme transmit high SFs and cause more congestion, and the network loses the advantage of orthogonality between different SFs. However, the proposed channel-adaptive SF scheme increases the data rate when ACK failures are reduced, thus lowering the SF and yielding a better SR of up to 7.5% and 7.8% for Figure 6 (a) and (b), respectively. Furthermore, the performance of both the SF approaches is lower in Figure 6 (b) than in Figure 6 (a). This is due to the signal strength being significantly decreased by the building penetration losses, which results in a lower SR. In the case of an urban environment, many EDs cannot reach the GW due to the unfavorable channel that leads to a high packet loss. As these EDs stay active and cause interference to the nearby EDs, the scalability of the LoRaWAN is retained. Another possibility is that the duty cycle limitations imposed by the LoRaWAN do not allow such transmissions if the EDs reach the maximum allowed time.

### 7.3.2 Analysis of G-ADR and EMA-ADR

The performance of the G-ADR and EMA-ADR are examined in terms of the convergence period, PSR, and energy consumption in both static and mobility

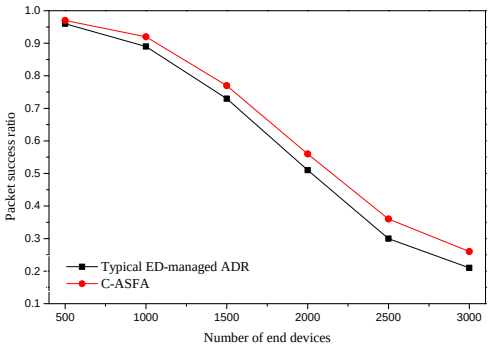


(a) PSR under log-distance

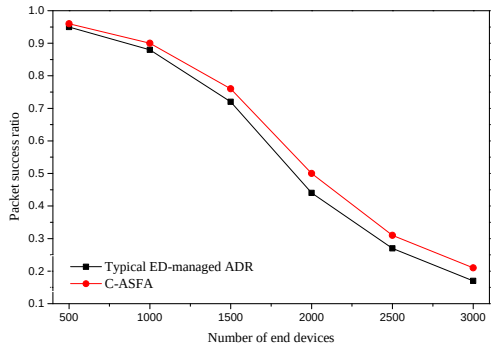


(b) PSR under Okumra-Hata

Figure 7.2: The success ratio of the SF allocation schemes in the unconfirmed mode under the condition of GW radius = 3410 m.

scenarios in a confirmed mode. In addition, the EDs choose a random speed of between 0.5 to 1.5 m/s (in [95], 2 m/s is used for outdoor positioning) and change direction after every 1000 m. Every ED transmits 24 packets/day during 4 days of the simulation time

#### 7.3.2.1 Convergence Period

The convergence period and *PSR* of static EDs during a simulation period of 4 days is shown in Figure 7.3. As indicated in Figure 7.3 (a), all schemes begin transmission with SF = 12 and TP = 14 dBm. In Figures 7.3 (a) and 7.3 (b) both typical ADR and ADR+ suffer from 20 h of converge period to reach a stable SF and PSR. This convergence period verifies the typical ADR features, as described in [50]. The primary reason for this high convergence period is that the frequency of a typical ADR (NS-managed ADR) is entirely arbitrary, which is activated after $M$ UL packets. This is a time-consuming process and thus yields a high convergence period. In general, an ED-managed ADR is intended to maximize the flexibility of DL traffic, which is restricted by the duty cycle limitations imposed by LoRaWAN. This helps the EDs to reestablish reliable communication links by steadily increasing the value of the SF ($SF < 12$). This flexibility increases the convergence period in the worst case, for example, when an ED employs a lower SF than needed to successfully deliver a packet to the nearest GW.

In contrast, G-ADR follows a similar trend with a convergence period of 14 h along with a better *PSR* when compared to both a typical ADR and ADR+ under the static scenario, as shown in Figure 7.3. Moreover, EMA-ADR outperforms the other schemes in the convergence period (i.e., 3 h) and *PSR*. As the reason for the quick convergence, the EMA filter resists against the rapid changes in the SNR

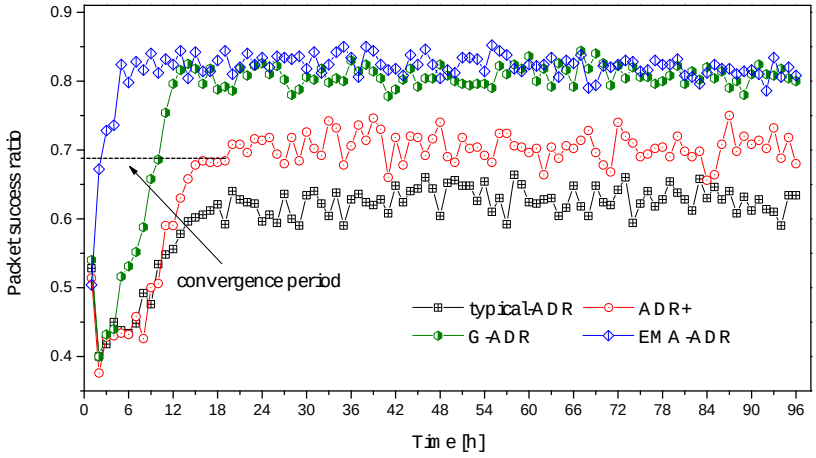


(a) Initial allocation of SF with 12

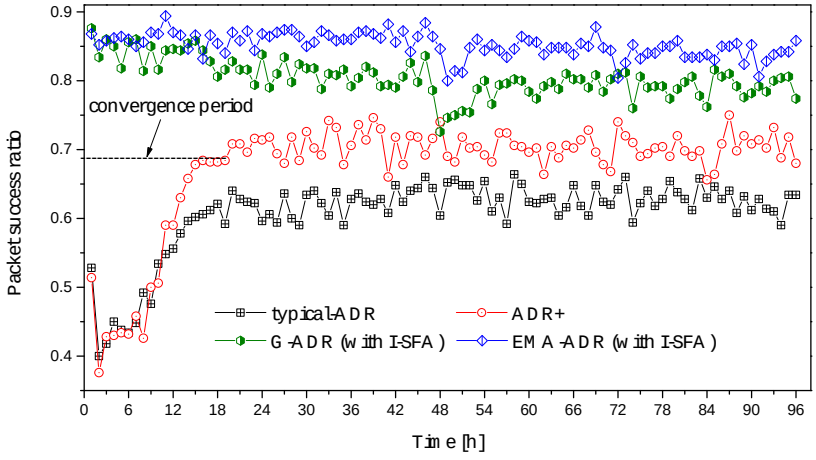


(b) Initial allocation of SF with 12 (for ADR and ADR+) and initial SF allocation with I-SFA (for G-ADR and EMA-ADR)

Figure 7.3: Convergence period and PSR of static EDs with N = 500.

of *M* packets and acts as a local averaging function. Thus, the proposed EMA-ADR scheme achieves a higher *PSR* compared with typical ADR and ADR+, as shown in Figure 7.3 (a). Figure 7.3 (b) presents another scenario in which G-ADR and EMA-ADR are employed using the I-SFA scheme. There is no convergence period when I-SFA is jointly utilized with G-ADR and EMA-ADR.

Figure 7.4 shows the convergence period and *PSR* of mobile EDs, where both typical ADR and ADR+ require 15 h and 14 h, respectively, to converge to a stable state. Further, in Figure 7.4 (a), Two types of convergence periods (in the case of typical ADR and ADR+) are observed: the initial convergence period and the convergence period caused by the mobility. The initial convergence period

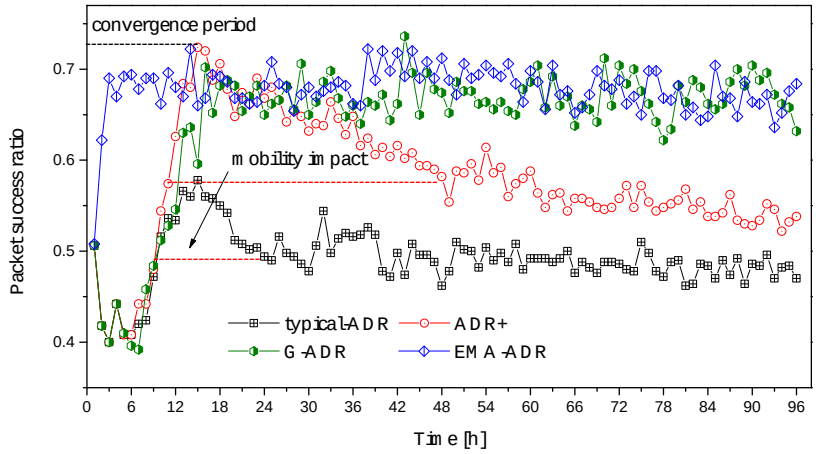


(a) Initial allocation of SF with 12

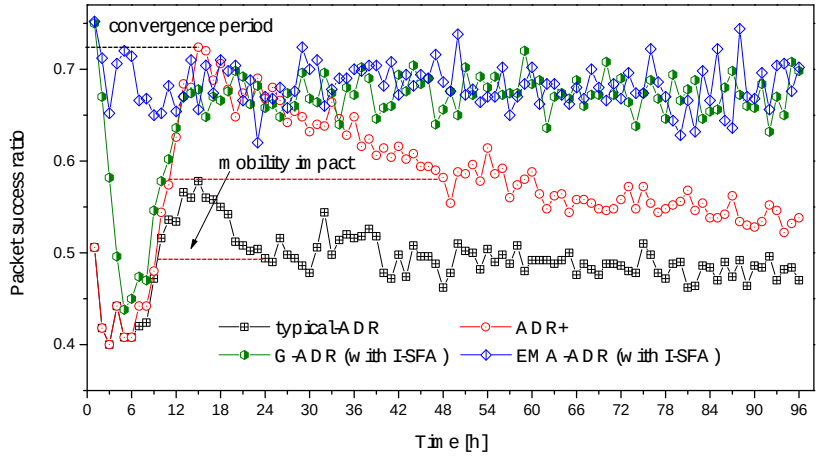


(b) Initial allocation of SF with 12 (for ADR and ADR+) and initial SF allocation with I-SFA (for G-ADR and EMA-ADR)

Figure 7.4: Convergence period and PSR of mobile EDs with N = 500.

occurs due to a high SF (all EDs initially start transmitting packets with SF = 12). However, after a short period of stability, the PSR decreases, and both the ADR and ADR+ suffer from a convergence period. This convergence period is caused when an ED is mobile and receives a new configuration (i.e., SF and TP) from the NS; the propagation scenario could have been drastically changed [24]. Therefore, the SF and the link budget will no longer be valid, which results in packet loss and massive retransmissions.

In Figure 7.4 (a), G-ADR and EMA-ADR take 16 h and 3 h for the initial convergence period, respectively, but do not suffer a second convergence period under a mobility scenario. Both of the proposed schemes employ filters, which helps

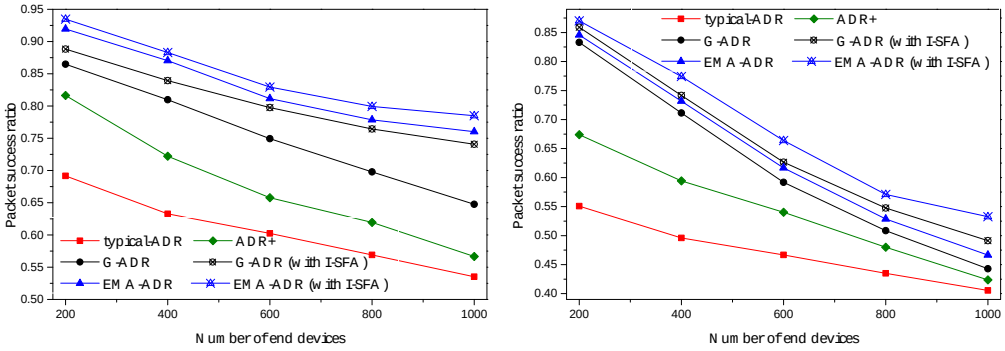


(a) Static EDs (b) Mobile EDs

Figure 7.5: Average PSR of static and mobile EDs (uplink period = 24 packets/day, total simulation time = 4 days).

reduce the convergence period and improve the PSR. As shown in Figure 7.4 (b), both G-ADR and EMA-ADR use I-SFA as an initial SF assignment during deployment. Unlike a static scenario, both the proposed G-ADR and EMA-ADR with the I-SFA scheme have a convergence period of 13 h and 3 h. In the case of G-ADR (with I-SFA), the mobility has a considerable impact on the convergence period because the parameters newly modified by the NS (i.e., both SF and TP) do not guarantee an efficient communication between the ED and GW. In such a case, the propagation environment may change radically when an ADR command reaches the mobile ED, and the newly assigned parameters may no longer be valid. Hence, a new packet from this ED with recently adopted parameters can be lost due to the inappropriate SF and TP use. However, EMA-ADR (with and without I-SFA) performs exceptionally well under the mobility conditions, resulting in a reduced convergence period and high PSR.

#### 7.3.2.2 Average Packet Success Ratio

The average *PSR* for a different number of static EDs is presented in Figure 7.5. Here, Figure 7.5 (a) shows a decreasing trend in *PSR* with a growing number of EDs in a confirmed mode. The declining tendency of *PSR* is due to high interference among the SFs when the EDs are transmitted with a high SF [96]. Because higher SFs are highly vulnerable to interference owing to the high ToA, they can negatively influence the capacity of the communication channel [29–33]. Thus, retransmissions from the EDs increase, causing significant congestion and massive packet loss. However, the proposed EMA-ADR with and without the I-SFA scheme outperforms the other schemes in terms of *PSR* because EMA-ADR frequently changes the SF and TP parameters by employing a low-pass filter and

Table 7.3: PSR improvement for static EDs in percentage.

| N | ADR | ADR+ | G-ADR | G-ADR (I-SFA) | EMA-ADR | EMA-ADR (I-SFA) |
|---|---|---|---|---|---|---|
| 200 | - | 12.5 | 17.3 | 19.7 | 22.8 | 24.3 |
| 400 | - | 8.9 | 17.7 | 20.7 | 23.8 | 25.0 |
| 600 | - | 5.5 | 14.7 | 19.5 | 20.9 | 22.7 |
| 800 | - | 5.1 | 12.9 | 21.5 | 21.0 | 23.0 |
| 1000 | - | 3.1 | 11.2 | 20.5 | 22.5 | 25.0 |

Table 7.4: PSR improvement for mobile EDs in percentage.

| N | ADR | ADR+ | G-ADR | G-ADR (I-SFA) | EMA-ADR | EMA-ADR (I-SFA) |
|---|---|---|---|---|---|---|
| 200 | - | 12.3 | 28.2 | 30.8 | 29.5 | 31.9 |
| 400 | - | 9.8 | 21.6 | 24.6 | 23.6 | 27.8 |
| 600 | - | 7.4 | 12.5 | 16.0 | 15.0 | 19.7 |
| 800 | - | 4.5 | 7.3 | 11.2 | 9.4 | 13.6 |
| 1000 | - | 1.8 | 3.8 | 8.6 | 6.1 | 12.7 |

averaging function. In addition, for a similar scenario, as presented in Figure 7.5 (a), Table 7.3 shows the average *PSR* improvement for ADR+ and the proposed schemes when compared to a typical ADR.

An analysis of the average *PSR* for a different number of mobile EDs is shown in Figure 7.5 (b). The mobility of the EDs has a high impact on the *PSR* because the mobility causes frequent changes in the topology, which influences the signal strength between an ED and a GW. As a result, the link budget used at the previous location after the ED movement would no longer be valid (assuming that the signal attenuation was applied at each ED). Thus, these EDs must alter their SF due to the variations in the received signal strength. However, when the NS changes the SF and TP (in a typical ADR and ADR+), these parameters are no longer valid owing to ED mobility. As a result, a packet transmitted from these EDs is lost because arriving under the sensitivity at the GW.

Another reason for this massive packet loss in Figure 7.5 (b) is due to the saturated receiver. The GW can demodulate up to 8 packets simultaneously. If a packet arrives at GW and there are no available receive paths, the packet is lost. Furthermore, for a scenario similar to that in Figure 7.5 (b), Table 7.4 shows the average *PSR* improvement for ADR+ and the proposed schemes when compared to typical ADRs.

#### 7.3.2.3 Average Energy Consumption

In general, the energy consumption of all schemes in the confirmed mode shows an increasing trend as the number of EDs increases, as shown in Figure 7.6 (a). However, the energy consumption of the proposed schemes is lower than that of an ADR and ADR+ because of the small number of retransmissions. Another

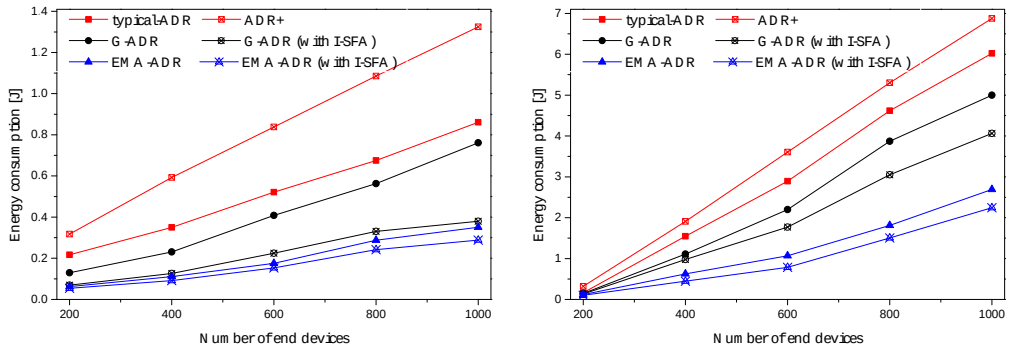


(a) Static EDs (b) Mobile EDs

Figure 7.6: Average energy consumption of static and mobile EDs (uplink period = 24 packets/day, total simulation time = 4 days).

cause of the low energy consumption of the proposed schemes is the higher *PSR*. However, in typical ADR and ADR+, a number of the EDs transmit packets with high parameters, including SF = 12 and TP = 14 dBm. As a result, the maximum number of packets is lost due to increased interference, resulting in EDs retransmitting packets with higher settings. Therefore, high energy consumption is observed in this case because the transmit energy consumption is primarily based on the values of SF, TP, and ToA, and the retransmissions [97].

The average energy consumption is shown in Figure 7.6 (b). Overall, the energy consumptions of the proposed G-ADR and EMA-ADR (with and without I-SFA) are lower because of the higher *PSR*. In general, the energy consumption of all schemes shows an increasing trend as the number of EDs increases. When a packet is retransmitted multiple times with a high SF and TP, it eventually increases the energy consumption. In addition, when packets are transmitted with higher SFs, it causes a high interference owing to the high ToA. Because higher SFs are highly susceptible to interference, they can negatively affect the energy consumption [29–33].

## 7.4 Experimental Analysis of Proactive Resource Allocation

This section presents the analysis of the M-ASFA, R-ARM, and AI-ERA.

### 7.4.1 Analysis of M-ASFA

M-ASFA is analyzed under confirmed and unconfirmed modes. Each ED transmits $\lambda$ = 48 packets during 48 h of simulation time, where 50% of the EDs are mobile (for pet-tracking application). The rest of the simulation parameters uti-

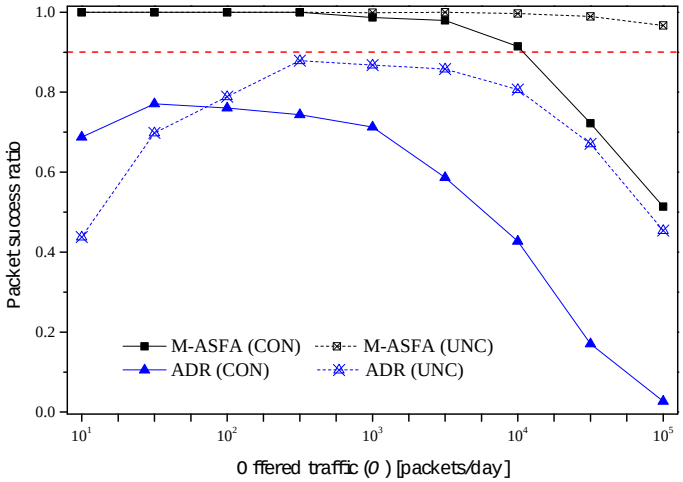


Figure 7.7: Average PSR of M-ASFA and ADR in confirmed and unconfirmed modes.

lized in the performance analysis of the M-ASFA are the same as shown in Table 7.2.

#### 7.4.1.1 Packet success ratio

Fig. 7.7 presents an analysis of the average PSRs of a typical ADR and the proposed M-ASFA schemes. Fig. 7.7 shows how the PSR generally varies when the offered traffic increases. In the case of the ADR in a confirmed mode (CON), the performance is significantly lower than that of the proposed M-ASFA scheme. The NS may not acknowledge the UL packet successful receipt by a GW due to the GW duty cycle constraints. Furthermore, the curves in Fig. 7.7 (ADR CON case) occur due to an extreme bottleneck caused by the unacknowledged packets. Therefore, the $PSR_{CON}$ is decreased. The unacknowledged packets increase the UL transmission traffic load from the EDs, which causes massive retransmissions. Due to ACK failures, more retransmissions are required to transmit a UL packet, which causes significant interference. The ACKs have priority over UL packet reception due to the transmission priority of the GW, resulting in UL packet loss, which, in turn, reduces $PSR_{CON}$ [47].

Meanwhile, the $PSR_{UNC}$ of ADR is higher than that of ADR in the confirmed mode ($PSR_{CON}$). Because the unconfirmed mode does not require DL ACK response from the GW, DL capacity is saved using a half-duplex GW. This achieves an improved $PSR_{UNC}$. However, in ADR, EDs using unconfirmed packets may periodically receive a DL ACK response from the GW after 64 UL packets by setting *ADRACKReq* bit in the UL frame header [10, 98]. An ED generally ob-

tains this confirmation response to validate its connectivity with the GW. When an ED completes 64 UL packets transmission and does not receive any DL response, the ED enables *ADRACKReq* for the subsequent 32 packets. In the absence of an ACK response from the NS, the ADR on the ED side is triggered to increase the SF (i.e., SF<12). However, the decreasing trend in 7.7, in terms of $PSR_{UNC}$ is due to mobility. This mobility reduces signal strength; therefore, many EDs could not reach the GW because of the unfavorable channel condition, resulting in a high packet loss. These EDs stay active and cause interference in the nearby EDs, thereby restricting the LoRaWAN scalability.

In the case of M-ASFA in the confirmed mode (CON), $PSR_{CON}$ also decreases owing to the increase in the offered traffic. Nonetheless, a satisfactory $PSR_{CON}$ of 90% is achieved with the offered traffic of 10,000 packets/day. The decreasing trend in Fig. 7.7 of the $PSR_{CON}$ with the increase in the offered traffic is caused by the duty cycle constraints of both ED and GW. Moreover, owing to the transmission priority of ACK over UL at the GW, the UL packets from EDs that arrive at the GW are lost. However, the proposed M-ASFA proactively responds to ED mobility, and the SFs have been applied adaptively, resulting in improved $PSR_{CON}$. In contrast to a typical ADR, the M-ASFA scheme in the unconfirmed mode achieves the highest $PSR_{UNC}$. It fulfills the PSR requirement of all the applications by adapting a mobility-aware approach.

#### 7.4.1.2 Convergence Period

Fig. 7.8 presents another scenario of per-hour $PSR_{CON}$ at an offered traffic of 3,168 (packets per day) for both M-ASFA and ADR. In Fig. 7.8a, M-ASFA satisfies the minimum $PSR_{CON}$ requirements, whereas ADR fails to meet similar needs. From Fig. 7.8 (a) The ADR requires 17 h of convergence period (represented with black line). This verifies the typical ADR features, as described in [50]. The primary reason for this convergence period is the time required by the NS, which monitors the $M$ of the UL packets (i.e., $M = 20$). However, the $PSR_{CON}$ fluctuates with time even after the convergence period. This is because the ADR cannot adapt to the variable channel and mobility conditions. Conversely, M-ASFA follows a similar trend of $PSR_{CON}$. Therefore, no convergence time is required, as shown in Fig. 7.8 (a). M-ASFA adaptively assigns an optimal SF before a UL packet transmission. Thus, M-ASFA achieves a higher $PSR_{CON}$ compared with that of ADR.

Per-hour $PSR_{UNC}$ at an offered traffic of 3,168 (packets per day) for both M-ASFA and ADR is presented in Fig. 7.8 (b). Fig. 7.8 (b) shows that ADR is unable to converge to a stable PSR owing to the ED movement. The new SF and TP do not guarantee the fulfillment of the mobile application requirements in terms of PSR and reliability. As a result, the ADR fails to adapt itself to a reliable

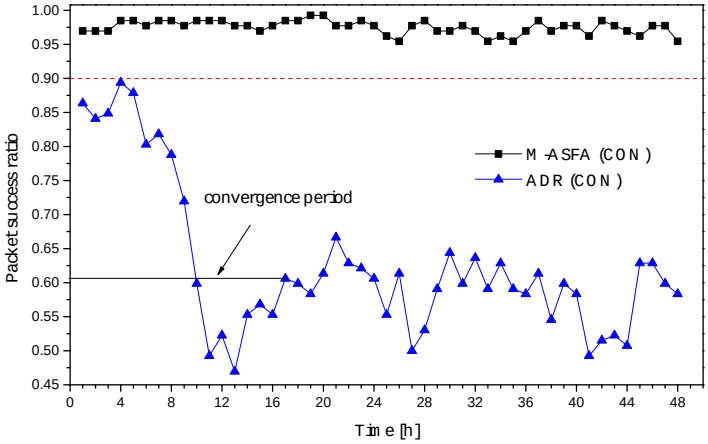


(a) Confirmed mode with PL = 50B and $\lambda$ = 48 packets/day

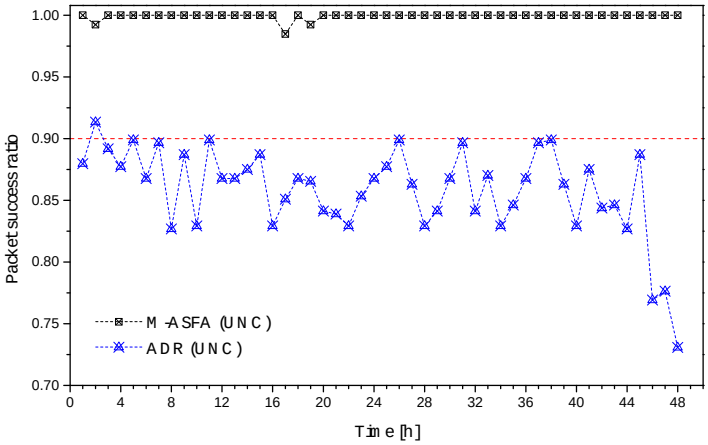


(b) Unconfirmed mode with PL = 50B and $\lambda$ = 48 packets/day

Figure 7.8: The per-hour of M-ASFA and ADR with offered traffic (O) [packets/day] = $N \times \lambda$.

and energy-efficient state. On the other hand, in Figs. 7.8 (b), no convergence period is observed because M-ASFA assigns the adaptive channel SF to the EDs, $PSR_{UNC}$ is shown to be larger and satisfied with the minimum PSR requirement of the pet-tracking application, compared with the $PSR_{UNC}$ in ADR.

#### 7.4.1.3 Energy consumption

Figs. 7.9 (a) and 7.9 (b) show energy consumption of M-ASFA and ADR in the confirmed and unconfirmed modes of communications, respectively. The cause of the low energy consumption of M-ASFA is the higher PSR. However, in the

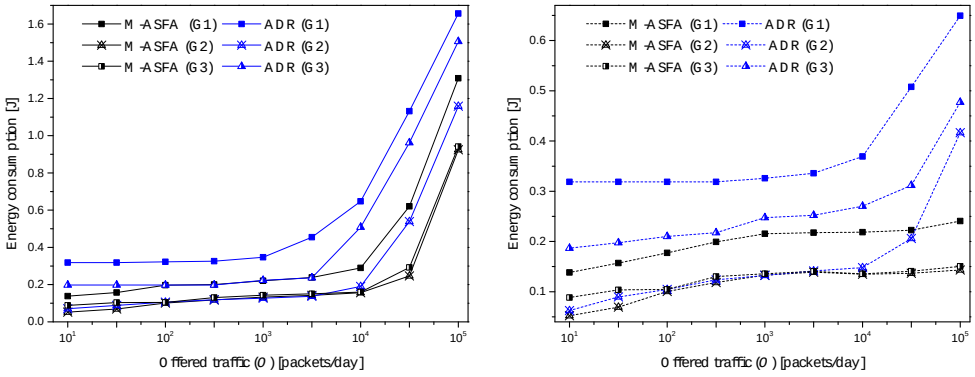


(a) Confirmed mode (b) Unconfirmed mode

Figure 7.9: Average energy consumption for M-ASFA and ADR.

case of ADR shown in Fig. 7.9 (a), when a mobile ED receives an ADR command from NS containing a new configuration of SF and/or TP, the propagation environment might have changed drastically. Therefore, the new configuration might not be valid, which results in packet loss. This situation causes massive retransmission, which results in a bottleneck at the GW. When a packet is retransmitted multiple times with high SF and TP, it eventually increases energy consumption, as shown in Fig. 7.9 (a). When packets are transmitted with higher SFs, it causes high interference. As higher SFs are highly susceptible to interference due to the high ToA, which can negatively affect energy consumption, as shown in Fig. 7.9 (b).

### 7.4.2 Analysis of R-ARM

This section presents detailed performance evaluation results of the proposed R-ARM compared with typical ADR approaches. The constraints of the proposed R-ARM and typical ADR approaches are listed in Table 7.5. The proposed R-ARM two mobile IoT applications as suggested by Semtech [11] and GSMA-3GPP [93]. Semtech in [11] introduced BADR and a pet-tracking application by sending GPS coordinates to the NS for monitoring real-time locations. Simultaneously, GSMA-3GPP suggests that agriculture-livestock tracking applications have different requirements compared to those of BADR. These application requirements are listed in Table 7.6.

#### 7.4.2.1 Packet success ratio

Fig. 7.10 shows the average PSR of the proposed R-ARM when compared with typical ADR approaches. Generally, the PSR decreases for all the methods when

Table 7.5: Constraints of the proposed R-ARM and typical ADR approaches under confirmed mode with SF = 12.

| Year | Scheme | ADR type | Simulation environment |
|---|---|---|---|
| 2017/2020 | typical ADR of LoRaWAN [2] | ED and NS sides | static EDs |
| 2018 | ADR+ [21] | NS side | static EDs |
| 2019 | blind ADR (BADR) [11] | ED side | mobile EDs |
| 2020 | enhanced ADR (EADR) [50] | ED and NS sides | static EDs |
| - | proposed R-ARM | ED and NS sides | mobile EDs |

Table 7.6: Mobile applications under confirmed mode.

| Application | Suggested by | Uplink interval [per day] | Packet size [bytes] |
|---|---|---|---|
| Pet-tracking | Semtech [11] | 144 (for a single ED) | 30 |
| Livestock tracking | GSMA-3GPP [93] | 100 (for a single ED) | 50 |

EDs increase. Thus, ED mobility affects PSR. Furthermore, given the changes in the location of EDs, the propagation environment around the ED can potentially be significantly altered when the ED receives a DL *LinkADRReq* command with SF and TP configuration in the case of ADR, ADR+, and EADR. Therefore, a packet with newly adapted SF and TP can not be successfully delivered to the GW, thereby resulting in massive packet loss.

Additionally, Fig. 7.10 exhibits a higher network load of 6 packets/hour (in the case of pet-tracking application), thereby leading to significant degradation in PSR and impairing scalability (in case of ADR, ADR+, and EADR). In the case of BADR, most of the transmitted packets that reach the GW are under the required sensitivity. Thus, congestion occurs in this situation, which causes massive PLR-S. Therefore, the proposed R-ARM performs significantly better compared with typical ADR approaches by selecting the best SF based on the number of retransmissions left regarding the GW sensitivity values.

#### 7.4.2.2 Combined PSR and PLR of the proposed R-ARM

Figure 7.11 represents the probabilities regarding the transmission of the proposed R-ARM for pet- and livestock applications. The sum of the probabilities of PSR and PLRs is equal to 1 in all cases. It is evident that the number of transmitted or retransmitted packets only contributes to either PSR or PLR.

#### 7.4.2.3 Convergence period

Fig. 7.12 shows the convergence period with per-hour PSR for the proposed R-ARM and typical ADR approaches at $N = 500$. ADR, ADR+, and R-ARM must initially wait for 20 UL packets to change the SF and TP. Therefore, 13- and 14-h convergence periods can be observed (in the pet-tracking application) for the

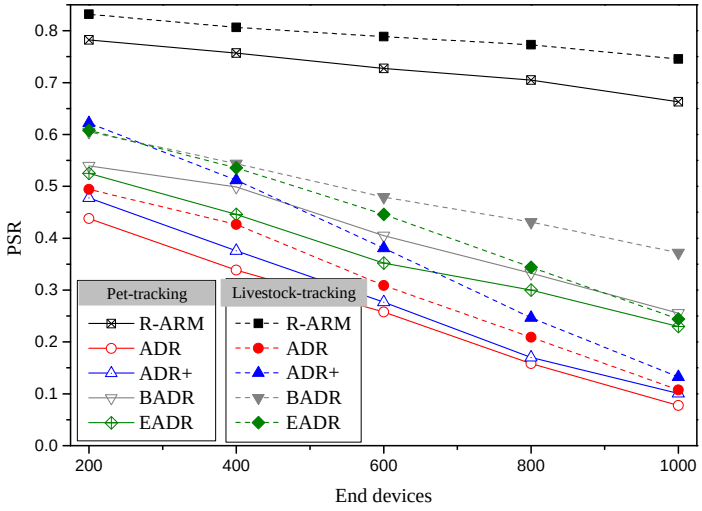


Figure 7.10: Average PSR of the proposed R-ARM and typical ADR approaches.

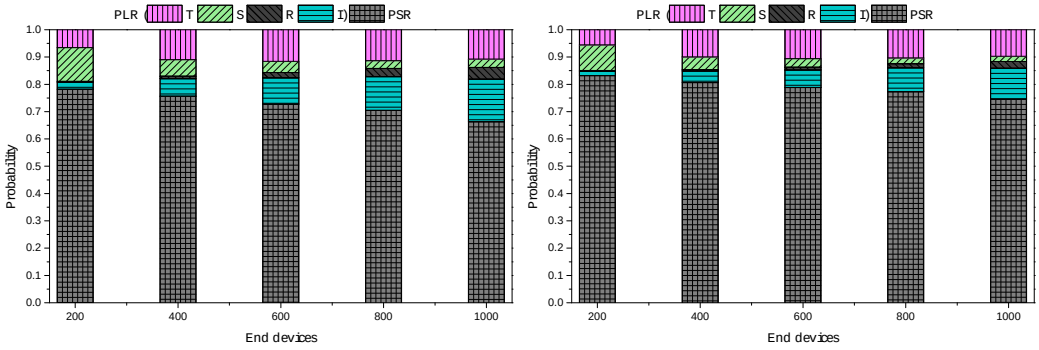


(a) Pet-tracking application (b) Livestock tracking application

Figure 7.11: Probability of PSR and PLRs of the proposed R-ARM ADR during the 1-d experiment.

ADR and ADR+, respectively. However, a livestock-tracking application requires 15 h and 16 h for the ADR and ADR+, respectively. For the ADR in livestock tracking, the PSR varies more with time, even after converging to a state of stability. The ADR and ADR+ fail to adapt to the underlying propagation model and mobility conditions.

As shown in Fig. 7.12, for converging to a steady-state in terms of the PSR, the EADR requires 4 h and 5 h, respectively. It is observed that when the UL interval is slower (in livestock tracking), the convergence period increases. In the case of a high UL interval (e.g., pet-tracking), the NS can quickly receive $M$ packets to

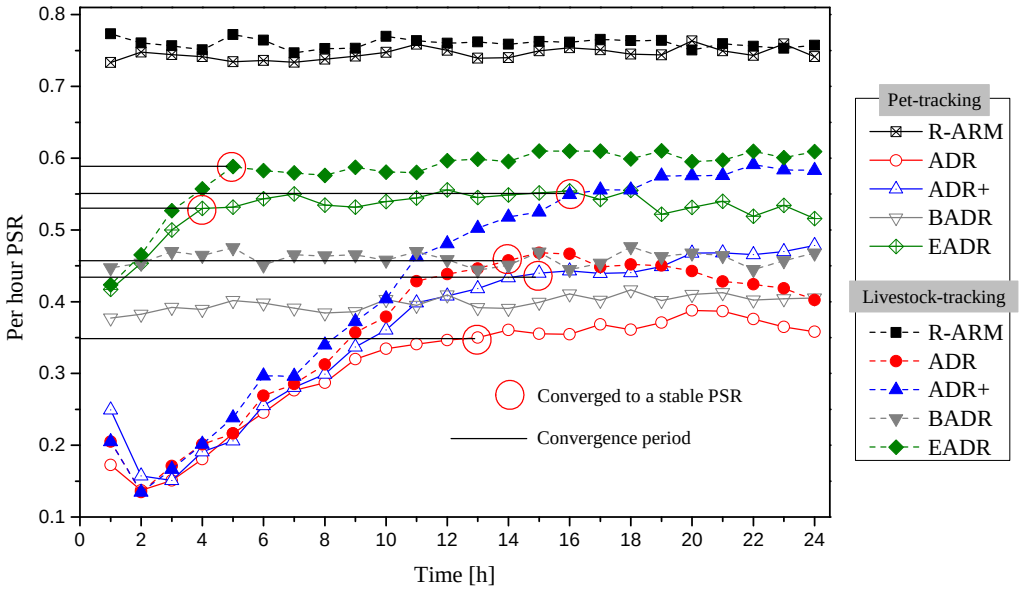


Figure 7.12: Convergence period with per-hour PSR of the proposed R-ARM and typical ADR approaches with $N = 500$.

determine the SF and TP. Additionally, EADR considers only $M = 5$ packets at the NS side and thus outperforms the ADR and ADR+ because it quickly adapts the SF and TP.

Conversely, BADR does not suffer from convergence by maintaining a stable PSR (lower PSR) than the EADR. Additionally, BADR does not require time to change the SF or TP and instead follows a fixed blind pattern (i.e., SF $\in$ [7, 10, 12]). The fixed and blind pattern can lead to packets arriving under the GW sensitivity at a lower SF. Conversely, the proposed R-ARM adaptively allocates the SF at the ED and NS sides and provides a stable PSR without a convergence time. Thus, the R-ARM realizes a higher PSR when compared to typical ADR approaches.

#### 7.4.2.4 Energy Consumption

It is observed that the energy consumption of R-ARM is stable and lower irrespective of the number of mobile EDs, as shown in Fig. 7.13. However, increases in the energy consumption pattern for typical ADR approaches are observed with increases in EDs and UL intervals. The packets are transmitted with SF = 12 and TP = 14, increasing interference (owing to a high ToA). Furthermore, the lost packets are retransmitted with similarly high SF and TP values. Therefore, higher energy consumption in a typical ADR approach is observed given that transmis-

sion energy consumption is mainly dependent on the SF, TP, ToA, and many retransmission attempts [66]. Another reason for this high energy consumption is that the ED moves away from the GW and may not receive an ACK in RX1. Therefore, the ED opens RX2, thereby resulting in additional energy consumption.

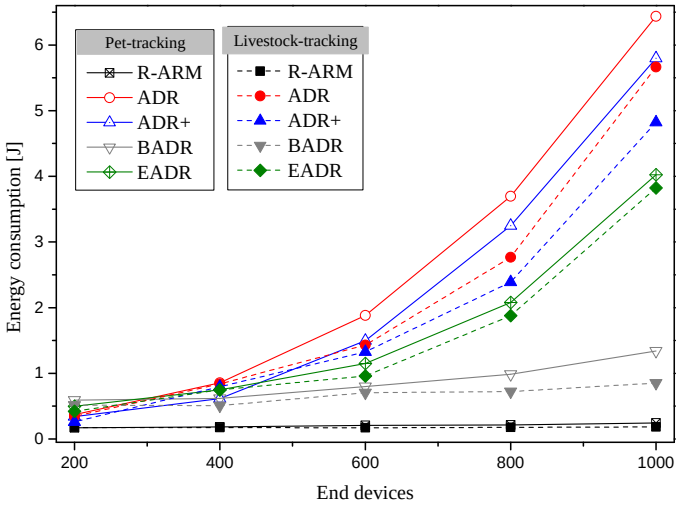


Figure 7.13: Average energy consumption.

#### 7.4.2.5 Fraction of end devices utilizing SF

Tables 7.7 and 7.8 show the fraction of the EDs utilizing final SF for pet- and livestock-tracking applications, while $N = 1000$. Evidently, in a massive LoRaWAN network, static ADRs can result in a situation where most of the EDs switch to the highest SF. This, in turn, increases the collision probability [10, 99]. A similar situation is observed for the static ADRs in Tables 7.7 and 7.8 with most of the EDs utilizing SF7 and SF12. The underlying mobility environment changes with ED movement, and the static ADRs cannot adapt to the channel conditions. However, the proposed R-ARM ADR proactively assigns a stable and suitable SF concerning the $P_{rx}$ and $\gamma$ at the ED side. However, at the NS side, R-ARM assigns the best SF by utilizing the two thresholds of Gaussian filter on $P_{rx}$ in conjunction with $\gamma$. Therefore, the utilization of a lower SF can result in fewer collisions [100].

Table 7.7: Fraction of the EDs (in percentage) utilizing SF in pet-tracking application with $N = 1000$.

| Spreading factor | ADR | ADR+ | EADR | BADR | R-ARM |
|---|---|---|---|---|---|
| SF 7 | 34 | 29.2 | 27.7 | 48.8 | 55.1 |
| SF 8 | 1.7 | 2.9 | 4.6 | 0 | 18.1 |
| SF 9 | 1.9 | 2.7 | 4.2 | 0 | 14.5 |
| SF 10 | 1.4 | 1.5 | 3.6 | 34.7 | 8.4 |
| SF 11 | 1.4 | 1.4 | 3.2 | 0 | 2.5 |
| SF 12 | 59.6 | 62.3 | 56.7 | 16.5 | 1.4 |

Table 7.8: Fraction of the EDs (in percentage) utilizing SF in livestock-tracking application with $N = 1000$.

| Spreading factor | ADR | ADR+ | EADR | BADR | R-ARM |
|---|---|---|---|---|---|
| SF 7 | 40.5 | 36.6 | 30.8 | 49 | 55.5 |
| SF 8 | 4.4 | 4.3 | 8 | 0 | 16.5 |
| SF 9 | 3.1 | 3.4 | 7 | 0 | 14.9 |
| SF 10 | 1.7 | 2.3 | 6.1 | 34.1 | 7.8 |
| SF 11 | 1.5 | 1.3 | 5.3 | 0 | 3.6 |
| SF 12 | 48.8 | 52.1 | 42.8 | 16.9 | 1.7 |

### 7.4.3 Analysis of AI-ERA Framework

In the case of AI-ERA framework, two IoT applications: electrical metering [89–91], and industrial asset tracking [92, 93] with requirements shown in Table 7.1 are considered.

#### 7.4.3.1 Evaluation of AI-ERA Framework in the Offline Mode

The AI-ERA framework model performance and confusion matrix are shown in Fig. 7.14. The model accuracy was recorded as 85%, as shown in Fig 7.14 (a). In Fig 7.14 (a), The accuracy and validation are increasing, and the loss is decreasing with the increasing number of epochs. The AI-ERA learns the pattern quickly and reaches good performance by efficiently predicting SF. Furthermore, the confusion matrix is shown in Fig 7.14 (b) shows the individual SF correct prediction.

Based on the performance of the model accuracy in the offline mode, the trained model was saved and thus will be utilized during the online mode to classify SF. Therefore, the proposed AI-ERA framework enhances the performance during the online mode owing to the best SF selection, reducing the chances of collision, interference and mitigating SF selection that can go under the required sensitivity threshold.

Table 7.9: Parameters and hyper-parameters utilized in the offline phase.

| Parameter | Value |
|---|---|
| Features | 4 |
| Python library | PyTorch: 1.9.0 |
| GPU | NVIDIA GeForce GTx 1050 Ti |
| Learning rate | 0.0001 |
| Hidden layers | 5 |
| Activation function | fully connected ReLu |
| Optimizer | Adam |
| Loss function | corss-entropy |

#### 7.4.3.2 AI-ERA Framework Analysis in the Online Mode

The pre-trained DNN model was trained using GPU; however, it uses CPU for SF classification when utilized in the online mode. Therefore, the proposed AI-ERA is lightweight.

#### 7.4.3.3 Packet success ratio

Fig. 7.15 shows the PSR, where the PSR decreases for all approaches with increasing EDs. The PSR decrease in the static scenario is due to the interference caused by Intra- and Inter-SF interferences. However, The PSR of BADR in both scenarios is static due to the use of only SF7, 10, 12.

The impact of PLR is higher in the mobility scenario compared to the static scenario. It is because ED mobility affects PSR. When ED moves around GW, the propagation environment changes dramatically. When ED employing ADR and GADR receives a DL *LinkADRReq* MAC command with newly configured SF and TP, a packet transmitted with these parameters can no longer be of assistance, causing packet loss.

Compared with typical ADR approaches, the proposed AI-ERA performs significantly better in static and mobility scenarios. The reason behind such an outstanding performance is that the DNN model learns the features for best of selection in the offline mode, thereby providing better SF classification for the transmitting ED before each UL transmission when utilized in the online mode. Thus, this proactive behavior of the AI-ERA framework reduces the chances of interference, resulting in improved PSR by 13% and 12% in static and mobility scenarios, respectively, when compared with ADR.

#### 7.4.3.4 Packet loss ratios (PLRs) of the Proposed AI-ERA Framework

Figure 7.16 represent the ratios of PSR and PLRs. Generally, the ratio of PSR and PLRs is equal to one. Thus, the amount of sent or retransmitted packets con-

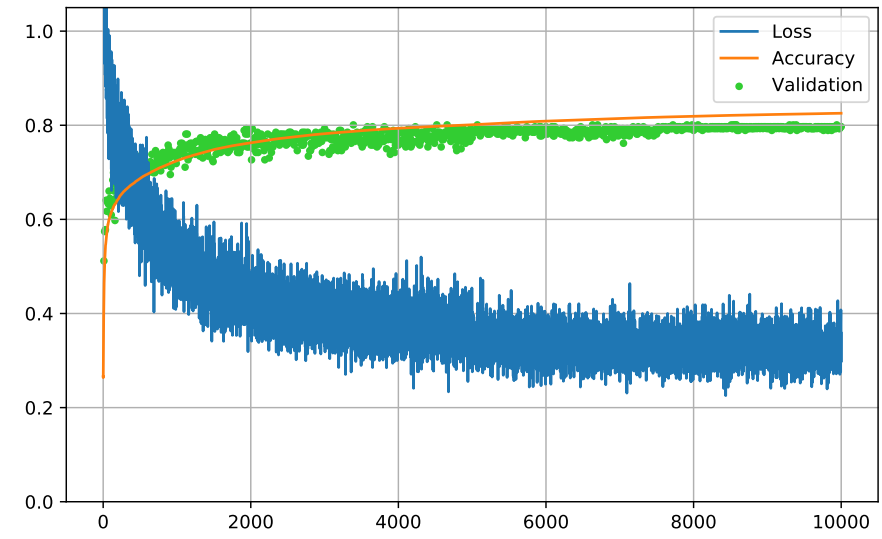


(a) Model accuracy

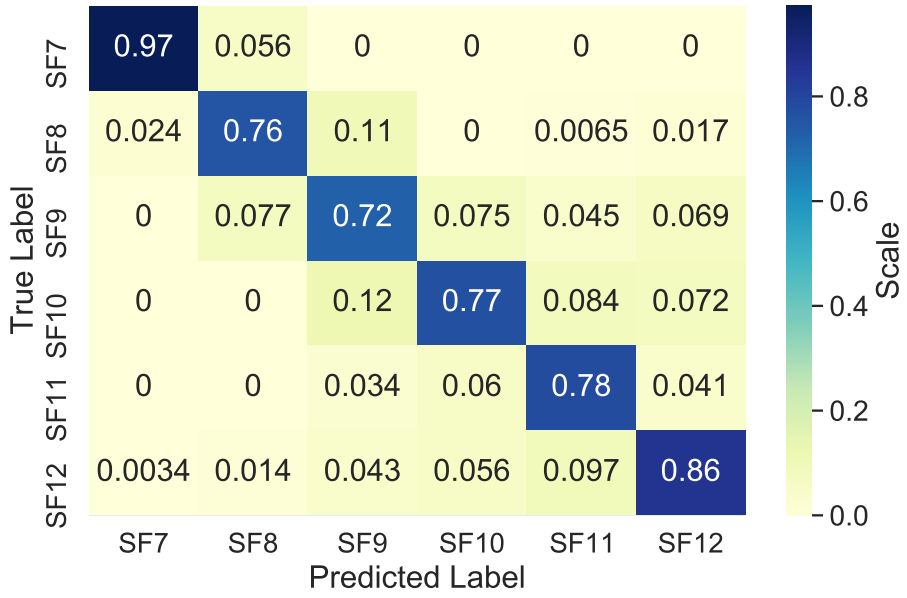


(b) Confusion matrix

Figure 7.14: Model performance during the offline mode.

tributes exclusively to either PSR or PLR.

As shown in Fig. 7.16 (a), AI-ERA is performing exceptionally well in terms of PLR-S under the static scenario owing to its proactive behavior of the online mode, classifying appropriate SF before UL packet transmission based on a se-

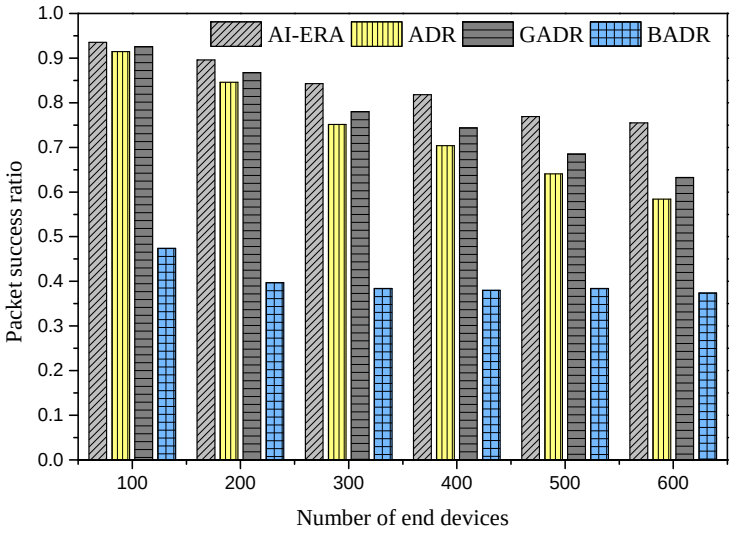


(a) Static scenario

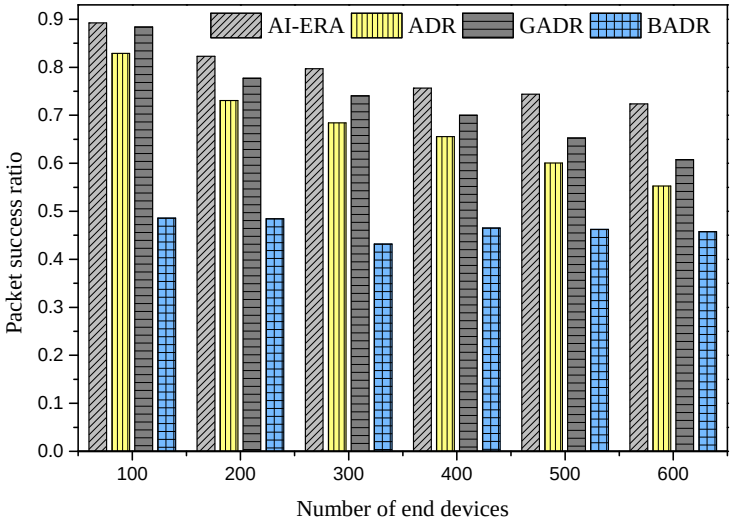


(b) Mobility scenario

Figure 7.15: Analysis of average packet success ratio.

quence of size $M$ (i.e., past 20 UL packets). Therefore, the static ED successfully delivers a packet with an adequately higher sensitivity than that is required. However, a small fraction of PLR-S is observed for the proposed AI-ERA framework due to a suitable SF classification.

On the other hand, in Fig. 7.16 (b), the impact of PLR-S is a little higher than that of static scenario owing to the ED movement. The ED movement causes drastic changes in location, $P_{rx}$, and SNR, resulting in an inaccurate SF classification

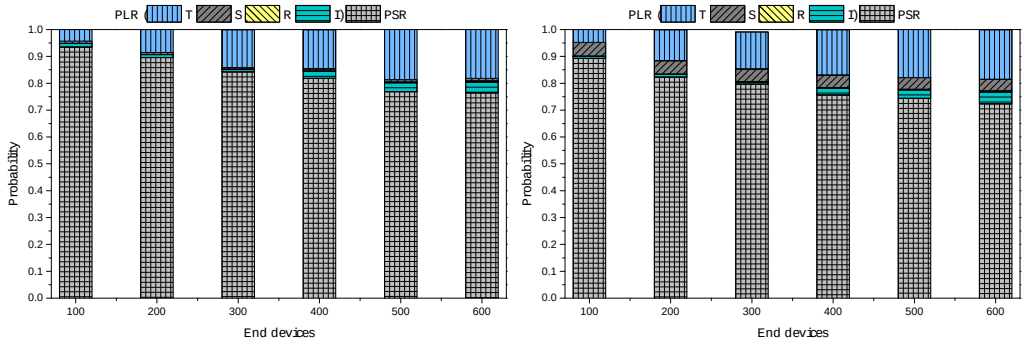


(a) Static scenario (b) Mobility scenario

Figure 7.16: Probability of PSR and PLRs for AI-ERA framework.

owing to the overfitting problem.

#### 7.4.3.5 Energy consumption

Fig. 7.17 shows the energy consumption, where the energy consumption trend increases for all approaches with increasing EDs.

(i) **Static Scenario:** The energy consumption of the proposed AI-ERA is much lower compared to the state-of-the-art ADR approaches, as shown in Fig. 7.17 (a). It is due to the proactive behavior of efficient SF selection at UL packet transmission. This behavior reduces the number of retransmissions. Another cause of the low energy consumption of the proposed AI-ERA is the higher *PSR* compared to other ADR approaches. Thus, the proposed AI-ERA outperforms state-of-the-art ADR approaches in the best SF classification for EDs and significantly reduces packet loss.

However, EDs employing ADR and GADR transmit packets with relatively high communication parameters (i.e., SF-12 and TP=14 dBm), resulting in massive packets owing to high interference. These lost packets are retransmitted with the same high communication parameters, increasing energy consumption. It is because the energy consumption of packet transmission is mainly based on SF, TP, ToA, and retransmissions parameters [68]. The energy consumption of BADR reveals that it is more energy-efficient when compared to the typical ADR and GADR.

(ii) **Mobility Scenario:** It is observed that the energy consumption of AI-ERA is lower compared to state-of-the-art ADR approaches, as shown in Fig. 7.17 (b). Since the SF selection in AI-ERA is based on prior knowledge, resulting

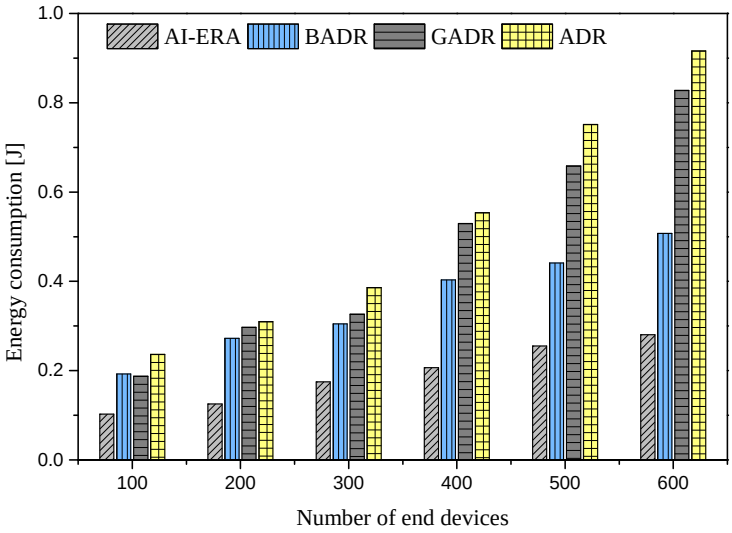


(a) Static scenario

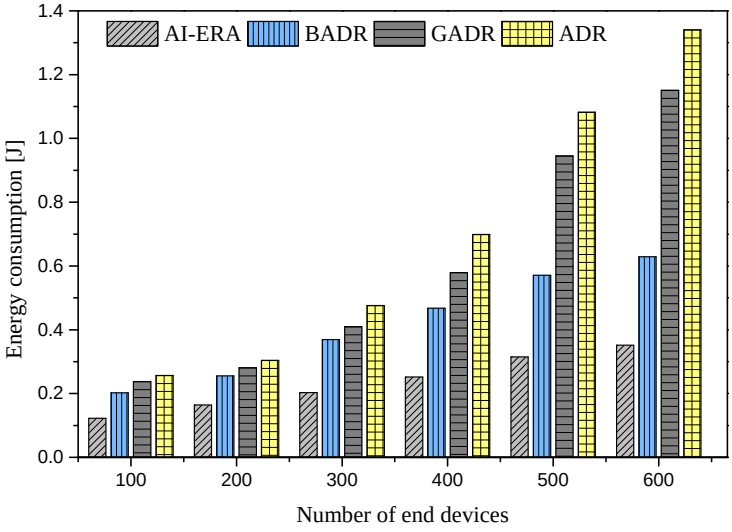


(b) Mobility scenario

Figure 7.17: Analysis of energy consumption in Joules.

in suitable SF classification. As a result, retransmission is significantly reduced, a primary reason for excessive energy consumption.

However, the energy consumption of ADR and GADR is increasing significantly. In the case of ADR and GADR, when a mobile ED receives an ADR command containing communication parameters (i.e., SF and TP) from NS, the propagation environment might have changed dramatically. Therefore, the new configuration might not be valid, resulting in packet loss. This situation causes

massive retransmission, creating a bottleneck at the GW. Thus, forcing ED to retransmit the lost packets with the same high transmission parameters increases the energy consumption, eventually. Furthermore, because higher SFs are highly susceptible to interference, they can negatively affect the energy consumption [33]. Furthermore, in a mobility scenario, ED migrates from one location to another, causing failure of ACK reception in RX1. Therefore, the ED opens RX2 with SF12, causing further energy consumption. In contrast, the primary aim of the BADR is to lower energy consumption, which is realized as shown in Fig. 7.17 (b). Thus, BADR outperforms typical ADR and GADR in terms of energy consumption.

#### 7.4.3.6 Convergence Period

Fig. 7.18 highlights the convergence period with per-hour PSR for the 24-h of simulation time with $N = 500$ concerning static and mobile scenarios. The EDs in all approaches begin UL packet transmission towards GW by employing SF12 with TP of 14 dBm, which is similar to that in [50, 51, 94, 101].

(i) **Static Scenario:** ADR and GADR must initially wait for $M$ (i.e., $M = 20$) UL packets to be received at the NS before altering SF and TP. Therefore, this waiting causes a convergence period of 12- and 15-h that can be noticed in a static ED scenario for ADR and GADR, respectively, as shown in Fig. 7.18 (a). Both ADR and GADR are activated after $M$ UL packets are received at the NS. However, when a UL packet is lost, both ADR and GADR have to wait longer since they start transmitting packets with SF12, which is susceptible to high interference owing to high ToA [18, 94, 102]. Therefore, this is a tedious operation, yielding a high convergence period.

Conversely, BADR suffers from a 7-h convergence period and then maintains a stable PSR (lower PSR) than the other approaches, as shown in Fig. 7.18 (a). Furthermore, BADR does not require time to alter the SF or TP. Instead, it follows a predetermined blind pattern using SF $\in$ [7, 10, 12]. The fixed and blind pattern can lead to packets arriving under the required threshold at GW at a lower SF.

In contrast to other approaches, the proposed AI-ERA only suffers from a 3-h convergence period in a static scenario, as highlighted in Fig. 7.18 (a). Although, AI-ERA transmits packets with SF12 with TP of 14 dBm during the initial period. It only waits for the first 20 UL packets (i.e., either received by the GW or lost) at the ED side before adapting an efficient SF. Therefore, this efficient, proactive approach of AI-ERA provides a stable PSR with only 4-h of convergence period, resulting in a higher PSR.

(ii) **Mobility Scenario:** Under the mobility scenario shown in Fig. 7.18 (b),

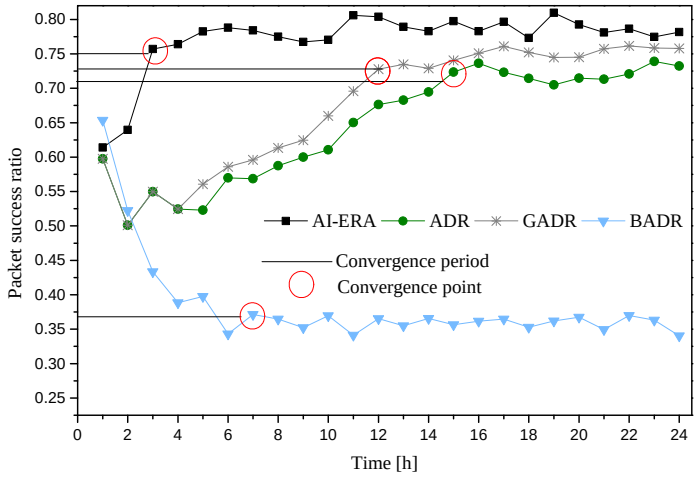


(a) Static scenario

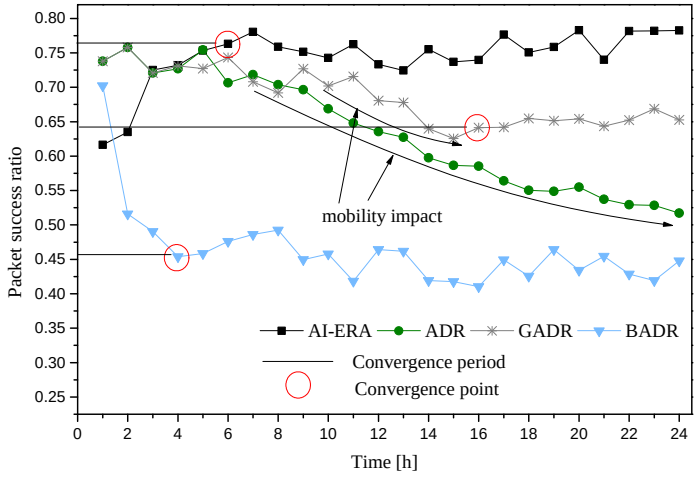


(b) Mobility scenario

Figure 7.18: Analysis of convergence period in hours.

GADR suffers from 16-h, while ADR failed to converge in 24-h of simulation time. This convergence time occurs while an ED is on the move and gets a new configuration (i.e., SF and TP) from the NS; the propagation scenario may have been substantially altered. As a result, the SF and link budget will be invalid, causing packet loss and huge retransmissions. Furthermore, due to massive retransmissions, some packets are lost due to ACK transmission priority at GW. In such a situation, the reception of a UL transmitted packet from ED gets interrupted at GW. As a result, the incoming packets from ED are lost at GW, increasing the wait time for the ADR and GADR to be initiated, causing a high

convergence period.

However, the convergence period of BADR has drastically decreased to 4-h. Eventually, a packet among SF $\in$ [7, 10, 12] can be received at the GW. For example, a packet lost with SF 7 at first try was lost, the next UL packet can be transmitted with SF 10 since the retransmission mechanism for the BADR is not explicitly defined in [11]. Therefore, the BADR blindly changes every ED SF for each UL packet transmission.

In contrast, the proposed AI-ERA suffers from the same convergence period (i.e., 6-h) under the mobility condition observed in a static scenario. Thus, it is evident that AI-ERA having 85% of accuracy in the offline mode classifies SF for every ED before UL packet transmission, yielding higher and stable PSR.

## 7.5 Experimental Analysis of Hybrid Resource Allocation

In this section, the analysis of the hybrid paradigm, namely HADR, is presented.

### 7.5.1 Analysis of HADR

Mobile EDs use Random Walk 2D mobility with a random speed between 2–4 m/s, as adapted in [94]. Both static and mobile ED transmit a UL packet every 10 minutes with a payload size of 30 bytes for a total simulation time of 24-h.

#### 7.5.1.1 Packet Success Ratio

Fig. 7.19 depicts the average PSR of the proposed HADR when compared with typical ADR and BADR approaches. In the mixed and static ED cases, ADR performs better than BADR because of the low variations in the channel conditions. In contrast, BADR shows improved performance in the mobility scenario only by blindly transmitting with SF 12, 10, and 7. However, ED mobility affects the PSR of ADR. In the case of ADR, when a DL *LinkADRReq* MAC command with new SF and TP parameters arrives at the GW, the propagation environment surrounding the ED might be drastically affected. As a result, the parameters are no longer helpful, resulting in packet loss owing to arriving under the required sensitivity thresholds

Compared to ADR and BADR, the proposed HADR performs significantly better by selecting the best SF using ADR+ for static EDs and blindly (without requiring prior knowledge, such as SNR or received power) transmitting with SF sequentially using the BADR+ for the mobile EDs. Thus, compared with typical ADR approaches, the proposed HADR enhanced the PSR, achieving its primary goal of PSR improvement in the mobility and mixed EDs scenarios, as shown in Fig. 7.20.

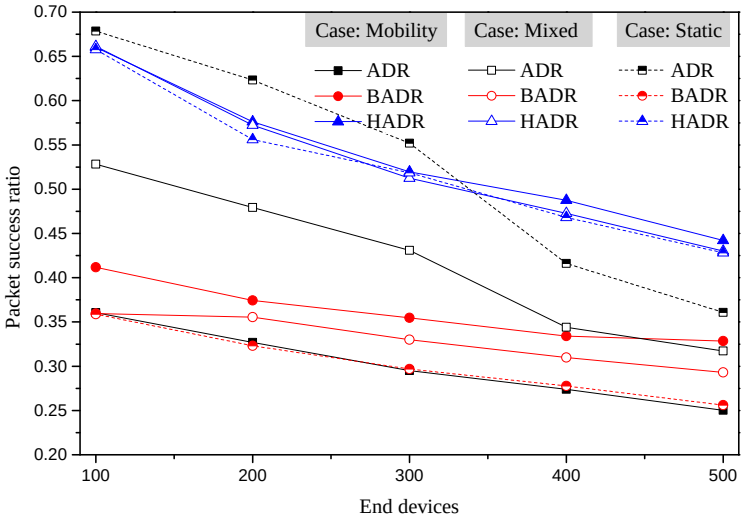


Figure 7.19: PSR of the HADR, BADR, and ADR under different ED conditions.

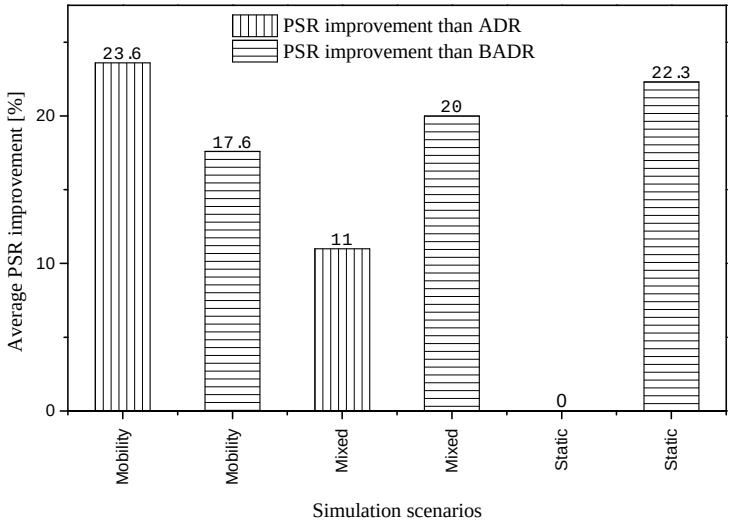


Figure 7.20: PSR improvement in the proposed HADR.

### 7.5.1.2 Packet Loss Ratios

Fig. 7.21 depicts the packet success and loss ratios under mixed scenarios (i.e., 50% of ED are static and 50% of the EDs are mobile). Generally, the ratios of PSR and PLRs equal one. Thus, the amount of sent or retransmitted packets contributes exclusively to PSR or PLR. In Fig. 7.21 (a), the ADR is primarily suffering from PLR-I and PLR-S, and PLR-T when the EDs increase. The PLR-I

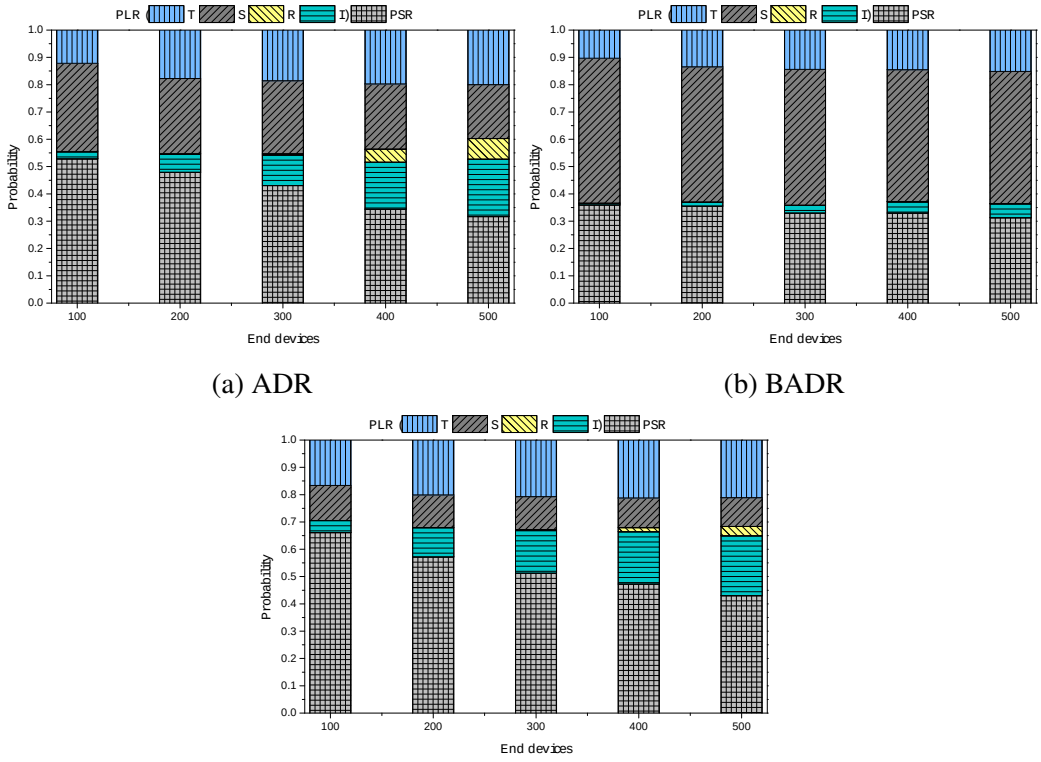


(a) ADR (b) BADR

(c) HADR

Figure 7.21: Packet success and loss ratios under mixed end devices (50% static and 50% mobile).

is caused due to high ToA when EDs transmit packets with SF of 12 during the initial deployment. A packet transmitted with these new SF and TP parameters arrives under the required threshold sensitivity at the GW, causing PLR-S. The PLR-T impact is approximately similar to all ADR approaches when the lost packets are retransmitted by ED (up to 7 times in the confirmed mode), increasing the network load in the UL direction and causing a collision with ACK. In the case of BADR shown in Fig. 7.21 (b), on average, 50% of the packets are lost owing to arriving under the required sensitivity threshold when transmitted with SF7 or SF10. Fig 7.21 (c) clearly shows that the proposed HADR resolves the issue of packets arriving under the required sensitivity by utilizing BADR+ and ADR+. Under a similar scenario, the final SF employed by the EDs is shown in Table 7.10.

Table 7.10: Final SF Utilization by the EDs in percentage for mixed end devices.

| Approach | SF7 | SF8 | SF9 | SF10 | SF11 | SF12 |
|---|---|---|---|---|---|---|
| ADR | 53.0 | 9.6 | 7.0 | 5.8 | 13.0 | 11.6 |
| BADR | 53.4 | 0 | 0 | 27.2 | 0 | 19.4 |
| HADR | 9.6 | 8.4 | 7.2 | 6.8 | 21.0 | 47.0 |

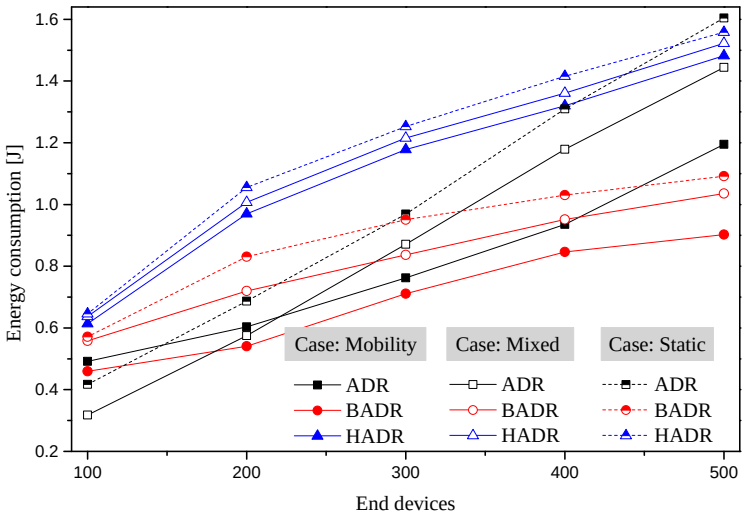


Figure 7.22: Average energy consumption in [J].

### 7.5.1.3 Energy Consumption

Fig. 7.22 shows an increase in energy consumption when the number of EDs is increased. The energy consumption of BADR is higher than ADR in the case of N = 100. With the increasing number of EDs, the energy consumption is gradually increased in ADR due to interference caused by an unsuitable SF and multiple retransmission attempts, thereby reducing the network scalability.

HADR utilizes ADR+ for static and BADR+ for mobile EDs. In the static ED scenario, the NS adjusts the SF and TP by taking the moving average of the SNR of the $M$ packets, reducing the energy consumption. However, when mobile EDs utilize BADR+, a packet can be retransmitted several times (up to 7 times in the confirmed mode) if an ED is not in the GW proximity. In such a situation, the retransmission mechanism in the proposed BADR+ can increase the SF (when SF $<$ 12) and allocate maximum allowed transmit power (i.e., TP = 14 dBm), at the cost of high energy consumption.

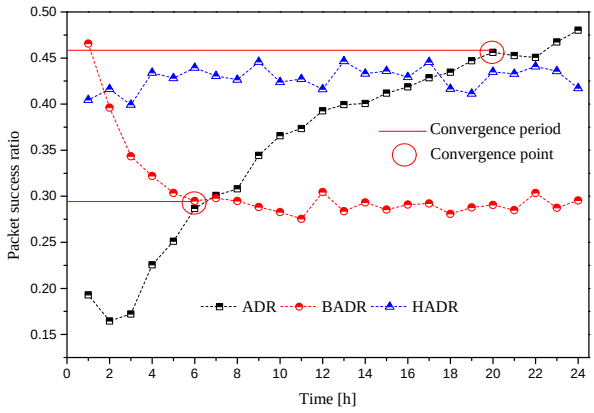


(a) Static scenario

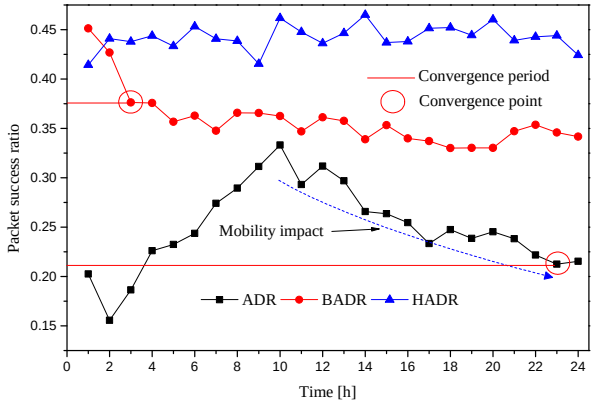


(b) Mobility scenario

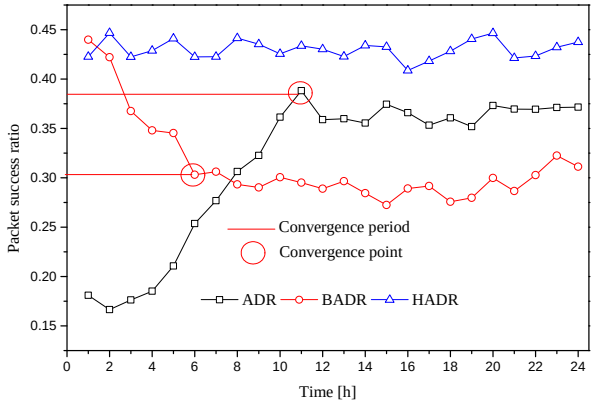


(c) Mixed scenario

Figure 7.23: Convergence period of ADR, BADR, and HADR with $N = 500$.

#### 7.5.1.4 Convergence Period Analysis

ADR is activated after $M$ UL packets are received at the NS. Therefore, waiting for $M$ packets cause a significant amount of convergence period up to 20, 23, and 11 hours in static, mobility, and mixed scenarios, respectively, as shown in Fig. 7.23. However, if a UL packet is lost, the ADR has to wait longer since it starts sending packets with SF12, which is susceptible to high interference owing to high ToA [18, 94, 102]. Therefore, this is a tedious operation, yielding a high convergence period. Conversely, BADR suffers from 6, 3, and 6 hours of convergence period and then maintains a stable PSR (lower PSR) than the other approaches, as shown in Fig. 7.18. Thus, the proposed HADR does not suffer from a convergence period in contrast to other approaches. Furthermore, the detailed convergence periods of all approaches in hours for static and mobile EDs are highlighted in Table 7.11.

Table 7.11: Convergence period in hours of ADR, BADR, and HADR with $N = 500$.

| **ADR** | | | **BADR** | | | **HADR** | | |
|---|---|---|---|---|---|---|---|---|
| static | mobile | mixed | static | mobile | mixed | static | mobile | mixed |
| 20 | 23 | 11 | 6 | 3 | 6 | 0 | 0 | 0 |

## 7.6 Summary

This chapter presented extensive simulation results of the proposed reactive, proactive, and hybrid paradigms. Through ns-3 simulation experiments, the proposed paradigms were extensively analyzed compared to typical ADR and state-of-the-art ADR approaches. As a result, the proposed paradigms significantly enhanced the PSR and reduced the energy consumption and convergence period.

# Chapter 8
# Conclusions and Future Directions

## 8.1 Conclusions

Resource management of LoRa-enabled devices deployed on a large scale is challenging due to underlying propagation conditions. LoRaWAN supports the ADR mechanism to manage the device resources, such as SF and TP. However, due to the sudden changes in the channel conditions, ADR cannot consider any appropriate measures to predict and provide evasive measures to alleviate the massive packet loss that is caused due to the unsuitable SF adapted by the devices. Therefore, this dissertation resolved the massive packet loss occurring due to inefficient SF by reactive, proactive, and hybrid approaches. Through extensive ns-3 simulation experiments, the proposed methods were compared to state-of-the-art methods. It was shown that the state-of-the-art methods suffer from a high convergence period owing to the time-consuming process and poor adaptation of the SF. Furthermore, it was observed that owing to the high convergence period, the state-of-the-art methods suffered from a high packet loss ratio and high energy consumption.

In contrast to the state-of-the-art approaches, the proposed methods adaptively assigned efficient resource parameters (e.g., SF and TP) to EDs. As a result, the proposed methods improved the PSR by reducing retransmissions and packets arriving under the required sensitivity thresholds. Furthermore, due to the assignment of efficient resource parameters to EDs, the reactive, proactive, and hybrid methods decreased energy consumption and the convergence period. Therefore, these proposed methods are suitable for IoT applications (e.g., smart metering and asset/livestock tracking) requiring reliability, low convergence period, high PSR, and ultra-low energy consumption.

## 8.2 Future directions

1. The proposed AI-ERA framework achieved significantly better results by efficiently allocating SF to ED. In the future, both SF and TP can be assigned to EDs simultaneously using the deep learning model (e.g., LSTM).

2. It was realized that the proposed AI-ERA framework at the ED side could be computationally costly. Therefore, it is intended to utilize the AI-ERA framework at the NS side in the future. As a result, the AI-ERA framework can decrease the computational cost and energy consumption.

3. In the future, the proposed pre-trained AI-ERA framework can be deployed in a real-world environment using a testbed.

# List of Publications

## Journals

1. **Arshad Farhad** and Jae-Young Pyun, "HADR: A Hybrid Adaptive Data Rate in LoRaWAN for Internet of Things," ICT Express, Jan. 2022, doi: 10.1016/J.ICTE.2021.12.013"

2. **Arshad Farhad**, Dae-Ho Kim, and Jae-Young Pyun, "R-ARM: Retransmission Assisted Resource Management in LoRaWAN for the Internet of Things." IEEE Internet of Things Journal, doi: 10.1109/JIOT.2021.3111167, pp: 1-1, (09 September, 2021).

3. **Arshad Farhad**, Dae-Ho Kim, Santosh Subedi, and Jae-Young Pyun, "Enhanced LoRaWAN Adaptive Data Rate for Mobile Internet of Things Devices." Sensors 20, no. 22 (2020): 6466.

4. **Arshad Farhad**, Dae-Ho Kim, Beom-Hun Kim, Alaelddin Fuad Yousif Mohammed, and Jae-Young Pyun, "Mobility-Aware Resource Assignment to IoT Applications in Long-Range Wide Area Networks." IEEE Access 8 (2020): pp.186111-186124.

5. **Arshad Farhad**, Dae-Ho Kim, and Jae-Young Pyun. "Resource Allocation to Massive Internet of Things in LoRaWANs." Sensors 20, no. 9 (2020): 2645.

## Conferences

1. **Arshad Farhad**, Dae-Ho Kim, Jeong-Sun Yoon, and Jae-Young Pyun, "Deep Learning-Based Channel Adaptive Resource Allocation in LoRaWAN" The 21st International Conference on Electronics, Information, and Communication (ICEIC 2022) (In Press at the time of thesis submission).

2. **Arshad Farhad**, Dae-Ho Kim, Jeong-Sun Yoon, and Jae-Young Pyun, "Feasibility Study of the LoRaWAN blind Adaptive Data Rate." In 2021 Twelfth International Conference on Ubiquitous and Future Networks, Jeju Island, Korea, 17-20 Aug. 2021, pp. 67-69. IEEE, 2021.

3. **Arshad Farhad**, Dae-Ho Kim, Daeyun Kwon, and Jae-Young Pyun, "An Improved Adaptive Data Rate for LoRaWAN Networks." In 2020 IEEE International Conference on Consumer Electronics-Asia (ICCE-Asia), Seoul, Korea, 1-3 Nov. 2020, pp. 1-4. IEEE, 2020.

4. **Arshad Farhad**, Dae-Ho Kim, and Jae-Young Pyun, "Scalability of LoRaWAN in an Urban Environment: A simulation Study." In 2019 Eleventh International Conference on Ubiquitous and Future Networks (ICUFN), Zagreb, Croatia, 2-5 July 2019, pp. 677-681. IEEE, 2019.

5. **Arshad Farhad**, Dae-Ho Kim, Pranesh Sthapit, and Jae-Young Pyun, "Interference Aware Spreading Factor Assignment Scheme for the Massive LoRaWAN Network." In 2019 International Conference on Electronics, Information, and Communication (ICEIC), Auckland, New Zealand, 22-25 Jan. 2019, pp. 1-2. IEEE, 2019

# Bibliography

[1] N. Ducrot, D. Ray, A. Saadani, O. Hersent, G. Pop, and G. Remond, "Lora device developer guide," 2016. [Online]. Available: https://developer.orange.com/wp-content/uploads/LoRa-Device-Developer-Guide-Orange.pdf

[2] LoRa, "Lorawan® regional parameters, rp002-1.0.2," Oct. 8 2020. [Online]. Available: https://lora-alliance.org/wp-content/uploads/2020/11/RP_2-1.0.2.pdf

[3] B. Citoni, F. Fioranelli, M. A. Imran, and Q. H. Abbasi, "Internet of things and lorawan-enabled future smart farming," *IEEE Internet of Things Magazine*, vol. 2, no. 4, pp. 14–19, 2019.

[4] T. T. Nguyen, H. H. Nguyen, R. Barton, and P. Grossetete, "Efficient design of chirp spread spectrum modulation for low-power wide-area networks," *IEEE Internet of Things Journal*, vol. 6, no. 6, pp. 9503–9515, 2019.

[5] U. Raza, P. Kulkarni, and M. Sooriyabandara, "Low power wide area networks: An overview," *IEEE Communications Surveys & Tutorials*, vol. 19, no. 2, pp. 855–873, 2017.

[6] A. Augustin, J. Yi, T. Clausen, and W. M. Townsley, "A study of lora: Long range & low power networks for the internet of things," *Sensors*, vol. 16, no. 9, p. 1466, 2016.

[7] Semtech, "Lora® and lorawan®: A technical overview," 2020. [Online]. Available: https://lora-developers.semtech.com/uploads/documents/files/LoRa_and_LoRaWAN-A_Tech_Overview-Downloadable.pdf

[8] R. Kufakunesu, G. P. Hancke, and A. M. Abu-Mahfouz, "A survey on adaptive data rate optimization in lorawan: Recent solutions and major challenges," *Sensors*, vol. 20, no. 18, p. 5044, 2020.

[9] V. Hauser and T. Hégr, "Proposal of adaptive data rate algorithm for lorawan-based infrastructure," in *2017 IEEE 5th International Conference on Future Internet of Things and Cloud (FiCloud), 21-23 Aug. 2017, Prague, Czech Republic*, 2017, pp. 85–90.

[10] J. Haxhibeqiri, E. De Poorter, I. Moerman, and J. Hoebeke, "A survey of lorawan for iot: From technology to application," *Sensors*, vol. 18, no. 11, p. 3995, 2018.

[11] Semtech, "Lorawan mobile applications: Blind adr," 2019. [Online]. Available: https://lora-developers.semtech.com/uploads/documents/files/LoRaWAN_Mobile_Apps-Blin_ADR_Downloadable.pdf

[12] G. Pasolini, "On the lora chirp spread spectrum modulation. signal properties and their impact on transmitter and receiver architectures." *IEEE Transactions on Wireless Communications*, pp. 1–1, 2021.

[13] C. Goursaud and J.-M. Gorce, "Dedicated networks for iot: Phy/mac state of the art and challenges," *EAI endorsed transactions on Internet of Thingsl*, 2015. [Online]. Available: https://hal.archives-ouvertes.fr/hal-01231221/

[14] B. Xie, Y. Yin, and J. Xiong, "Pushing the limits of long range wireless sensing with lora," *Proceedings of the ACM on Interactive, Mobile, Wearable and Ubiquitous Technologies*, vol. 5, no. 3, pp. 1–21, 2021.

[15] S. Corporation, "Lora modulation basics," 2015. [Online]. Available: https://www.frugalprototype.com/wp-content/uploads/2016/08/an1200.22.pdf

[16] Semtech, "Semtech sx1301 wireless & sensing products datasheet," 2017. [Online]. Available: https://www.semtech.com/products/wireless-rf/lora-gateways/sx1301

[17] ——, "Semtech wireless & sensing products, sx1272," 2019. [Online]. Available: https://semtech.my.salesforce.com/sfc/p/#E0000000JelG/a/440000001NCE/v_VBhk1IolDgxwwnOpcS_vTFxPfSEPQbuneK3mWsXlU

[18] A. Farhad, D.-H. Kim, and J.-Y. Pyun, "Resource allocation to massive internet of things in lorawans," *Sensors*, vol. 20, no. 2645, pp. 1–20, 2020.

[19] Semtech, "An in-depth look at lorawan® class a devices," 2019. [Online]. Available: https://lora-developers.semtech.com/uploads/documents/files/LoRaWAN_Class_A_Devices_In_Depth_Downloadable.pdf

[20] S. Li, U. Raza, and A. Khan, "How agile is the adaptive data rate mechanism of lorawan," in *IEEE Global Communications Conference (GLOBECOM), Abu Dhabi, United Arab Emirates, 9-13 Dec.* IEEE, 2018, pp. 206–212.

[21] M. Slabicki, G. Premsankar, and M. Di Francesco, "Adaptive configuration of lora networks for dense iot deployments," in *IEEE/IFIP Network Operations and Management Symposium*. IEEE, 2018, pp. 1–9.

[22] F. Van den Abeele, J. Haxhibeqiri, I. Moerman, and J. Hoebeke, "Scalability analysis of large-scale lorawan networks in ns-3," *IEEE Internet of Things Journal*, vol. 4, no. 6, pp. 2186–2198, 2017.

[23] S. Li, U. Raza, and A. Khan, "How agile is the adaptive data rate mechanism of lorawan?" in *2018 IEEE Global Communications Conference (GLOBECOM)*. IEEE, 2018, pp. 206–212.

[24] K. Kousias, G. Caso, Ö. Alay, and F. Lemic, "Empirical analysis of lorawan adaptive data rate for mobile internet of things applications," in *Proceedings of the 2019 on Wireless of the Students, by the Students, and for the Students Workshop, October, 2019*, 2019, pp. 9–11.

[25] Semtech, "Understanding the lora adaptive data rate," 2019. [Online]. Available: https://lora-developers.semtech.com/uploads/documents/files/Understanding_LoRa_Adaptive_Data_Rate_Downloadable.pdf

[26] ETSI, "System reference document (srdoc); technical characteristics for low power wide area networks and chirp spread spectrum (lpwan-css) operating in the uhf spectrum below 1 ghz; etsi tr 103 526 v1.1.1 (2018-04)," 2018. [Online]. Available: https://www.etsi.org/deliver/etsi_tr/103500_103599/103526/01.01.01_60/tr_103526v010101p.pdf

[27] B. Reynders, W. Meert, and S. Pollin, "Power and spreading factor control in low power wide area networks," in *IEEE International Conference on Communications (ICC), Paris, France, 21-25 May 2017*. IEEE, 2017, pp. 1–6.

[28] J.-T. Lim and Y. Han, "Spreading factor allocation for massive connectivity in lora systems," *IEEE Communications Letters*, vol. 22, no. 4, pp. 800–803, 2018.

[29] I. E. Korbi, Y. Ghamri-Doudane, and L. A. Saidane, "Lorawan analysis under unsaturated traffic, orthogonal and non-orthogonal spreading factor conditions," in *2018 IEEE 17th International Symposium on Network Computing and Applications (NCA)*. IEEE, 2018, pp. 1–9.

[30] D. Croce, M. Gucciardo, I. Tinnirello, D. Garlisi, and S. Mangione, "Impact of spreading factor imperfect orthogonality in lora communications," in *International Tyrrhenian Workshop on Digital Communication*. Springer, 2017, pp. 165–179.

[31] G. Zhu, C.-H. Liao, M. Suzuki, Y. Narusue, and H. Morikawa, "Evaluation of lora receiver performance under co-technology interference," in *2018 15th IEEE Annual Consumer Communications & Networking Conference (CCNC), Las Vegas, NV, USA, 12-15 Jan. 2018*. IEEE, 2018, pp. 1–7.

[32] A. Waret, M. Kaneko, A. Guitton, and N. El Rachkidy, "Lora throughput analysis with imperfect spreading factor orthogonality," *IEEE Wireless Communications Letters*, vol. 8, no. 2, pp. 408–411, 2018.

[33] C. Caillouet, M. Heusse, and F. Rousseau, "Optimal sf allocation in lorawan considering physical capture and imperfect orthogonality," in *GLOBECOM 2019 - IEEE Global Communications Conference, Dec 2019, Waikoloa, United States, hal-02267218*, 2019, pp. 1–8.

[34] R. B. Sørensen, D. M. Kim, J. J. Nielsen, and P. Popovski, "Analysis of latency and mac-layer performance for class a lorawan," *IEEE Wireless Communications Letters*, vol. 6, no. 5, pp. 566–569, 2017.

[35] J. Haxhibeqiri, F. Van den Abeele, I. Moerman, and J. Hoebeke, "Lora scalability: A simulation model based on interference measurements," *Sensors*, vol. 17, no. 6, p. 1193, 2017.

[36] D. Zorbas, G. Z. Papadopoulos, P. Maille, N. Montavont, and C. Douligeris, "Improving lora network capacity using multiple spreading factor configurations," in *2018 25th International Conference on Telecommunications (ICT)*. IEEE, 2018, pp. 516–520.

[37] L. Feltrin, C. Buratti, E. Vinciarelli, R. De Bonis, and R. Verdone, "Lorawan: Evaluation of link-and system-level performance," *IEEE Internet of Things Journal*, vol. 5, no. 3, pp. 2249–2258, 2018.

[38] B. Reynders, Q. Wang, P. Tuset-Peiro, X. Vilajosana, and S. Pollin, "Improving reliability and scalability of lorawans through lightweight scheduling," *IEEE Internet of Things Journal*, vol. 5, no. 3, pp. 1830–1842, 2018.

[39] V. Gupta, S. K. Devar, N. H. Kumar, and K. P. Bagadi, "Modelling of iot traffic and its impact on lorawan," in *GLOBECOM 2017-2017 IEEE*

*Global Communications Conference, Rome, Italy, 9-11 Oct. 2017*. IEEE, 2017, pp. 1–6.

[40] S. Kim, H. Lee, and S. Jeon, "An adaptive spreading factor selection scheme for a single channel lora modem," *Sensors*, vol. 20, no. 4, p. 1008, 2020.

[41] D. Garlisi, I. Tinnirello, G. Bianchi, and F. Cuomo, "Capture aware sequential waterfilling for lorawan adaptive data rate," *IEEE Transactions on Wireless Communications*, vol. 20, no. 3, pp. 2019–2033, 2021.

[42] F. Cuomo, M. Campo, A. Caponi, G. Bianchi, G. Rossini, and P. Pisani, "Explora: Extending the performance of lora by suitable spreading factor allocations," in *2017 IEEE 13th International Conference on Wireless and Mobile Computing, Networking and Communications (WiMob)*, 2017, pp. 1–8.

[43] F. Cuomo, J. C. C. Gámez, A. Maurizio, L. Scipione, M. Campo, A. Caponi, G. Bianchi, G. Rossini, and P. Pisani, "Towards traffic-oriented spreading factor allocations in lorawan systems," in *2018 17th Annual Mediterranean Ad Hoc Networking Workshop (Med-Hoc-Net)*, 2018, pp. 1–8.

[44] A. Peruzzo and L. Vangelista, "A power efficient adaptive data rate algorithm for lorawan networks," in *2018 21st International Symposium on Wireless Personal Multimedia Communications (WPMC)*. IEEE, 2018, pp. 90–94.

[45] D. Bankov, E. Khorov, and A. Lyakhov, "On the limits of lorawan channel access," in *2016 International Conference on Engineering and Telecommunication (EnT), Moscow, Russia, 29-30 Nov. 2016*. IEEE, 2016, pp. 10–14.

[46] ——, "Mathematical model of lorawan channel access with capture effect," in *2017 IEEE 28th Annual International Symposium on Personal, Indoor, and Mobile Radio Communications (PIMRC), Montreal, QC, Canada, 8-13 Oct. 2017*. IEEE, 2017, pp. 1–5.

[47] M. Capuzzo, D. Magrin, and A. Zanella, "Mathematical modeling of lora wan performance with bi-directional traffic," in *2018 IEEE Global Com-*

*munications Conference (GLOBECOM), Abu Dhabi, United Arab Emirates, 9-13 Dec. 2018*. IEEE, 2018, pp. 206–212.

[48] D.-Y. Kim, S. Kim, H. Hassan, and J. H. Park, "Adaptive data rate control in low power wide area networks for long range iot services," *Journal of computational science*, vol. 22, pp. 171–178, 2017.

[49] J. Park, K. Park, H. Bae, and C.-k. Kim, "Earn: Enhanced adr with coding rate adaptation in lorawan," *IEEE Internet of Things Journal*, 2020.

[50] J. Finnegan, R. Farrell, and S. Brown, "Analysis and enhancement of the lorawan adaptive data rate scheme," *IEEE Internet of Things Journal*, vol. 7, no. 8, pp. 7171–7180, 2020.

[51] A. Farhad, D.-H. Kim, S. Subedi, and J.-Y. Pyun, "Enhanced lorawan adaptive data rate for mobile internet of things devices," *Sensors*, vol. 20, no. 22, p. 6466, 2020.

[52] "Network simulator (ns)-3," Accessed: Jan. 10, 2021. [Online]. Available: https://www.nsnam.org/

[53] V. Moysiadis, T. Lagkas, V. Argyriou, A. Sarigiannidis, I. D. Moscholios, and P. Sarigiannidis, "Extending adr mechanism for lora enabled mobile end-devices," *Simulation Modelling Practice and Theory*, vol. 113, p. 102388, 2021.

[54] K. Anwar, T. Rahman, A. Zeb, I. Khan, M. Zareei, and C. Vargas-Rosales, "Rm-adr: Resource management adaptive data rate for mobile application in lorawan," *Sensors*, vol. 21, no. 23, 2021. [Online]. Available: https://www.mdpi.com/1424-8220/21/23/7980

[55] T. Hossain, Y. Doi, T. Tazin, M. A. R. Ahad, and S. Inoue, "Study of lorawan technology for activity recognition," in *Proceedings of the 2018 ACM International Joint Conference and 2018 International Symposium on Pervasive and Ubiquitous Computing and Wearable Computers*, 2018, pp. 1449–1453.

[56] C. A. Gomez, A. Shami, and X. Wang, "Machine learning aided scheme for load balancing in dense iot networks," *Sensors*, vol. 18, no. 11, p. 3779, 2018.

[57] T. Yatagan and S. Oktug, "Smart spreading factor assignment for lorawans," in *2019 IEEE Symposium on Computers and Communications (ISCC)*. IEEE, 2019, pp. 1–7.

[58] F. Cuomo, D. Garlisi, A. Martino, and A. Martino, "Predicting lorawan behavior: How machine learning can help," *Computers*, vol. 9, no. 3, p. 60, 2020.

[59] S. Cui and I. Joe, "Collision prediction for a low power wide area network using deep learning methods," *Journal of Communications and Networks*, vol. 22, no. 3, pp. 205–214, 2020.

[60] M. C. Bor, U. Roedig, T. Voigt, and J. M. Alonso, "Do lora low-power wide-area networks scale?" in *Proceedings of the 19th ACM International Conference on Modeling, Analysis and Simulation of Wireless and Mobile Systems*, 2016, pp. 59–67.

[61] D. Magrin, M. Centenaro, and L. Vangelista, "Performance evaluation of lora networks in a smart city scenario," in *IEEE International Conference on communications (ICC), Paris, France, 21-25 May 2017*. IEEE, 2017, pp. 1–7.

[62] M. Capuzzo, D. Magrin, and A. Zanella, "Confirmed traffic in lorawan: Pitfalls and countermeasures," in *2018 17th Annual Mediterranean Ad Hoc Networking Workshop (Med-Hoc-Net), Capri, Italy, 20-22 June*. IEEE, 2018, pp. 1–7.

[63] S. S. Borkotoky, J. F. Schmidt, U. Schilcher, P. Battula, and S. Rathi, "Reliability and energy consumption of lora with bidirectional traffic," *IEEE Communications Letters*, pp. 1–1, 2021.

[64] 3GPP, "Cellular system support for ulta-low complexity and low throughput internet of things (ciot)," 2016. [Online]. Available: https://itectec.com/archive/3gpp-specification-tr-45-820/

[65] F. S. D. Silva, E. P. Neto, H. Oliveira, D. Rosário, E. Cerqueira, C. Both, S. Zeadally, and A. V. Neto, "A survey on long-range wide-area network technology optimizations," *IEEE Access*, vol. 9, pp. 106 079–106 106, 2021.

[66] A. Farhad, D. H. Kim, B. H. Kim, A. F. Y. Mohammed, and J. Y. Pyun, "Mobility-aware resource assignment to iot applications in long-range wide area networks," *IEEE Access*, vol. 8, pp. 186 111–186 124, 2020.

[67] A. Farhad, D. Kim, and J. Pyun, "Scalability of lorawan in an urban environment: A simulation study," in *Eleventh International Conference on Ubiquitous and Future Networks (ICUFN), Zagreb, Croatia, 2-5 July 2019*, July 2019, pp. 677–681.

[68] J. Finnegan, K. Niotaki, and S. Brown, "Exploring the boundaries of ambient rf energy harvesting with lorawan," *IEEE Internet of Things Journal*, pp. 1–1, 2020.

[69] A. Farhad, D. H. Kim, D. Kwon, and J. Y. Pyun, "An improved adaptive data rate for lorawan networks," in *2020 IEEE International Conference on Consumer Electronics - Asia (ICCE-Asia), 1-3 Nov., Seoul, Korea*, 2020, pp. 1–4.

[70] M. Aernouts, N. BniLam, N. Podevijn, D. Plets, W. Joseph, R. Berkvens, and M. Weyn, "Combining tdoa and aoa with a particle filter in an outdoor lorawan network," in *2020 IEEE/ION Position, Location and Navigation Symposium (PLANS)*. IEEE, 2020, pp. 1060–1069.

[71] S. Subedi and J.-Y. Pyun, "Practical fingerprinting localization for indoor positioning system by using beacons," *Journal of Sensors*, vol. 2017, 2017.

[72] S. Subedi, H.-S. Gang, N. Y. Ko, S.-S. Hwang, and J.-Y. Pyun, "Improving indoor fingerprinting positioning with affinity propagation clustering and weighted centroid fingerprint," *IEEE Access*, vol. 7, pp. 31 738–31 750, 2019.

[73] L. Alliance, "Lorawan 1.1 regional parameters," 2017. [Online]. Available: https://lora-alliance.org/sites/default/files/2018-04/lorawantm_regional_parameters_v1.1rb_-_final.pdf

[74] A. Carlsson, I. Kuzminykh, R. Franksson, and A. Liljegren, "Measuring a lora network: performance, possibilities and limitations," in *Internet of Things, Smart Spaces, and Next Generation Networks and Systems, 29 September 2018*. Springer, 2018, pp. 116–128.

[75] C. Demeslay, P. Rostaing, and R. Gautier, "Theoretical performance of lora system in multi-path and interference channels," *IEEE Internet of Things Journal*, pp. 1–1, 2021.

[76] S. Narieda, T. Fujii, and K. Umebayashi, "Energy constrained optimization for spreading factor allocation in lorawan," *Sensors*, vol. 20, no. 16, p. 4417, 2020.

[77] G. G. M. de Jesus, R. D. Souza, C. Montez, and A. Hoeller, "Lorawan adaptive data rate with flexible link margin," *IEEE Internet of Things Journal*, vol. 8, no. 7, pp. 6053–6061, 2020.

[78] STM32, "Stm32 lora® expansion package for stm32cube," 2021.

[79] L. Alliance, "Fuota process summary technical recommendation, tr002 v1.0.0," 2019. [Online]. Available: https://lora-alliance.org/sites/default/files/2019-04/tr002-fuota_process_summary-v1.0.0.pdf

[80] I. Goodfellow, Y. Bengio, and A. Courville, *Deep learning*. MIT press, 2016.

[81] Y. Zhou, Z. M. Fadlullah, B. Mao, and N. Kato, "A deep-learning-based radio resource assignment technique for 5g ultra dense networks," *IEEE Network*, vol. 32, no. 6, pp. 28–34, 2018.

[82] C. Zhang, P. Patras, and H. Haddadi, "Deep learning in mobile and wireless networking: A survey," *IEEE Communications surveys & tutorials*, vol. 21, no. 3, pp. 2224–2287, 2019.

[83] J. Wang, J. Tang, Z. Xu, Y. Wang, G. Xue, X. Zhang, and D. Yang, "Spatiotemporal modeling and prediction in cellular networks: A big data enabled deep learning approach," in *IEEE INFOCOM 2017-IEEE Conference on Computer Communications*. IEEE, 2017, pp. 1–9.

[84] A. Furno, M. Fiore, and R. Stanica, "Joint spatial and temporal classification of mobile traffic demands," in *IEEE INFOCOM 2017-IEEE Conference on Computer Communications*. IEEE, 2017, pp. 1–9.

[85] T. J. O'Shea, S. Hitefield, and J. Corgan, "End-to-end radio traffic sequence recognition with recurrent neural networks," in *2016 IEEE Global Conference on Signal and Information Processing (GlobalSIP)*. IEEE, 2016, pp. 277–281.

[86] S. Rajendran, W. Meert, D. Giustiniano, V. Lenders, and S. Pollin, "Deep learning models for wireless signal classification with distributed low-cost spectrum sensors," *IEEE Transactions on Cognitive Communications and Networking*, vol. 4, no. 3, pp. 433–445, 2018.

[87] N. E. West and T. O'Shea, "Deep architectures for modulation recognition," in *2017 IEEE International Symposium on Dynamic Spectrum Access Networks (DySPAN)*. IEEE, 2017, pp. 1–6.

[88] G. Shen, J. Zhang, A. Marshall, L. Peng, and X. Wang, "Radio frequency fingerprint identification for lora using deep learning," *IEEE Journal on Selected Areas in Communications*, 2021.

[89] S. Corporation, "Real-world lorawan® network capacity for electrical metering applications," 2017. [Online]. Available: https://info.semtech.com/network_capacity_white_paper_download

[90] ——, "Lora® devices: Smart utilities real world solutions," 2018. [Online]. Available: https://info.semtech.com/smart-utilities-e-book

[91] ——, "Why lorawan® is the logical choice for asset-tracking connectivity?" 2020. [Online]. Available: https://lora-alliance.org/wp-content/uploads/2020/11/WhitePaper_AssetTracking.pdf

[92] ——, "Smart supply chain and logistics," 2017. [Online]. Available: https://www.semtech.com/uploads/technology/LoRa/app-briefs/Semtech_SupChain_AssetTracking-Airport_AppBrief-FINAL.pdf

[93] GSMA-3GPP, "3gpp low power wide area technologies," 2016. [Online]. Available: https://www.gsma.com/iot/wp-content/uploads/2016/10/3GPP-Low-Power-Wide-Area-Technologies-GSMA-White-Paper.pdf

[94] A. Farhad, D.-H. Kim, and J.-Y. Pyun, "R-arm: Retransmission-assisted resource management in lorawan for the internet of things," *IEEE Internet of Things Journal*, pp. 1–1, 2021.

[95] N. Podevijn, D. Plets, J. Trogh, L. Martens, P. Suanet, K. Hendrikse, and W. Joseph, "Tdoa-based outdoor positioning with tracking algorithm in a public lora network," *Wireless Communications and Mobile Computing*, vol. 2018, 2018.

[96] K. Staniec and M. Kowal, "Lora performance under variable interference and heavy-multipath conditions," *Wireless communications and mobile computing*, vol. 2018, 2018.

[97] J. Finnegan, S. Brown, and R. Farrell, "Modeling the energy consumption of lorawan in ns-3 based on real world measurements," in *2018 Global Information Infrastructure and Networking Symposium (GIIS)*. IEEE, 2018, pp. 1–4.

[98] L. Alliance, "Lorawan™ 1.1 specification," 2017, available online: https://lora-alliance.org/sites/default/files/2018-04/lorawantm_specification_-v1.1.pdf, (Accessed on 02 Jan. 2020).

[99] N. Chinchilla-Romero, J. Navarro-Ortiz, P. Muñoz, and P. Ameigeiras, "Collision avoidance resource allocation for lorawan," *Sensors*, vol. 21, no. 4, p. 1218, 2021.

[100] R. Marini, W. Cerroni, and C. Buratti, "A novel collision-aware adaptive data rate algorithm for lorawan networks," *IEEE Internet of Things Journal*, vol. 8, no. 4, pp. 2670–2680, 2021.

[101] K. Anwar, T. Rahman, A. Zeb, Y. Saeed, M. A. Khan, I. Khan, S. Ahmad, A. E. Abdelgawad, and M. Abdollahian, "Improving the convergence period of adaptive data rate in a long range wide area network for the internet of things devices," *Energies*, vol. 14, no. 18, p. 5614, 2021.

[102] A. Farhad, D.-H. Kim, P. Sthapit, and J.-Y. Pyun, "Interference-aware spreading factor assignment scheme for the massive lorawan network," in *International Conference on Electronics, Information, and Communication (ICEIC), Auckland, New Zealand, 06 May 2019*. IEEE, 2019, pp. 1–2.